



National Library  
of Canada

Acquisitions and  
Bibliographic Services Branch

395 Wellington Street  
Ottawa, Ontario  
K1A 0N4

Bibliothèque nationale  
du Canada

Direction des acquisitions et  
des services bibliographiques

395, rue Wellington  
Ottawa (Ontario)  
K1A 0N4

*Your file* *Votre référence*

*Our file* *Notre référence*

## NOTICE

The quality of this microform is heavily dependent upon the quality of the original thesis submitted for microfilming. Every effort has been made to ensure the highest quality of reproduction possible.

If pages are missing, contact the university which granted the degree.

Some pages may have indistinct print especially if the original pages were typed with a poor typewriter ribbon or if the university sent us an inferior photocopy.

Reproduction in full or in part of this microform is governed by the Canadian Copyright Act, R.S.C. 1970, c. C-30, and subsequent amendments.

## AVIS

La qualité de cette microforme dépend grandement de la qualité de la thèse soumise au microfilmage. Nous avons tout fait pour assurer une qualité supérieure de reproduction.

S'il manque des pages, veuillez communiquer avec l'université qui a conféré le grade.

La qualité d'impression de certaines pages peut laisser à désirer, surtout si les pages originales ont été dactylographiées à l'aide d'un ruban usé ou si l'université nous a fait parvenir une photocopie de qualité inférieure.

La reproduction, même partielle, de cette microforme est soumise à la Loi canadienne sur le droit d'auteur, SRC 1970, c. C-30, et ses amendements subséquents.

Canada

**Effects of Ischemia and Preservation Solutions  
on Morphology and Transport  
of Renal Proximal Tubules**

by

YongDong You

Submitted in partial fulfillment of the requirements  
for the degree of Doctor of Philosophy

at

Dalhousie University  
Halifax, Nova Scotia, Canada  
July, 1993

©1993 by YongDong You



National Library  
of Canada

Acquisitions and  
Bibliographic Services Branch

395 Wellington Street  
Ottawa, Ontario  
K1A 0N4

Bibliothèque nationale  
du Canada

Direction des acquisitions et  
des services bibliographiques

395, rue Wellington  
Ottawa (Ontario)  
K1A 0N4

*Your file* *Votre référence*

*Our file* *Notre référence*

**The author has granted an irrevocable non-exclusive licence allowing the National Library of Canada to reproduce, loan, distribute or sell copies of his/her thesis by any means and in any form or format, making this thesis available to interested persons.**

**L'auteur a accordé une licence irrévocable et non exclusive permettant à la Bibliothèque nationale du Canada de reproduire, prêter, distribuer ou vendre des copies de sa thèse de quelque manière et sous quelque forme que ce soit pour mettre des exemplaires de cette thèse à la disposition des personnes intéressées.**

**The author retains ownership of the copyright in his/her thesis. Neither the thesis nor substantial extracts from it may be printed or otherwise reproduced without his/her permission.**

**L'auteur conserve la propriété du droit d'auteur qui protège sa thèse. Ni la thèse ni des extraits substantiels de celle-ci ne doivent être imprimés ou autrement reproduits sans son autorisation.**

ISBN 0-315-93760-2

**Canada**

Name YongDong You

Dissertation Abstracts International is arranged by broad, general subject categories. Please select the one subject which most nearly describes the content of your dissertation. Enter the corresponding four-digit code in the spaces provided.

Physiology

**0433 UMI**

SUBJECT TERM

SUBJECT CODE

**Subject Categories**

**THE HUMANITIES AND SOCIAL SCIENCES**

**COMMUNICATIONS AND THE ARTS**

Architecture .....0729  
 Art History .....0377  
 Cinema .....0900  
 Dance .....0378  
 Fine Arts .....0357  
 Information Science .....0723  
 Journalism .....0391  
 Library Science .....0399  
 Mass Communications .....0708  
 Music .....0413  
 Speech Communication .....0459  
 Theater .....0465

**EDUCATION**

General .....0515  
 Administration .....0514  
 Adult and Continuing .....0516  
 Agricultural .....0517  
 Art .....0273  
 Bilingual and Multicultural .....0282  
 Business .....0688  
 Community College .....0275  
 Curriculum and Instruction .....0727  
 Early Childhood .....0518  
 Elementary .....0524  
 Finance .....0277  
 Guidance and Counseling .....0519  
 Health .....0680  
 Higher .....0745  
 History of .....0520  
 Home Economics .....0278  
 Industrial .....0521  
 Language and Literature .....0279  
 Mathematics .....0280  
 Music .....0522  
 Philosophy of .....0998  
 Physical .....0523

Psychology .....0525  
 Reading .....0535  
 Religious .....0527  
 Sciences .....0714  
 Secondary .....0533  
 Social Sciences .....0534  
 Sociology of .....0340  
 Special .....0529  
 Teacher Training .....0530  
 Technology .....0710  
 Tests and Measurements .....0288  
 Vocational .....0747

**LANGUAGE, LITERATURE AND LINGUISTICS**

Language  
 General .....0679  
 Ancient .....0289  
 Linguistics .....0290  
 Modern .....0291  
 Literature  
 General .....0401  
 Classical .....0294  
 Comparative .....0295  
 Medieval .....0297  
 Modern .....0298  
 African .....0316  
 American .....0591  
 Asian .....0305  
 Canadian (English) .....0352  
 Canadian (French) .....0355  
 English .....0593  
 Germanic .....0311  
 Latin American .....0312  
 Middle Eastern .....0315  
 Romance .....0313  
 Slavic and East European .....0314

**PHILOSOPHY, RELIGION AND THEOLOGY**

Philosophy .....0422  
 Religion  
 General .....0318  
 Biblical Studies .....0321  
 Clergy .....0319  
 History of .....0320  
 Philosophy of .....0322  
 Theology .....0469

**SOCIAL SCIENCES**

American Studies .....0323  
 Anthropology  
 Archaeology .....0324  
 Cultural .....0326  
 Physical .....0327  
 Business Administration  
 General .....0310  
 Accounting .....0272  
 Banking .....0770  
 Management .....0454  
 Marketing .....0338  
 Canadian Studies .....0385  
 Economics  
 General .....0501  
 Agricultural .....0503  
 Commerce-Business .....0505  
 Finance .....0508  
 History .....0509  
 Labor .....0510  
 Theory .....0511  
 Folklore .....0358  
 Geography .....0366  
 Gerontology .....0351  
 History  
 General .....0578

Ancient .....0579  
 Medieval .....0581  
 Modern .....0582  
 Black .....0328  
 African .....0331  
 Asia, Australia and Oceania .....0332  
 Canadian .....0334  
 European .....0335  
 Latin American .....0336  
 Middle Eastern .....0333  
 United States .....0337  
 History of Science .....0585  
 Law .....0398  
 Political Science  
 General .....0615  
 International Law and Relations .....0616  
 Public Administration .....0617  
 Recreation .....0814  
 Social Work .....0452  
 Sociology  
 General .....0626  
 Criminology and Penology .....0627  
 Demography .....0938  
 Ethnic and Racial Studies .....0631  
 Individual and Family Studies .....0628  
 Industrial and Labor Relations .....0629  
 Public and Social Welfare .....0630  
 Social Structure and Development .....0700  
 Theory and Methods .....0344  
 Transportation .....0709  
 Urban and Regional Planning .....0999  
 Women's Studies .....0453

**THE SCIENCES AND ENGINEERING**

**BIOLOGICAL SCIENCES**

Agriculture  
 General .....0473  
 Agronomy .....0285  
 Animal Culture and Nutrition .....0475  
 Animal Pathology .....0476  
 Food Science and Technology .....0359  
 Forestry and Wildlife .....0478  
 Plant Culture .....0479  
 Plant Pathology .....0480  
 Plant Physiology .....0817  
 Range Management .....0777  
 Wood Technology .....0746  
 Biology  
 General .....0306  
 Anatomy .....0287  
 Biostatistics .....0308  
 Botany .....0309  
 Cell .....0379  
 Ecology .....0329  
 Entomology .....0353  
 Genetics .....0369  
 Limnology .....0793  
 Microbiology .....0410  
 Molecular .....0307  
 Neuroscience .....0317  
 Oceanography .....0416  
 Physiology .....0433  
 Radiation .....0821  
 Veterinary Science .....0778  
 Zoology .....0472  
 Biophysics  
 General .....0786  
 Medical .....0760  
**EARTH SCIENCES**  
 Biogeochemistry .....0425  
 Geochemistry .....0996

Geodesy .....0370  
 Geology .....0372  
 Geophysics .....0373  
 Hydrology .....0388  
 Mineralogy .....0411  
 Paleobotany .....0345  
 Paleocology .....0426  
 Paleontology .....0418  
 Paleozoology .....0985  
 Palynology .....0427  
 Physical Geography .....0368  
 Physical Oceanography .....0415

**HEALTH AND ENVIRONMENTAL SCIENCES**

Environmental Sciences .....0768  
 Health Sciences  
 General .....0566  
 Audiology .....0300  
 Chemotherapy .....0992  
 Dentistry .....0567  
 Education .....0350  
 Hospital Management .....0769  
 Human Development .....0758  
 Immunology .....0982  
 Medicine and Surgery .....0564  
 Mental Health .....0347  
 Nursing .....0569  
 Nutrition .....0570  
 Obstetrics and Gynecology .....0380  
 Occupational Health and Therapy .....0354  
 Ophthalmology .....0381  
 Pathology .....0571  
 Pharmacology .....0419  
 Pharmacy .....0572  
 Physical Therapy .....0382  
 Public Health .....0573  
 Radiology .....0574  
 Recreation .....0575

Speech Pathology .....0460  
 Toxicology .....0383  
 Home Economics .....0386

**PHYSICAL SCIENCES**

**Pure Sciences**  
 Chemistry  
 General .....0485  
 Agricultural .....0749  
 Analytical .....0486  
 Biochemistry .....0487  
 Inorganic .....0488  
 Nuclear .....0738  
 Organic .....0490  
 Pharmaceutical .....0491  
 Physical .....0494  
 Polymer .....0495  
 Radiation .....0754  
 Mathematics .....0405  
 Physics  
 General .....0605  
 Acoustics .....0986  
 Astronomy and Astrophysics .....0606  
 Atmospheric Science .....0608  
 Atomic .....0748  
 Electronics and Electricity .....0607  
 Elementary Particles and High Energy .....0798  
 Fluid and Plasma .....0759  
 Molecular .....0609  
 Nuclear .....0610  
 Optics .....0752  
 Radiation .....0756  
 Solid State .....0611  
 Statistics .....0463  
**Applied Sciences**  
 Applied Mechanics .....0346  
 Computer Science .....0984

Engineering  
 General .....0537  
 Aerospace .....0538  
 Agricultural .....0539  
 Automotive .....0540  
 Biomedical .....0541  
 Chemical .....0542  
 Civil .....0543  
 Electronic and Electrical .....0544  
 Heat and Thermodynamics .....0348  
 Hydraulic .....0545  
 Industrial .....0546  
 Marine .....0547  
 Materials Science .....0794  
 Mechanical .....0548  
 Metallurgy .....0743  
 Mining .....0551  
 Nuclear .....0552  
 Packaging .....0549  
 Petroleum .....0765  
 Sanitary and Municipal System Science .....0790  
 Geotechnology .....0428  
 Operations Research .....0796  
 Plastics Technology .....0795  
 Textile Technology .....0994

**PSYCHOLOGY**

General .....0621  
 Behavioral .....0384  
 Clinical .....0622  
 Developmental .....0620  
 Experimental .....0623  
 Industrial .....0624  
 Personality .....0625  
 Physiological .....0989  
 Psychobiology .....0349  
 Psychometrics .....0632  
 Social .....0451



I dedicate this thesis to my parents and grandparents

# Contents

List of Figures . . . . .	viii
List of Tables . . . . .	x
Abstract . . . . .	xi
List of Abbreviations and Symbols . . . . .	xii
Acknowledgements . . . . .	xvii
<b>1 INTRODUCTION</b>	<b>1</b>
1.1 Renal Ischemia . . . . .	2
1.1.1 Energy metabolism and transport in proximal tubules . . . . .	2
1.1.2 Effects of ischemia on energy metabolism and transport . . . . .	6
1.1.3 Morphological changes following hypoxia and ischemia . . . . .	9
1.2 Renal Preservation Solutions . . . . .	14
1.2.1 Cold storage of kidney for transplantation . . . . .	14
1.2.2 Experimental and clinical comparison of EC and UW solutions . . . . .	16
1.3 Electrophysiology of Proximal Tubular Transport . . . . .	17
1.3.1 General scheme of proximal tubular transport . . . . .	18
1.3.2 Electrical potentials associated with tubular transport . . . . .	19
1.4 Rationale . . . . .	25
1.4.1 Rationale for study of hypoxia/ischemia . . . . .	26
1.4.2 Rationale for study of preservation solutions . . . . .	28
1.4.3 Summary . . . . .	29
<b>2 METHODOLOGY</b>	<b>31</b>
2.1 Solutions . . . . .	31
2.1.1 Hypoxic and ischemic solutions . . . . .	31
2.1.2 Preservation solutions . . . . .	34
2.2 Isolation and Perfusion of Tubules . . . . .	35
2.3 Electrophysiological Techniques . . . . .	37
2.3.1 Potential difference measurements . . . . .	37
2.3.2 Intracellular Na <sup>+</sup> -activity measurement . . . . .	38
2.3.3 Measurements of K <sup>+</sup> transference numbers of basolateral and apical cell membranes . . . . .	39
2.3.4 Tubular resistance measurements . . . . .	40
2.4 Morphological Methods . . . . .	42
2.4.1 Light microscopy . . . . .	42
2.4.2 Electron microscopy . . . . .	43

2.5	Measurement of Tubular ATP Content . . . . .	44
2.6	Experimental Protocols . . . . .	45
2.6.1	Hypoxic and ischemic perfusion . . . . .	46
2.6.2	Temperature studies . . . . .	47
2.6.3	Preservative solution studies . . . . .	48
2.7	Statistical Analysis . . . . .	48
<b>3</b>	<b>RESULTS I: Hypoxia and Ischemia</b>	<b>49</b>
3.1	Electrophysiological Effects of Hypoxia . . . . .	49
3.1.1	Basolateral membrane and transepithelial potentials . . . . .	49
3.1.2	Basolateral $K^+$ transference number and intracellular $Na^+$ activity . . . . .	53
3.1.3	Transepithelial resistance . . . . .	54
3.2	Electrophysiological Effects of Ischemia . . . . .	57
3.2.1	Basolateral membrane and transepithelial potentials . . . . .	57
3.2.2	Basolateral $K^+$ transference number and intracellular $Na^+$ activity . . . . .	60
3.2.3	Tubular resistances . . . . .	60
3.3	Electrophysiological Effects of Ouabain . . . . .	65
3.4	Hypoxia/Ischemia and Proximal Tubular Ultrastructure . . . . .	65
3.5	Hypoxia/Ischemia and Intracellular ATP Content . . . . .	68
<b>4</b>	<b>RESULTS II: Temperature and Preservation Solutions</b>	<b>73</b>
4.1	Effects of Cooling . . . . .	73
4.2	Comparison of EC and UW Solutions at 22°C and 37°C . . . . .	82
4.2.1	Effects of EC and UW solutions at 22°C . . . . .	82
4.2.2	Effects of EC and UW solutions at 37°C . . . . .	83
4.3	Further Investigation of Osmotic Effects of EC solution at 37°C . . . . .	94
<b>5</b>	<b>DISCUSSION I: Electrophysiology of Proximal Tubular Transport</b>	<b>97</b>
5.1	The Control Proximal Tubule . . . . .	97
5.1.1	Diffusional potentials . . . . .	97
5.1.2	Transepithelial and transmembrane potentials . . . . .	98
5.1.3	Basolateral cell membrane . . . . .	101
5.1.4	Apical cell membrane . . . . .	105
5.1.5	Loop current . . . . .	108
5.2	Effects of Hypoxia and Ischemia . . . . .	110
5.2.1	Basolateral membrane potential and $K^+$ transference number . . . . .	111
5.2.2	Intracellular $Na^+$ activity . . . . .	112
5.2.3	Transepithelial potential and tubular resistances . . . . .	114
5.3	Effects of Cooling . . . . .	117
5.3.1	Cooling to 22°C . . . . .	117
5.3.2	Cooling to 4°C . . . . .	119

<b>6</b>	<b>DISCUSSION II: Tubular Metabolism and Morphology</b>	<b>123</b>
6.1	Effects of Hypoxia and Ischemia . . . . .	123
6.1.1	Morphological changes . . . . .	124
6.1.2	Metabolic changes . . . . .	125
6.2	Effects of Temperature and Preservation Solutions . . . . .	129
6.2.1	Maintenance of cell volume at 37°C . . . . .	129
6.2.2	Effects of temperature on cell volume . . . . .	130
6.2.3	Effects of high-K <sup>+</sup> content in preservation solutions . . . . .	131
6.2.4	Effects of membrane impermeants in preservation solutions . . . . .	133
6.2.5	Correlation between cell swelling and deterioration of transepithelial potential . . . . .	136
<b>7</b>	<b>CONCLUDING REMARKS</b>	<b>139</b>
<b>A</b>	<b>Cable Analysis in Mammalian Proximal Tubules</b>	<b>141</b>
A.1	General Theory . . . . .	142
A.2	Intraluminal Current Injection and Luminal Cable . . . . .	144
A.3	Intraluminal Current Injection and Voltage Divider Ratio . . . . .	145
A.3.1	$\alpha$ and $R_{lis}$ . . . . .	145
A.3.2	$\alpha$ and intercellular current exchange . . . . .	146
A.4	Intracellular Current Injection and Cellular Cable . . . . .	147
A.4.1	Cross talk . . . . .	147
A.4.2	Point-current distortion . . . . .	147
A.5	Data Analysis . . . . .	149
•	<b>Bibliography</b>	<b>160</b>

# List of Figures

1.1	Ionic and substrate transport systems in proximal tubules . . . . .	20
2.1	The tubular perfusion apparatus . . . . .	36
2.2	Effect of temperature on the resistivity of Ringer solution . . . . .	41
3.1	Effects of hypoxia on $V_{bl}$ & $V_{te}$ : Representative tracings . . . . .	51
3.2	Effects of hypoxia on $V_{bl}$ & $V_{te}$ : Summary . . . . .	52
3.3	Effects of hypoxia on $t_{K(bl)}$ & $a_i^{Na}$ : Representative tracings . . . . .	55
3.4	Effects of hypoxia on $R_{te}$ . . . . .	56
3.5	Effects of ischemia on $V_{bl}$ , $V_{te}$ & $a_i^{Na}$ : Representative tracings . . . . .	58
3.6	Effects of ischemia on $V_{bl}$ & $V_{te}$ : Summary . . . . .	59
3.7	Effect of ischemia on $R_{te}$ . . . . .	62
3.8	Cellular cable analysis: $\Delta V_{bl} \sim x$ relationship . . . . .	63
3.9	Correlation between the effects of hypoxia/ischemia on $V_{te}$ & $R_{te}$ . . . . .	66
3.10	Effects of ouabain on $a_i^{Na}$ , $V_{bl}$ & $V_{te}$ . . . . .	67
3.11	Ultrastructural appearance of control isolated perfused proximal straight tubules . . . . .	69
3.12	Effects of hypoxia and ischemia on the ultrastructure . . . . .	70
3.13	Effects of hypoxia/ischemia on tubular ATP content . . . . .	72
4.1	Effects of cooling to 4°C on $V_{bl}$ , $t_{K(bl)}$ & $V_{te}$ . . . . .	75
4.2	Effects of cooling to 22°C on $V_{bl}$ , $t_{K(bl)}$ & $V_{te}$ . . . . .	76
4.3	Effects of cooling to 22°C & to 4°C on $a_i^{Na}$ . . . . .	77
4.4	Effects of temperature on cell volume: Photomicrographs . . . . .	79
4.5	Effects of temperature on cell volume: Time courses . . . . .	80
4.6	Effects of temperature on cell ultrastructures . . . . .	81
4.7	Effects of EC solution on cell volume at 22°C: Photomicrographs . . . . .	84
4.8	Effects of UW solution on cell volume at 22°C: Photomicrographs . . . . .	85
4.9	Effects of EC & UW solutions on cell volume: Summary . . . . .	86
4.10	Recovery of $V_{te}$ following EC & UW perfusion at 22°C . . . . .	87
4.11	Effects of EC solution on cell volume at 37°C: Photomicrographs . . . . .	88
4.12	Effects of UW solution on cell volume at 37°C: Photomicrographs . . . . .	89
4.13	Effects of EC, ECM & UW solutions on cell volume: Summary . . . . .	90
4.14	Effects of EC & UW perfusion at 37°C on cell ultrastructures . . . . .	92
4.15	Recovery of $V_{te}$ following EC, ECM & UW perfusion at 37°C . . . . .	93

4.16 Cell ultrastructures during control reperfusion following EC, ECM or UW perfusion at 37°C . . . . .	95
5.1 Equivalent electrical circuit for the proximal tubules . . . . .	100
A.1 Equivalent electrical circuit for cable analysis . . . . .	143

# List of Tables

2.1	Concentrations of components in Ringer solutions . . . . .	32
2.2	Concentrations of components in preservation solutions . . . . .	33
3.1	Effects of ischemia on tubular resistances . . . . .	64
4.1	Effects of temperature on tubular resistances . . . . .	78
6.1	Estimated cell membrane $K^+$ conductances . . . . .	132

## Abstract

This study investigated the electrophysiological and morphological alterations in renal proximal tubules following exposure to ischemic conditions and preservation solutions, using an *in vitro* single-tubule perfusion model.

Isolated mouse proximal straight tubules were subjected to simulated ischemic conditions by perfusion with hypoxic and ischemic solutions ( $P_{O_2}$  4 mmHg); the latter solution was high in  $K^+$  and lactate, devoid of glucose, and low in pH. Twenty-minute tubular perfusion with the hypoxic or ischemic solution on both the luminal and the basolateral sides at 37°C did not significantly alter cell membrane potential, cell membrane ionic conductance, and intracellular  $Na^+$  activity. The ultrastructure of the tubular cells was also well preserved following the perfusion. However, such a perfusion decreased both the transepithelial potential and resistance by 40%. These results suggest that tubular cells are able to maintain their structural and electrochemical integrity after short-term exposure to hypoxic or ischemic conditions. The compromised transepithelial transport would seem to indicate that cell-to-cell junctions are damaged by these insults.

Proximal tubules were also perfused with Euro-Collins' (EC) and University of Wisconsin (UW) solutions at 22°C and 37°C. Perfusion with the EC solution on both the luminal and the basolateral sides led to significant cell swelling, accompanied by deterioration of the transepithelial potential upon reperfusion with the Ringer solution. When the EC solution was perfused on the luminal and the basolateral sides separately, it was found that the deteriorating effect of this solution is associated with its presence on the basolateral side. In comparison, perfusion with the UW solution had no effect on cell volume, and no subsequent damage to the transepithelial potential was observed. Furthermore, substitution of glucose with mannitol abolished the damaging effect of the EC solution. These data emphasize the importance of effective membrane impermeants in the preservation solutions in maintaining cell volume, and suggest that cell swelling in the EC solution at warm temperatures could lead to acute tubular necrosis and delayed graft function in clinical renal transplantation.

## List of Abbreviations and Symbols

- 0-sub  $\equiv$  Organic substrate-free Ringer
- 20-K<sup>+</sup>  $\equiv$  20 mM-K<sup>+</sup> Ringer
- $\alpha$   $\equiv$  voltage divider ratio
- $\Delta E_{ap}$   $\equiv$  deflection of apical membrane diffusional potential (mV)
- $\Delta E_{bl}$   $\equiv$  deflection of basolateral membrane diffusional potential (mV)
- $\Delta V_{ap}$   $\equiv$  deflection of apical membrane potential (mV)
- $\Delta V_{bl}$   $\equiv$  deflection of basolateral membrane potential (mV)
- $\Delta V_c$   $\equiv$  deflection of transepithelial potential at the collection end (mV)
- $\Delta V_p$   $\equiv$  deflection of transepithelial potential at the perfusion end (mV)
- $\Delta V_{te}$   $\equiv$  deflection of transepithelial potential (mV)
- $\eta$   $\equiv$  combined double cable length constant (cm)
- $\vartheta$   $\equiv$  combined double cable length constant (cm)
- $\lambda_c$   $\equiv$  intrinsic length constant of cellular cable (cm)
- $\lambda_l$   $\equiv$  intrinsic length constant of luminal cable (cm)
- $\mu\text{L}$   $\equiv$  microlitre
- $\mu\text{m}$   $\equiv$  micrometre
- $\mu\text{A}$   $\equiv$  microampere
- $\rho$   $\equiv$  resistivity of the Ringer solution ( $\Omega\cdot\text{cm}$ )
- $\Omega$   $\equiv$  ohm
- $a$   $\equiv$  radius of the tubule (cm)
- $a_i^K$   $\equiv$  intracellular potassium activity (mM)
- $a_i^{\text{Na}}$   $\equiv$  intracellular sodium activity (mM)
- $a_o^K$   $\equiv$  extracellular K<sup>+</sup> activity (mM)
- $a_o^{\text{Na}}$   $\equiv$  extracellular Na<sup>+</sup> activity (mM)
- ATP  $\equiv$  adenosine 5'-triphosphate
- [ATP]<sub>i</sub>  $\equiv$  intracellular ATP content (mM or pmoles/mmTL)

- BB  $\equiv$  brush borders
- cm  $\equiv$  centimetre
- $d$   $\equiv$  interspace depth (cm)
- DGF  $\equiv$  delayed graft function
- $E_{ap}$   $\equiv$  diffusional potential of the apical membrane (mV)
- $E_{bl}$   $\equiv$  diffusional potential of the basolateral membrane (mV)
- $E_{Cl}$   $\equiv$  transmembrane  $Cl^-$  diffusional potential (mV)
- $E_K$   $\equiv$  transmembrane  $K^+$  diffusional potential (mV)
- $E_{Na}$   $\equiv$  transmembrane  $Na^+$  diffusional potential (mV)
- $E_{te}$   $\equiv$  transepithelial diffusional potential (mV)
- EC  $\equiv$  Euro-Collins' solution
- ECM  $\equiv$  Euro-Collins' mannitol solution
- $F$   $\equiv$  Faraday constant
- F-actin  $\equiv$  filament actin
- FCCP  $\equiv$  carbonyl cyanide-*p*-trifluoromethoxyphenylhydrazone
- g  $\equiv$  gram
- $g_K$   $\equiv$  membrane  $K^+$  conductance (mho/cm<sup>2</sup>)
- $g'_K$   $\equiv$  corrected membrane  $K^+$  conductance (mho/cm<sup>2</sup>)
- $g_{K(ap)}$   $\equiv$  apical  $K^+$  conductance (mho/cm<sup>2</sup>)
- $g'_{K(ap)}$   $\equiv$  corrected apical  $K^+$  conductance (mho/cm<sup>2</sup>)
- $g_{K(bl)}$   $\equiv$  basolateral  $K^+$  conductance (mho/cm<sup>2</sup>)
- $g'_{K(bl)}$   $\equiv$  corrected basolateral  $K^+$  conductance (mho/cm<sup>2</sup>)
- $G\Omega$   $\equiv$  gigaohm
- HES  $\equiv$  hydroxyethylstarch
- Hz  $\equiv$  hertz
- $I_0$   $\equiv$  amplitude of injected current (nA)
- $I_c$   $\equiv$  current flow along the cellular cable (nA)

- $I_g \equiv$  transepithelial electrogenic  $\text{Na}^+$ -transport current (pEq/mmTL/min)
- $I_l \equiv$  current flow along the luminal cable (nA)
- $I_{\text{loop}} \equiv$  loop current ( $\mu\text{A}/\text{cm}^2$ )
- $I_{\text{sc}} \equiv$  equivalent short-circuit current ( $\mu\text{A}/\text{cm}^2$ )
- ID  $\equiv$  inner diameter
- $J_{\text{Na}} \equiv$  transepithelial  $\text{Na}^+$  flux (pEq/mmTL/min)
- $J_v \equiv$  transepithelial volume flux (nL/mmTL/min)
- $K_m \equiv$  the substrate concentration that allows the reaction to proceed at one-half its maximum rate (mM)
- L  $\equiv$  litre
- LDH  $\equiv$  lactate dehydrogenase
- $l \equiv$  total linear extent (cm/cm<sup>2</sup> epithelium)
- M  $\equiv$  moles/litre
- $M\Omega \equiv$  megaohm
- mg  $\equiv$  milligram
- min  $\equiv$  minute
- mL  $\equiv$  millilitre
- mM  $\equiv$  millimolar
- mm  $\equiv$  millimetre
- mmHg  $\equiv$  millimetre of mercury
- mmTL  $\equiv$  millimetre tubule length
- mOsm  $\equiv$  milliosmoles
- mV  $\equiv$  millivolt
- MW  $\equiv$  molecular weight (grams/mole)
- $n \equiv$  number of measurements
- nA  $\equiv$  nanoampere
- NADH  $\equiv$  nicotinamide-adenine dinucleotide

- nL  $\equiv$  nanolitre
- nm  $\equiv$  nanometre
- OD  $\equiv$  outer diameter
- $P$   $\equiv$  probability
- $P_{\text{Cl}}$   $\equiv$  permeability of  $\text{Cl}^-$
- $P_{\text{HCO}_3}$   $\equiv$  permeability of  $\text{HCO}_3^-$
- $P_{\text{K}}$   $\equiv$  permeability of  $\text{K}^+$
- $P_{\text{Na}}$   $\equiv$  permeability of  $\text{Na}^+$
- $P_{\text{O}_2}$   $\equiv$  oxygen tension
- PCT  $\equiv$  proximal convoluted tubule
- pEq  $\equiv$  picoequivalent
- pmoles  $\equiv$  picomoles
- PST  $\equiv$  proximal straight tubule
- $Q_{\text{O}_2}$   $\equiv$  oxygen consumption
- $R$   $\equiv$  gas constant
- $R_{\text{ap}}$   $\equiv$  specific apical resistance per unit area ( $\Omega \cdot \text{cm}^2$ )
- $r_{\text{ap}}$   $\equiv$  transverse apical resistance per unit length ( $\Omega \cdot \text{cm}$ )
- $R_{\text{bl}}$   $\equiv$  specific basolateral resistance per unit area ( $\Omega \cdot \text{cm}^2$ )
- $r_{\text{b}}$   $\equiv$  transverse basolateral resistance per unit length ( $\Omega \cdot \text{cm}$ )
- $r_{\text{c}}$   $\equiv$  core resistance of cellular cable per unit length ( $\Omega/\text{cm}$ )
- $R_{\text{input}}$   $\equiv$  input resistance ( $\Omega$ )
- $r_{\text{l}}$   $\equiv$  core resistance of luminal cable per unit length ( $\Omega/\text{cm}$ )
- $R_{\text{lis}}$   $\equiv$  specific resistance of lateral intercellular space per unit area ( $\Omega \cdot \text{cm}^2$ )
- $R_{\text{s}}$   $\equiv$  specific shunt resistance per unit area ( $\Omega \cdot \text{cm}^2$ )
- $r_{\text{s}}$   $\equiv$  transverse shunt resistance per unit length ( $\Omega \cdot \text{cm}$ )
- $R_{\text{te}}$   $\equiv$  specific transepithelial resistance per unit area ( $\Omega \cdot \text{cm}^2$ )
- $R_{\text{tj}}$   $\equiv$  specific resistance of tight junction per unit area ( $\Omega \cdot \text{cm}^2$ )

- $R_v \equiv$  relative cell volume
- $R_z \equiv$  parallel specific resistance of apical and basolateral membranes per unit area ( $\Omega \cdot \text{cm}^2$ )
- S.E.  $\equiv$  standard error of mean
- sec  $\equiv$  second
- $T \equiv$  temperature ( $^{\circ}\text{C}$  or Kelvin)
- $t_{\text{K}(\text{bl})} \equiv$  basolateral  $\text{K}^+$  transference number
- $t'_{\text{K}(\text{bl})} \equiv$  corrected basolateral  $\text{K}^+$  transference number
- $t_{\text{K}(\text{ap})} \equiv$  apical  $\text{K}^+$  transference number
- $t'_{\text{K}(\text{ap})} \equiv$  corrected apical  $\text{K}^+$  transference number
- U  $\equiv$  unit
- UW  $\equiv$  University of Wisconsin solution
- $V_{\text{ap}} \equiv$  apical membrane potential (mV)
- $V_{\text{bl}} \equiv$  basolateral membrane potential (mV)
- $V_{\text{Na}} \equiv$  potential readings from intracellular  $\text{Na}^+$ -electrode (mV)
- $V_{\text{te}} \equiv$  transepithelial potential (mV)
- $w_i \equiv$  interspace width (cm)
- $X \equiv$  tubule length (cm)
- $x \equiv$  distance from the current-injection site (cm)
- $Z \equiv$  valence of an ion

## Acknowledgements

I would like to thank those who have made the completion of my graduate work possible.

I extend my deepest gratitude to my supervisor, Dr. Nikolas S. Morgunov, and my co-supervisor, Dr. David J. Hirsch, for their guidance, patience and motivation throughout my graduate years, especially during the final preparation of this thesis. I would also like to thank the members of my examining committee, Dr. Patrick Vinay (Hôpital Notre-Dame, Montréal), Dr. Michael West (Department of Medicine), Dr. B. Milan Horacek, and Dr. Siegfried Pelzer, for their critical review of this study.

I am indebted to Dr. Ian G. Mobbs and Stephen Whitefield of the Department of Anatomy for teaching me the electron microscopic techniques, and to Dr. David Byers of the Atlantic Research Centre for Mental Retardation for his kind loan of the luminometer. Appreciation is also extended to Brian Hoyt, Dr. B. Milan Horacek and Paul MacInnis for their help and advice on processing and printing of this thesis.

I am grateful to Stephen G. Foster for his assistance in the lab, and to my fellow graduate students for their valuable support and friendship.

Finally, I would like to acknowledge the Faculty of Graduate Studies and the Iazzk Walton Killam Foundation for their financial support of my graduate program.

# Chapter 1

## INTRODUCTION

Occurrence of delayed graft function (DGF) in recipients of cadaveric kidney transplants is a major clinical complication, which leads to poorer graft survival rates and higher mortality [41, 89, 156, 167, 168]. Immediate graft function is important to the successful immunosuppression regimen following the implantation [98, 150, 184]. DGF has been attributed to several factors, among which are warm ischemia [28, 64] and the type of solutions used in renal preservation [156]. Great research effort has been directed towards understanding and prevention of renal ischemia and towards developing more efficient renal preservation solutions for transplantation. This introduction reviews some aspects of renal ischemia and kidney preservation, as well as provides background information on electrophysiology of proximal tubular transport — the main investigative technique used in this study. The introduction is concluded by emphasizing the rationale of this study.

## 1.1 Renal Ischemia

### 1.1.1 Energy metabolism and transport in proximal tubules

Renal tubular energy metabolism refers to the utilization of substrates as fuels to generate direct energy source (adenosine 5'-triphosphate, or ATP), which in turn maintains tubular integrity and function. Different nephron segments differ dramatically in their energy metabolism. Only the energy metabolism of proximal tubules is reviewed here, because this is the only nephron segment investigated in the present study.

Proximal tubules are responsible for the bulk reabsorption of ions, small nutrient molecules such as glucose and amino acids, and water filtered by glomeruli (for reviews see [21], [22], [60], [135], and [170]). Such reabsorption is mainly driven by the  $\text{Na}^+, \text{K}^+$ -ATPase localized in the basolateral membrane of the proximal tubular cells. The  $\text{Na}^+, \text{K}^+$ -ATPase is a primary active transport system that directly requires the expenditure of metabolic energy (ATP). In mammalian proximal tubules under physiological conditions, most of the ATP is generated aerobically by oxidative phosphorylation, a process localized in mitochondria (for reviews on oxidative phosphorylation, see [88] and [177]). Proximal tubular cells can utilize a variety of substrates as metabolic fuels to synthesize ATP (for reviews see [85], [129], [179], and [210]). Substrates like glucose, lactate, fatty acids and amino acids can enter proximal tubular cells either across the apical membrane via  $\text{Na}^+$ -dependent cotransport systems or across the basolateral membrane via  $\text{Na}^+$ -independent mechanisms [14, 110, 178, 180].

Although glucose is the most common metabolic fuel for many tissues, including the renal medulla [119, 120], it is not an effective fuel for proximal tubules, especially for proximal convoluted tubules [85]. In microdissected  $S_1$  and  $S_2$  segments from the mouse kidney, the intracellular ATP content ( $[ATP]_i$ ) was barely detectable with glucose as the only substrate in the incubation medium, whereas glucose was almost as effective as glutamine and lactate in maintaining  $[ATP]_i$  in  $S_3$  segment [196]. In isolated suspensions of proximal convoluted tubules (PCT), presence of glucose as the sole substrate supported neither aerobic respiration (oxygen consumption, or  $Q_{O_2}$ ) nor  $[ATP]_i$ , whereas in suspensions of proximal straight tubules (PST), glucose was partially effective in supporting  $Q_{O_2}$  but not effective in maintaining a higher  $[ATP]_i$  level than found in substrate-free medium [159]. As pointed out by Ruegg and Mandel in their paper [159], the different effects of glucose on  $Q_{O_2}$  and  $[ATP]_i$  in suspensions of PST may be due to the fact that aside from being a metabolic fuel, glucose also facilitates apical  $Na^+$  entry and hence accelerates tubular  $Na^+$  transport (see Section 1.3), which represents an additional drain of intracellular ATP level. In sum, studies in isolated proximal tubules indicate that glucose is not an effective fuel in PCT, but can support at least a portion of energy metabolism in PST. This general conclusion is in agreement with the heterogeneity of glycolytic enzyme distribution along  $S_1$ ,  $S_2$  and  $S_3$  segments of proximal tubules [199].

Lactate can be used as a metabolic fuel by all segments of proximal tubules. In microdissected proximal tubular segments from the mouse kidney,  $[ATP]_i$  was well maintained in the presence of 2 mM of lactate [196]. In isolated suspensions of rabbit proximal tubules, lactate has been shown to stimulate  $Q_{O_2}$  and increase

the mitochondrial content of reduced nicotinamide-adenine dinucleotide (NADH) [11]. NADH is the major source of electrons for the respiratory chain which, in cooperation with the  $F_0F_1$ -type  $H^+$ -ATPase, generates ATP via electron transfer. However, in the presence of fatty acids, lactate uptake and oxidation are inhibited [17, 80]. Considering that the plasma fatty acid level is quite high [13], fatty acids appear to be the major metabolic fuel for proximal tubules *in vivo*. In agreement with this notion, in isolated suspensions of rabbit proximal tubules, lower concentrations of short-chain fatty acids than lactate are required to increase mitochondrial NADH level [11]. Lactate that is not metabolized can either be converted to glucose inside tubular cells via gluconeogenesis [48, 49, 80, 82], or exit the cell across the basolateral membrane via  $Na^+$ -independent mechanisms [14, 178, 198].

The proximal tubule is capable of metabolizing a variety of amino acids, among which glutamine is one of the main fuels in this tubular segment. Release of  $^{14}CO_2$  from labelled glutamine was demonstrated in early studies [112], although isotopic dilution was not taken into account in these experiments. In isolated single mouse proximal tubule, 30 min of substrate-free incubation at  $37^\circ C$  decreased  $[ATP]_i$  to 20% of the preincubation level. However, 75% of  $[ATP]_i$  was maintained after the incubation when 2 mM of glutamine was added to the substrate-free medium [196]. Another amino acid metabolized by proximal tubules is alanine. However, although alanine may be converted to pyruvate, which can be further metabolized through the tricarboxylic acid cycle to generate ATP, the amount of alanine being metabolized this way is small under physiological conditions [47]. It appears that alanine in the Ringer solution used for tubule perfusion in the studies reported here is a substrate

for  $\text{Na}^+$ -coupled cotransport (see Section 1.3) rather than a substrate for energy metabolism by the proximal tubule.

The energy production and the  $\text{Na}^+$  reabsorption in proximal tubules are tightly coupled. Factors that modulate  $\text{Na}^+$  reabsorption also modulate energy production. In suspensions of rabbit proximal tubules [84], glucose and  $\alpha$ -methyl-D-glucoside increased aerobic ATP production ( $Q_{\text{O}_2}$ ) by stimulating the  $\text{Na}^+, \text{K}^+$ -ATPase-powered transepithelial  $\text{Na}^+$  reabsorption (see Section 1.3.1). In addition, stimulation of  $\text{Na}^+, \text{K}^+$ -ATPase by nystatin, a  $\text{Na}^+$  ionophore, drastically augmented the oxygen consumption in proximal tubule suspensions from the dog [186] and rabbit [84, 159, 181] kidneys. On the other hand,  $\text{Na}^+, \text{K}^+$ -ATPase inhibition with ouabain decreased  $Q_{\text{O}_2}$  [84, 159, 186]. It is generally believed that cytosolic and mitochondrial levels of ATP, ADP and free phosphate ( $\text{P}_i$ ) are among the factors that couple the mitochondrial ATP production to the transepithelial active transport [85]. Cytosolic and mitochondrial concentrations of ATP, ADP and  $\text{P}_i$  not only reflect a balance between energy production and consumption processes, but also participate in the modulation of these two processes. For example, elevation of mitochondrial ADP level, which can be brought about by activation of energy utilization, stimulate the ATP synthesis [3, 100, 130]. Rotenone and antimycin A, inhibitors of mitochondrial ATP production, concomitantly inhibited  $\text{Na}^+$ -dependent reabsorption of fluid, phosphate and glucose [83]. The activity of  $\text{Na}^+, \text{K}^+$ -ATPase, a key transporter in proximal tubular  $\text{Na}^+$  reabsorption, increases linearly with the increase in  $[\text{ATP}]_i$ , showing no saturation up to physiological  $[\text{ATP}]_i$  range (4 to 5 mM) [182].

In summary, proximal tubules utilize a variety of substrates to generate ATP as

their direct energy source to power the process of  $\text{Na}^+$  and fluid reabsorption. The order of substrate preference in proximal tubules appears to be ketone bodies > fatty acids > lactate > glutamine [85]. This order may change when the metabolic status of the tubule is altered, an example of which is acidosis [86, 185]. Proximal tubular reabsorption is tightly coupled to the mitochondrial ATP synthesis, emphasizing reabsorption as the predominant energy-requiring process in this tubular segment under physiological conditions.

### **1.1.2 Effects of ischemia on energy metabolism and transport**

Renal ischemia leads to profound changes in cell structure and function (for reviews see [27], [35], [36], [102], [136], and [206]). However, renal cells can recover from 25 to 60 min of ischemic insult with little irreversible damage to their morphology and function [102]. This section deals with the alterations in energy metabolism and transport in proximal tubules during and after short-term warm ischemia.

When proximal tubular cells are deprived of oxygen (hypoxia or anoxia), several aspects of metabolism and transport are altered. Dickman and Mandel, using isolated proximal tubule suspensions, demonstrated the effects of several respiratory inhibitors on energy metabolism [57]. Their experimental results are summarized as follows. (1) Forty-five minutes of hypoxia (1%  $\text{O}_2$ ) and anoxia (0%  $\text{O}_2$ ) reduced intracellular ATP level ( $[\text{ATP}]_i$ ) and intracellular  $\text{K}^+$  content ( $[\text{K}^+]_i$ ). (2) The extent of  $[\text{ATP}]_i$  and  $[\text{K}^+]_i$  reduction during experimental periods, however, was greater under anoxic conditions than under hypoxic conditions. Consequently, compared with anoxia, hypoxia resulted in less cell injury — as measured by percentage of lactate

dehydrogenase (LDH) release — and better recovery of  $[ATP]_i$  and  $[K^+]_i$  during reoxygenation. The remaining  $[ATP]_i$  during hypoxia may be provided by one of the following two processes, or both: first, it is likely that some ATP comes from residual oxidative phosphorylation; second, glycolytic ATP may also contribute to the intracellular ATP pool because glycolysis is stimulated by hypoxia (as indicated by the increase in lactate production), but not by anoxia. (3) To further confirm the protective effect of glycolytic ATP, respiratory inhibitors rotenone, carbonyl cyanide-*p*-trifluoromethoxyphenylhydrazone (FCCP) and antimycin A were used to block aerobic ATP synthesis. It was found that rotenone and FCCP stimulated glycolysis, whereas antimycin A failed to do so. As a result, antimycin A decreased  $[ATP]_i$  and  $[K^+]_i$  to a greater degree than did rotenone and FCCP. Correspondingly, rotenone and FCCP caused less LDH release from proximal tubule suspensions than did antimycin A. (4) Combined treatment of rotenone and 2-deoxyglucose, inhibitor of glycolysis, resulted in a greater LDH release compared with treatment of rotenone alone. The authors concluded from the above observations that stimulation of glycolysis is important to maintain minimal energy stores and hence preserve the integrity of proximal tubular cells when aerobic ATP production is suppressed [57]. It appears that a critical level of  $[ATP]_i$  is required to prevent irreversible cell injury. Such an energy threshold was shown to be necessary for maintaining cell viability in cultured renal epithelial cells subjected to chemical depletion of  $[ATP]_i$  [202].

Ischemia is different from hypoxia or anoxia in that it refers to a situation in which both oxygen and substrate supplies are terminated [102, 206]. Numerous studies using whole-kidney models (either *in vivo* or *in vitro*) have documented dramatic

alterations in tubular metabolism and transport following 15 to 60 min of total loss of blood flow. Decrement of renal cortical ATP level was observed within 10 sec of the onset of ischemia in both isolated [16] and *in situ* [109] whole-kidney models. This ATP depletion would inhibit the  $\text{Na}^+, \text{K}^+$ -ATPase and disturb the cellular electrolyte balance. Indeed, occlusion of renal artery for 20 min resulted in an elevation of intracellular  $\text{Na}^+$  and  $\text{Cl}^-$  concentrations, and a drop in intracellular  $\text{K}^+$  concentration in proximal and distal tubules [132]. These disturbances of metabolic and ionic balances would inevitably compromise the tubular transport process during the ischemic insult.

Effects of hypoxia/anoxia and ischemia on energy metabolism and transport may persist during the reperfusion period, when the supplies of blood and oxygen to the kidney is restored. The reperfusion injury of renal cells following the ischemic insult has been an area of great research interest in recent years. Studies using whole-kidney ischemic models *in vivo* indicate that the ability of kidneys to regenerate ATP during reperfusion decreases with the increase in duration of warm ischemia [29]. Aerobic production of ATP, as measured by renal oxygen consumption ( $Q_{\text{O}_2}$ ) was depressed during initial phase of reperfusion (0 to 15 min) [91]. The  $Q_{\text{O}_2}$  then overshoot but became uncoupled to  $\text{Na}^+$  reabsorption at 30 to 45 min of reflow, suggesting significant ATP consumption in cellular repair processes [91]. In isolated proximal tubule suspensions, both proximal convoluted tubules (PCT) and proximal straight tubules (PST) showed depressed  $Q_{\text{O}_2}$  and  $[\text{ATP}]_i$  after 60 min of recovery from a 40-min hypoxia or anoxia [160]. Alterations in renal energy metabolism are accompanied by changes in tubular transport. In whole-kidney models *in vivo*,

compromised tubular reabsorption following 20- to 60-min occlusion of blood flow is suggested by the depressed urine-to-plasma inulin concentration ratio [132] and by the elevated fractional sodium excretion despite a decrease in filtered sodium load [91]. Using micropuncture techniques, Johnston and coworkers observed marked reduction in fluid reabsorption during the recovery period (0 to 4 hours) after 35 min of total renal artery occlusion in rat kidney [101]. In addition, PCT and PST isolated from rabbit kidneys 10 min after recovering from a 60-min ischemia showed large decrease in fluid reabsorption ( $J_v$ ) and the transepithelial potential (an electrical potential that is closely associated with  $\text{Na}^+$  and substrate reabsorption, see Section 1.3) [87].

In summary, hypoxia/anoxia and ischemia lead to decrease in  $[\text{ATP}]_i$  and disturbance of cellular ionic balance. Following the hypoxic and ischemic insults, proximal tubular reabsorption is greatly compromised. Cellular energy-generating process not only is impaired, but also becomes uncoupled to the transport function. These alterations represent the metabolic and functional aspects of acute renal failure.

### **1.1.3 Morphological changes following hypoxia and ischemia**

Renal tubules are composed of a single layer of epithelial cells joined together side by side by intercellular junctions. To accomplish vectorial transport of ions, nutrients and water across the tubular epithelium (namely, reabsorption or secretion), tubular cells must be polarized in the direction perpendicular to the tubular wall. Such polarity is established by having distinct apical membrane (facing the tubular lumen) and basolateral membrane (facing the interstitium) on the surface of each cell. Apical

and basolateral membrane domains are separated by cell-to-cell junctions.

In proximal tubules, the apical and the basolateral cell membrane domains are different in many respects. Structurally, the apical membrane takes the form of microvilli to increase the effective contact surface with the luminal fluid and facilitate reabsorption. The surface area of the basolateral membrane is increased by basolateral infoldings, as described by Welling and Welling [208]. Functionally, apical and basolateral membranes contain different transport proteins that work in series to enable transepithelial movement of water and solutes. Taking  $\text{Na}^+$  reabsorption as an example,  $\text{Na}^+$  moves across the apical membrane via the  $\text{Na}^+$ -substrate cotransporter and the  $\text{Na}^+$ - $\text{H}^+$  exchanger (probably NHE-3 isoform [194]), transport proteins that are unique to the apical membrane. The influx of  $\text{Na}^+$  increases the intracellular  $\text{Na}^+$  concentration, which in turn stimulates the extrusion of  $\text{Na}^+$  through the activity of the  $\text{Na}^+$ , $\text{K}^+$ -ATPase, a primary active transport system that is unique to the basolateral membrane.

Studies using the *in vivo* ischemic model demonstrated a scope of ultrastructural alterations in proximal tubules following both warm ischemia and subsequent reperfusion. One of the most distinct morphological alterations following 30 to 35 min of warm renal ischemia is the loss of microvilli within 60 min of reperfusion [91, 101]. Regeneration of microvilli was observed between 60 to 240 min of reperfusion [91, 101]. Repair of microvilli and other organelles is accompanied by the uncoupling of energy consumption and transport [91], suggesting that energy is expended on repair processes. In addition to the damage to microvilli, a variety of subcellular changes was observed following 10 to 60 min of *in vivo* ischemia and 3 to

24 hour of reperfusion. These changes include clumping of chromatin in the nuclei, dilatation of endoplasmic reticulum, swelling of mitochondria, and increase in size and number of second-degree lysosomes and residual bodies [71, 72, 73, 74, 134, 158].

Recent investigation into the morphological aspects of ischemic injury has revealed more subtle alterations in tubular cell membranes. A number of studies by Molitoris' group have demonstrated an alteration of membrane protein and lipid composition in proximal-tubule cells during renal ischemia. For example, the  $\text{Na}^+, \text{K}^+$ -ATPase, a protein unique to the basolateral membrane under physiological conditions, accumulated in the cortical apical membrane fractions after 15 to 50 min of ischemia, induced by clamping of renal pedicle [137, 140, 142]. Following the same ischemic protocol, redistribution of many other membrane proteins and lipids was also evident [137, 140, 141, 142]. Based on these observations, Molitoris has proposed that loss of membrane polarity in proximal tubules is an important consequence of cell injury that impairs tubular reabsorption following ischemia [137].

Newer experimental observations have suggested that the polarity loss may result from: a) the opening of tight junctions and b) the disruption of cytoskeletal network.

The loosening of the tight junction following ischemia has been suggested by several studies. In an *in vivo* ischemic model in rat kidney, the integrity of the tight junction was assessed using an electron-dense marker, ruthenium red [138]. This marker, when delivered into the tubular lumen through a micropipette, stained only the apical membrane. It was excluded from the basolateral membrane because of the tight junction. Induction of renal ischemia by renal pedicle clamping for 5 to 30 min led to a stepwise increase in ruthenium-red staining of the basolateral membrane,

suggesting damage to the tight junction. Similar results were observed in a chemical ischemic model (ATP depletion) using confluent LLC-PK<sub>1</sub> monolayers, in which 2 hours of ATP depletion using 0.1  $\mu\text{M}$  antimycin A resulted in the coating of the basolateral membrane with ruthenium red [42]. Cultured LLC-PK<sub>1</sub> cell originates from and possesses many important structural and functional properties of proximal tubular cells [42]. Morphological observations on the damage to the tight junction was supported by the concomitant decrease in transepithelial resistance ( $R_{te}$ ) recorded using electrophysiological techniques [42, 128].  $R_{te}$  describes the electrical tightness of an epithelium (see Section 5.2.3).

Another early event that contributes to loss of cell polarity is the disruption of the cytoskeletal network [136]. Like other epithelial cells, proximal tubule cells possess extensive membrane-associated cytoskeletal networks that are responsible for establishing and maintaining both the architecture and protein composition of the apical and the basolateral membranes. At the apical side, the membrane of microvilli is supported by a sophisticated submembranous cytoskeleton, with filament actin (F-actin) being the primary component [54]. A complicated cytoskeletal web also lies under the basolateral cell membrane. This fodrin-based network links membrane proteins such as Na<sup>+</sup>,K<sup>+</sup>-ATPase to the F-actin cytoskeletal structure and anchors those proteins in the basolateral membrane domain [40, 145, 146, 147, 148]. Ischemia disrupts the assembly of cytoskeletal proteins. In an isolated perfused kidney model, after anti-actin antibody staining, proximal tubules from control-perfused kidneys showed concentrated actin immunofluorescence associated with the brush border, which may correspond to the F-actin-based membrane skeleton [108]. Fifteen min-

utes of ischemia resulted in large gaps of actin staining at the brush border, which correlated with the disappearance of microvilli observed under the light microscope [108]. In a more recent study, decrease in actin fluorescence (rhodamine-phalloidin staining) at the apical membrane was observed after 5 min of ischemia, induced *in vivo* by pedicle clamping [107]. Confluent-monolayer model was also used to study the effect of ischemia on cytoskeletal structure. Fluorescent staining of F-actin in control cultured LLC-PK<sub>1</sub> cells, however, showed different distribution pattern compared with normal cells, with F-actin fluorescence mainly associated with the basolateral membrane [139]. Such F-actin networks may therefore be crucial to anchor the basolateral membrane-proteins such as Na<sup>+</sup>,K<sup>+</sup>-ATPase. A redistribution of F-actin fluorescence in LLC-PK<sub>1</sub> cells was observed following 30 to 120 min of ATP depletion using 1.5 μM antimycin A [139]. Such a redistribution of F-actin was accompanied by the dissociation of Na<sup>+</sup>,K<sup>+</sup>-ATPase from the cytoskeletal structure, suggesting mobilization and redistribution of Na<sup>+</sup>,K<sup>+</sup>-ATPase in the cell membrane [139].

In summary, renal ischemia leads to a loss of membrane polarity, including loss of brush border and redistribution of apical and/or basolateral membrane-specific proteins. These morphological and biochemical changes are probably initiated by the disruption of the cytoskeletal network and the opening of cell-to-cell junctions. Alterations in cell morphology and membrane composition correlate with the impairment of cell-transport function.

## 1.2 Renal Preservation Solutions

### 1.2.1 Cold storage of kidney for transplantation

Successful kidney preservation for extended time period (for example, 24 hours) allows completion of such procedures as tissue matching, selection of a recipient, transport of the organ and preparation of the recipient for surgery. Kidney preservation is thus essential to all cadaveric transplantation programs [131].

Storage at temperatures close to 0°C has proven to be the most effective way to preserve an organ. Following nephrectomy, the supply of oxygen and metabolic fuel for energy production within the kidney is greatly reduced. Cold temperature slows down all the enzymatic reactions within the cell (namely cell metabolism) and therefore curtails both energy production and consumption. According to van Hoff's law, with a 2- to 3-fold reduction in reaction rate for every 10°C decrease in temperature (namely,  $Q_{10} = 2 \sim 3$ ), cooling from 37°C to 0°C slows down cell metabolism by 13 to 50 times [19]. An early study by Levy has shown that cooling to 0°C reduced oxygen consumption of the kidney to less than 3% of the 37°C control [122]. Therefore, with the reduction of their metabolic rates, organs preserved in cold temperatures are able to maintain their metabolic integrity for a longer period in the face of limited oxygen and substrate supply.

However, cold temperature has potential damaging effects on cell morphology. It inhibits the activity of Na<sup>+</sup>,K<sup>+</sup>-ATPase [45, 62] and results in the loss of cellular K<sup>+</sup> content and the gain of cellular Na<sup>+</sup> and Cl<sup>-</sup> from the interstitium [193]. The entry of NaCl disturbs the transmembrane osmotic balance, resulting in cell swelling [193].

Renal preservation solutions were designed to counteract the adverse effects of cold temperature described above (for reviews, see references [19], [28], [51], and [131]). The two most commonly used preservation solutions are Euro-Collins' (EC) and University of Wisconsin (UW) solutions. One of the most important components in preservation solutions is an effective membrane-impermeable osmolyte to counterbalance the osmotic pressure originating from the negatively charged intracellular protein. Glucose is used as such a membrane-impermeable osmolyte in EC solution, whereas lactobionate and raffinose are added to UW solution to provide the osmotic balance. To preserve the intracellular ionic content when  $\text{Na}^+, \text{K}^+$ -ATPase is inactivated at cold temperatures, both EC and UW solutions contain high concentrations of  $\text{K}^+$  and low concentrations of  $\text{Na}^+$ . Theoretically, this should reduce the energy expended in restoration of ionic balance upon rewarming [28]. Both EC and UW solutions are well buffered to minimize the changes in intracellular pH. In addition, UW solution also contains adenosine as a precursor of ATP synthesis, glutathione as a reducing agent, allopurinol to inhibit the formation of free  $\text{O}_2$  radicals and hydroxyethyl starch as a colloid in plasma compartment to counterbalance the oncotic pressure in interstitium and prevent tissue edema [19].

In summary, cold storage reduces cell metabolic rate and the minimal energy supply required to maintain cell viability. Renal preservation solutions are used in place of interstitial fluid at cold temperatures to preserve intracellular ionic content and prevent cell swelling. Cold storage using preservation solutions allows kidney cells to survive longer in the face of ischemia.

## **1 2.2 Experimental and clinical comparison of EC and UW solutions**

Since the development of UW solution in late 1980's, a number of experimental and clinical studies have compared the effectiveness of this solution in kidney preservation with the widely used EC solution, which was developed almost 20 years earlier.

In the isolated perfused canine kidney model, the percentage of Na<sup>+</sup> reabsorption following 48- and 72-hour cold storage in UW solution was significantly higher than the percentage of Na<sup>+</sup> reabsorption in kidneys stored in EC solution for the same lengths of time [155]. In the autotransplant model, the graft survival rate of reimplanted kidneys was 100% after storage in UW solution for 48 and 72 hours. However, the graft survival was only 80% after 48-hour storage, and 0% after 72-hour storage in EC solution [155]. In another autotransplant study [197], animals implanted with kidneys preserved in EC solution for 72 hours showed decreased urine output and elevated plasma serum creatinine level during reperfusion. Fifteen-day survival rate was 17% (1 out of 6) for this group. In comparison, animals implanted with kidneys preserved in UW solutions for the same length of time had much higher urine outputs and lower serum creatinine levels. Fifteen-day survival rate was 100% (6 out of 6). Moreover, the renal microvascular structure, visualized with silicon rubber one hour after revascularization, was much better preserved in UW-preserved kidneys than in EC-preserved kidneys. This finding was further confirmed by histological comparison of renal vasculature in UW- and EC-preserved kidneys [197].

The first comprehensive clinical comparison of UW and EC solutions, in which the outcome of 695 recipients of cadaver renal transplants was studied, was recently

published [156]. Occurrence of delayed graft function (DGF) was significantly lower in UW-preserved kidneys compared with that in EC-preserved kidneys. Serum creatinine level was lower and urine output was higher in recipients of UW-preserved kidneys compared with that in recipients of EC-preserved kidneys. These functional differences between UW- and EC-preserved kidneys correlated with the significantly higher rate of 1-year graft survival of UW-preserved kidneys.

In summary, both experimental and clinical studies indicate that the UW solution is superior to the EC solution in preserving the structure and function of the kidney graft.

### **1.3 Electrophysiology of Proximal Tubular Transport**

Fluid entering the proximal straight tubules *in vivo* is essentially free of organic nutrients and bicarbonate because of the powerful reabsorption process in proximal convoluted tubules [21]. Although proximal straight tubules function mainly to reabsorb filtered NaCl *in vivo*, this segment shows many electrophysiological characteristics of proximal convoluted tubules when presented with plasma-like Ringer solution during *in vitro* experiments [66, 113]. Thus proximal straight tubule appears to share the intrinsic transport systems found in proximal convoluted tubule, although activities of some transport systems may differ quantitatively [99, 106]. This section provides a brief overview of the electrophysiology of proximal tubular transport, with emphasis on NaCl reabsorption, under both *in vivo* and *in vitro* conditions.

### 1.3.1 General scheme of proximal tubular transport

Figure 1.1 illustrates the main ionic and substrate transport mechanisms identified so far in mammalian proximal tubules. Reabsorption of water and solutes across the tubular epithelium occurs via the following two pathways: 1) transcellular pathway and 2) paracellular pathway.

Transcellular transport requires coordinated function of transporters in both the apical and the basolateral membranes. For example, transcellular reabsorption of  $\text{Na}^+$ , the major cation in glomerular ultrafiltrate, involves several apical entry steps in series with a basolateral exit step (Figure 1.1). The basolateral extrusion of  $\text{Na}^+$  is accomplished by the  $\text{Na}^+, \text{K}^+$ -ATPase, which is powered by the metabolic energy released from ATP hydrolysis (*primary active transport*). Through the active extrusion of  $\text{Na}^+$  and the active uptake of  $\text{K}^+$ , the  $\text{Na}^+, \text{K}^+$ -ATPase sets up the transmembrane concentration gradients of both  $\text{Na}^+$  and  $\text{K}^+$ . The transmembrane  $\text{K}^+$  gradient in turn generates the inside-negative membrane electrical potential (see Section 1.3.2). Electrochemical potentials of  $\text{Na}^+$  and  $\text{K}^+$  across the cell membrane, especially that of  $\text{Na}^+$ , can be utilized by the coupled-transporters to power the uphill movement of other ions (for example,  $\text{H}^+$ ,  $\text{HCO}_3^-$ , and  $\text{Cl}^-$ ) or small organic solutes (for example, glucose and amino acids — *secondary active transport*).

Paracellular reabsorption occurs when solutes move from lumen across the tight junction and lateral intercellular space into the interstitium (Figure 1.1). This transport pathway is passive, depending on the electrochemical gradients across the tight junction that are set up by transcellular transport processes. Aside from the elec-

electrochemical gradients, permeabilities of solutes through the tight junction also determine the rate of transport [21, 22]. In mammalian proximal tubules, paracellular NaCl reabsorption can account for no more than 15% of total NaCl reabsorption [21]. Passive water reabsorption, either transcellularly or paracellularly, occurs due to the high water permeability across the epithelium, although the transepithelial osmotic gradient is small [170].

In summary, proximal tubule cells employ both passive and active transport pathways to reabsorb glomerular ultrafiltrate across the tubular epithelium. All these transport processes are primarily energized by the  $\text{Na}^+, \text{K}^+$ -ATPase, which, by utilizing the energy from ATP hydrolysis, maintains electrochemical gradients of  $\text{Na}^+$  and  $\text{K}^+$  across the cell membrane. The net effect of all proximal tubular transport processes is that major organic (glucose, amino acids, lactate) and inorganic ( $\text{Na}^+$ ,  $\text{K}^+$ ,  $\text{HCO}_3^-$ ,  $\text{Cl}^-$ , and  $\text{HPO}_4^{2-}$ ) solutes and water are reabsorbed, whereas  $\text{H}^+$  is secreted.

### **1.3.2 Electrical potentials associated with tubular transport**

Electrical potentials across the cell membranes and across the tight junction can be recorded in a functional proximal tubule. These electrical potentials are set up by the ionic gradients and transport currents across each barrier. Thus, recording and analysis of these potentials may provide one with information on ionic distributions and permeability characteristics of cell membranes and the tight junction, and help one in assessing various aspects of the tubular transport.

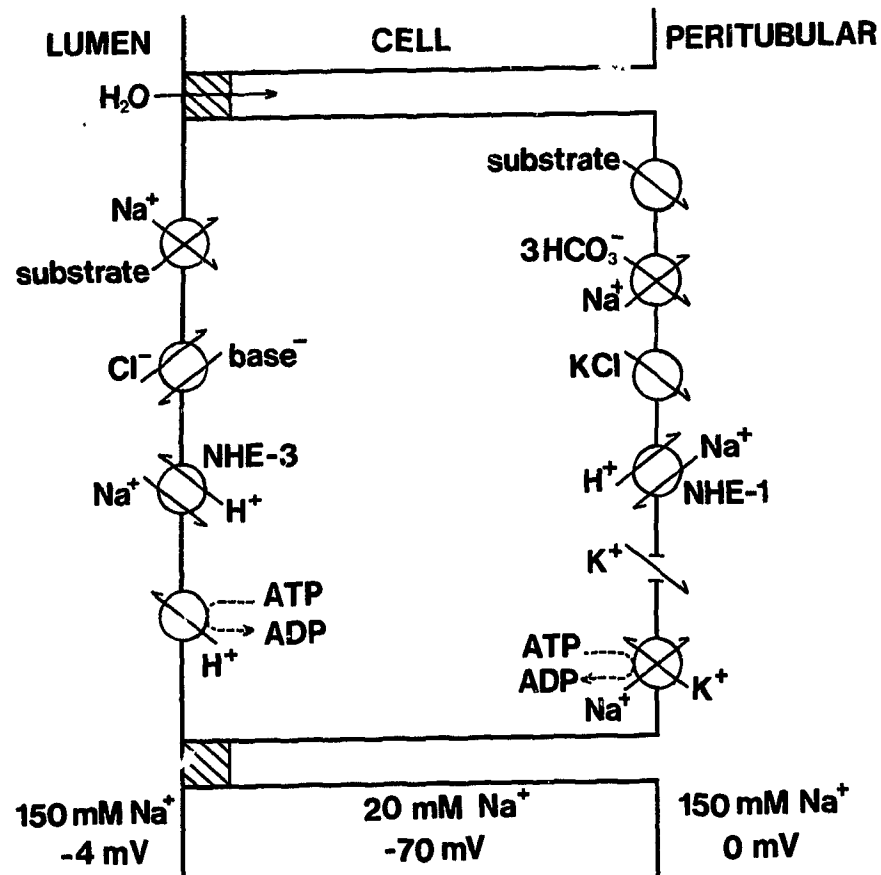


Figure 1.1: Ionic and substrate transport systems in mammalian proximal tubules. "Substrate" refers to small nutrient molecules such as glucose and amino acids, whereas "base<sup>-</sup>" refers to  $HCO_3^-$  and  $OH^-$ . NHE-1 is a "housekeeping" isoform of  $Na^+$ - $H^+$  exchanger and is present in the basolateral cell membrane [26, 195], whereas NHE-3 is probably an isoform of  $Na^+$ - $H^+$  exchanger specific for  $Na^+$  and  $H^+$  transport [194]. Arrows pointing upward represent movement against the electrochemical gradients and those pointing downward represent movement down the electrochemical gradients. The movement of water across the tight junction is an example of paracellular reabsorption (Illustration modified from reference [37]).

### The cell membrane potential

Like most mammalian cells, proximal tubule cells have high-K<sup>+</sup> and low-Na<sup>+</sup> content, whereas the interstitial fluid is high in Na<sup>+</sup> and low in K<sup>+</sup>. The transmembrane Na<sup>+</sup> and K<sup>+</sup> gradients are maintained by the Na<sup>+</sup>,K<sup>+</sup>-ATPase. It is well known that a concentration gradient of any ion  $Y$  across a barrier can generate a *Nernst potential* ( $E_Y$ ), if the barrier is permeable to  $Y$ :

$$E_Y = \frac{RT}{ZF} \ln \frac{a_o^Y}{a_i^Y} \quad (1.1)$$

where  $R$ ,  $T$ ,  $Z$  and  $F$  represent gas constant, absolute temperature, valence of the ion  $Y$  and Faraday constant, respectively;  $a$  refers to the activity of  $Y$  and subscripts  $o$  and  $i$  denote the outside and the inside of the cell, respectively. Since the basolateral membrane of renal proximal tubules is highly permeable to K<sup>+</sup>, but much less permeable to Na<sup>+</sup>, the Nernst potential of K<sup>+</sup> contributes a large portion of the basolateral membrane potential [30, 31]. Aside from the diffusional potential of K<sup>+</sup>, several transport systems also contribute to the membrane potential. For example, the Na<sup>+</sup>,K<sup>+</sup>-ATPase extrudes three Na<sup>+</sup> ions and takes up two K<sup>+</sup> ions with each cycle of pumping, resulting in one positive charge being removed from the cytosol per cycle (for reviews see [8], [68], [75], and [187]). This type of transport system is called *electrogenic*. The charge movement (or pump current) generated by the Na<sup>+</sup>,K<sup>+</sup>-ATPase hyperpolarizes the basolateral membrane. It has been well documented that the cardiac glycoside ouabain inhibits the Na<sup>+</sup>,K<sup>+</sup>-ATPase (see, for example, [94]) and causes depolarization of the membrane potential. The effect

of ouabain on membrane potential could be accounted for by: 1) the suppression of the hyperpolarizing pump current; 2) the dissipation of the  $K^+$  gradient across the membrane, which decreases the  $K^+$ -diffusion potential; and 3) the reduction of basolateral  $K^+$  conductance [200], which uncouples the  $K^+$ -diffusion potential and the membrane potential.

Compared with the basolateral membrane, ionic permeabilities across the apical membrane have not been well documented, although it appears that the  $Na^+$  permeability across the apical membrane is much higher than that across the basolateral membrane [31]. If comparable  $Na^+$  and  $K^+$  permeabilities are assumed, the apical membrane potential will be affected by both  $Na^+$ - and  $K^+$ -diffusion potentials (see Section 5.1.1). Several electrogenic transport systems in the apical membrane, among which are  $Na^+$ -substrate cotransport systems, also contribute to the membrane potential (see Figure 1.1). These transport proteins move positively-charged  $Na^+$  ions across the apical membrane along with electroneutral substrates, such as glucose, glycine and alanine, resulting in the accumulation of positive charges inside the cell. Thus, activation of  $Na^+$ -coupled cotransport systems depolarizes the apical membrane potential. Experimentally, inhibition of the cotransport systems by removal of substrates from the tubular lumen hyperpolarizes the apical membrane potential [143]. Membrane hyperpolarization was also observed when the cotransport systems were inhibited by cooling or by specific transport blockers such as phlorizin [200].

## The transepithelial potential

Transepithelial potential ( $V_{te}$ ) recorded from proximal tubules *in situ* varies considerably from segment to segment [32]. Under physiological conditions, at least two sources contribute to the  $V_{te}$  [32]. 1)  $V_{te}$  may originate from the diffusional potentials of anions such as  $Cl^-$  and  $HCO_3^-$ , the chemical gradients of which are set up by transcellular active transport processes. The overall diffusional potential depends not only on the directions and magnitudes of these ionic gradients, but also on the relative permeability of each ion across the tight junction. 2) The  $Na^+$ -transport current (also known as the loop current, see Section 5.1.5) flowing through the tight junction may also contribute to the  $V_{te}$ .

To eliminate the first source and study the effect of transcellular electrogenic transport on  $V_{te}$ , proximal tubules were perfused using symmetrical luminal perfusate and peritubular (bath) superfusate in the isolated perfused tubule model [39, 43, 113, 114, 126] and in the micropuncture model [66, 133]. When proximal tubules were exposed to artificial solutions that mimic the composition of glomerular ultrafiltrate on both luminal and basolateral sides, the recorded  $V_{te}$  was lumen-negative [39, 43, 113, 114, 126, 143, 200]. The lumen-negative potential was greatly suppressed or eliminated by ouabain [39, 113] and poisons of energy metabolism, such as cyanide [66], suggesting that active  $Na^+$  transport is essential for maintaining the potential. Furthermore, removal of organic solutes from solutions facing the luminal membrane also eliminated the lumen-negative potential [66, 113, 133, 143], suggesting that the electrogenic  $Na^+$ -substrate cotransport system is the cause of this potential. This

conclusion is further supported by the fact that phlorizin, a blocker of  $\text{Na}^+$ -glucose cotransport, depolarized the lumen-negative  $V_{te}$  [15, 113, 143].

In stop-flow experiments, when ionic gradients developed across the epithelium with time, the  $V_{te}$  changed its sign and became lumen-positive in rat proximal tubules [66, 67]. Such a lumen-positive  $V_{te}$  was reproduced in isolated perfused proximal tubules, by perfusion of the lumen with a solution resembling late proximal tubular fluid and the bath with a solution resembling glomerular ultrafiltrate [113]. Luminal perfusate in this experiment was free of organic substrate and with  $\text{HCO}_3^-$  partly replaced by  $\text{Cl}^-$  [113]. Under these circumstances, since the  $\text{Na}^+$ -coupled transport current is absent, the  $V_{te}$  is entirely due to the combined diffusional potential of  $\text{HCO}_3^-$  and  $\text{Cl}^-$  across the tight junction. From the sign of the  $V_{te}$  and the existing ionic gradients of  $\text{HCO}_3^-$  and  $\text{Cl}^-$ , it is easy to predict that the  $\text{HCO}_3^-$  permeability ( $P_{\text{HCO}_3}$ ) cross the tight junction must be lower than that of  $\text{Cl}^-$  ( $P_{\text{Cl}}$ ) in order for  $V_{te}$  to be lumen-positive (see Equation 5.1). Ratios of  $P_{\text{HCO}_3}/P_{\text{Cl}}$  less than unity were observed experimentally in the same tubular segment [23, 95, 203].

The knowledge of the origin of transepithelial potential obtained from the studies described above is useful in interpreting the observed  $V_{te}$  in proximal tubules *in vivo*. The  $V_{te}$  recorded from the first loop of proximal tubular segment that immediately follows the glomerulus ( $S_1$  segment) is lumen-negative [15, 67]. This potential is mainly due to the  $\text{Na}^+$ -coupled cotransport current as explained above. The contribution of diffusional potentials is small in this early phase of reabsorption because sizable ionic gradients are yet to be established. In contrast, the net electrogenic transport current is small in the late segment of the proximal tubule ( $S_2$  and  $S_3$ ),

because of the exhaustion of luminal organic solutes. The  $V_{te}$  recorded relates to the diffusional potentials of  $\text{Cl}^-$  (lumen-positive) and  $\text{HCO}_3^-$  (lumen-negative) that are set up across the tight junction by active reabsorption of  $\text{NaHCO}_3$  in the early segment [21]. A lumen-positive  $V_{te}$  has been recorded in the late segment of the rat proximal tubule *in situ* by means of micropuncture technique [15, 67], suggesting a higher transepithelial  $\text{Cl}^-$  permeability. This result is in complete agreement with the results from *in vitro* tubule-perfusion experiments [113].

In summary, the activity of certain electrogenic transport systems and the distributions of membrane- or tight-junction-permeable ions can be analyzed by measuring membrane and transepithelial potentials. It has to be pointed out that although electrophysiology provides a simple way of assessing tubular transport, the information obtained using such a technique is complicated and requires great care to interpret (see Chapter 5 for further explanation).

## 1.4 Rationale

The clinical renal preservation of cadaveric kidney involves three stages: 1) flushing of the kidney with ice-cold preservation solutions immediately after nephrectomy, 2) static ice storage of the organ, and 3) rewarming of the preserved organ during anastomosis. The transport function of renal tubules subjected to these nonphysiological conditions has not been characterized in detail at the cellular level. The aim of the present study was to investigate the alterations in tubular transport and morphology under conditions that the tubules could be exposed during renal preservation.

### 1.4.1 Rationale for study of hypoxia/ischemia

Ischemia is unavoidable during renal preservation. First, warm ischemia can start even before the kidneys are removed from a cadaveric donor if a hypotension has occurred. Second, cold ischemia during ice storage of the organ can last for 24 to 72 hours. From the consideration that the same pathophysiological events occur in cold ischemia as in warm ischemia, only with a slower time course (see discussion in Section 1.2.1), it is of clinical relevance to study the effect of warm ischemia using experimental animal models.

The classic model of renal ischemia in experimental animals involves clamping of renal pedicle *in situ* for up to one to two hours. Damaging effects of warm ischemia on both structure and function of renal tubules, especially proximal tubules, have been documented (see Section 1.1). However, although information on renal tubule injury following ischemia is ample, the triggering mechanism of cell injury remains largely unknown. The mechanistic issue is difficult to address using the whole-kidney model, because of the complexity of the system.

Recently developed ischemic models are based on simpler systems, such as isolated tubule suspension [103, 159] and cultured tubule cells [42, 139]. Experimental conditions were carefully controlled so that the effect of single factors (e.g. low  $P_{O_2}$ , ATP depletion) can be studied individually. New pathogenic aspects of renal cell injury have been documented partially because of the development of these simple model systems [35, 136, 206]. However, functional aspects of ischemic tubule injury have not been extensively investigated.

The single perfused tubule, isolated from fresh kidney slices, allows one to assess tubular transport and cell integrity continuously during the entire course of experiment. The tubule is subjected to a full transport load due to the rapid luminal perfusion and basolateral superfusion of the tubule with experimental solutions. We were interested in investigating the effects of warm hypoxia and ischemia on renal tubular transport using this tubule-perfusion system. Such a model allows one to monitor the electrogenic  $\text{Na}^+$  transport in detail by means of electrophysiological techniques. Therefore, the effects of hypoxia and ischemia on each component of electrogenic  $\text{Na}^+$  transport can be characterized. From the previous knowledge of cellular aspects of ischemic injury [102, 206], our hypothesis is that restriction of oxygen supply during hypoxia and ischemia would impair the process of mitochondrial oxidative phosphorylation and decrease cellular ATP content. This would in turn compromise the function of  $\text{Na}^+, \text{K}^+$ -ATPase and decrease the overall tubular transport, including the electrogenic  $\text{Na}^+$  reabsorption.

In the present study, hypoxia (low  $P_{\text{O}_2}$ ) and ischemia (a combination of low  $P_{\text{O}_2}$ , low pH, high  $\text{K}^+$  and lactate accumulation) were simulated in the perfusion chamber, and the effects of these two experimental conditions on tubular transport and ultrastructure were investigated. Isolated perfused proximal straight tubules of the mouse kidney were subjected to the simulated hypoxic or ischemic conditions for 20 minutes at  $37^\circ\text{C}$ . The proximal straight tubule was chosen as the subject of this study primarily because it is one of the most vulnerable segments to ischemic insult [58, 72, 73, 201]. Fortunately, this segment also happens to be the easiest segment to isolate from the mouse kidney slice by free-hand dissection, without col-

lagenase treatment. Twenty minutes of exposure time was chosen to detect the early events of hypoxic and ischemic injury. Renal ischemia *in vivo* for a similar length of time results in mild and reversible damage to tubular structure and function [102]. Electrophysiological techniques were applied to continuously monitor the effects of hypoxia and/or ischemia on electrochemical integrity and electrogenic transport of the tubular epithelium during the entire course of the experimental protocol. After 20 minutes of exposure to hypoxia and/or ischemia, tubules were also perfusion-fixed and subjected to electron-microscopic evaluation.

#### **1.4.2 Rationale for study of preservation solutions**

Since the development of UW solution, the effectiveness of this solution has been compared with the traditional EC solution in several clinical and experimental studies (see Section 1.2.2).

We were interested in characterizing the mechanism(s) underlying the beneficial effect of UW solution in preventing the occurrence of DGF. According to previous studies described above, increased anastomosis time, rather than cold storage time, appears to be closely associated with the occurrence of DGF [156].

Standard surgical protocol states that preserved kidneys need not be flushed free of preservation solutions prior to implantation (H. Bitter-Suermann, personal communication). Therefore, renal tubules are exposed to preservation solutions when kidneys are rewarmed during anastomosis (stage 3 of preservation, see above). We hypothesize that UW solution is superior to EC solution because at the room temperature to body temperature range, the former protects the tubule integrity better than

the latter does. Indeed, several studies have suggested that EC solution may lose its protective ability at warm temperatures [93, 189]. In fact, Andrews and Coffey have proposed that a good preservation solution should be able to protect the kidney tubules from warm ischemia during the performance of surgical transplantation [7].

This study was conducted to characterize, at the cellular level, the effects of preservation solutions on renal tubules at warm temperatures, using the isolated-perfused-tubule model. Similar model systems have been used to evaluate tubular integrity and function following kidney storage or tubule perfusion with different preservation solutions at 4°C to 10°C [63, 154]. In those studies, preservation solutions were quickly washed out by Ringer solution when tubules were rewarmed up to 37°C during reperfusion periods. Therefore, tubules were never exposed to preservation solutions at temperatures above 22°C. Effects of *in vitro* warm perfusion with EC and UW solutions have not been reported.

In addition, the effects of temperature on membrane conductive pathways and electrogenic transport mechanisms were also analyzed using electrophysiological techniques. Electrical properties of plasma membranes at different temperatures were then used to explain the observed morphological changes during EC or UW perfusion. These morphological changes were correlated with changes in the overall electrogenic transport, represented by the transepithelial potential.

### **1.4.3 Summary**

In summary, the objective of this thesis is to investigate cellular transport and morphological characteristics associated with various stages of renal transplantation,

namely, warm ischemia during nephrectomy, and rewarming in preservation solutions during anastomosis. The thesis is divided into two parts with the following specific objectives, respectively:

*A.* to study the effect of warm hypoxia and warm ischemia on tubular transport and morphology;

*B.* to study the temperature modulation of membrane conductive properties and characterize the effects of EC and UW solutions on renal tubules at warm temperatures.

# Chapter 2

## METHODOLOGY

### 2.1 Solutions

All perfusion and dissection solutions used in this study are listed in Tables 2.1 and 2.2. The preparation and usage of several experimental solutions are described in detail below.

#### 2.1.1 Hypoxic and ischemic solutions

Oxyrase<sup>TM</sup> (Oxyrase, Inc., Mansfield, OH, USA), a membrane-bound oxygenase [151] has been used in isolated tubule suspensions to achieve total anoxia [103]. In this study, Oxyrase<sup>TM</sup> was added to the hypoxic and ischemic solutions at concentrations of 0.15 to 0.30 U/mL of Ringer solution. Both solutions were kept in water-jacketed reservoirs (at 40°C) under one atmosphere of 95%N<sub>2</sub>-5%CO<sub>2</sub>. The solutions were delivered to either bath or tubular lumen through gas impermeable Saran tubing (Clarkson Controls & Equipment Co., Detroit, MI, USA). In addition, the surface of the bath solution was exposed to a stream of 95%N<sub>2</sub>-5%CO<sub>2</sub> from a gas line attached to the upper edge of the chamber. Samples of bath superfusate and effluent from the luminal exchange-pipette (0.6 to 1.0 mL) were collected and

Table 2.1: Concentrations of components in Ringer solutions<sup>a</sup>

Components (mM)	Ringer Solutions					
	standard	0-sub	20-K	PVP	hypoxic	ischemic
Na <sup>+</sup>	140.0	140.0	125.0	136.9	140.0	131.0
K <sup>+</sup>	5.0	5.0	20.0	5.0	5.0	20.0
Mg <sup>2+</sup>	1.2	1.2	1.2	1.2	1.2	1.2
Ca <sup>2+</sup>	2.0	2.0	2.0	2.0	2.0	2.0
Cl <sup>-</sup>	117.4	121.4	117.4	121.8	117.4	127.4
HPO <sub>4</sub> <sup>2-</sup>	1.3	1.3	1.3	1.3	1.3	1.3
HCO <sub>3</sub> <sup>-</sup>	25.0	25.0	25.0	10.0	25.0	5.0
Lactate <sup>-</sup>	4.0	0.0	4.0	4.0	4.0	20.0
HEPES	2.5	2.5	2.5	10.0	2.5	2.5
Glucose	5.5	0.0	5.5	5.5	5.5	0.0
Alanine	6.0	0.0	6.0	6.0	6.0	0.0
Mannitol	0.0	11.5	0.0	0.0	0.0	0.0
PVP (g/L)	0.0	0.0	0.0	15.0	0.0	0.0
Oxy. (U/ml)	0.0	0.0	0.0	0.0	.15-.3	.15-.3
95%O <sub>2</sub> -5%CO <sub>2</sub>	+	+	+	-	-	-
95%N <sub>2</sub> -5%CO <sub>2</sub>	-	-	-	-	+	+
pH (37°C)	7.4	7.4	7.4	7.4 <sup>b</sup>	7.4	7.0
P <sub>O<sub>2</sub></sub> (mmHg)	408-524	ND	ND	ND	0-6	0-8
Osm. (mOsm/L)	300	300	300	316	300	300

<sup>a</sup>HEPES, N-2-hydroxyethylpiperazine-N'-2-ethanesulfonic acid; PVP, polyvinylpyrrolidone; Oxy., Oxyrase<sup>TM</sup>; Osm., osmolarity; ND, not determined. Control Ringer contains 0.75 g/L dye [85% FD&C blue #1 (H. Kohhstamm & Co., New York, NY, USA) and 15% FD&C yellow #5 (Warner Jenkinson, St. Louis, MO, USA)] when used as luminal perfusate to better visualize luminal flow and detect damaged cells. 0-sub Ringer, 20-K Ringer and PVP Ringer denote organic substrate-free Ringer, high-[K<sup>+</sup>] (20 mM) Ringer, and dissection Ringer (containing PVP), respectively.

<sup>b</sup>The pH of PVP solution was measured at 4°C.

Table 2.2: Concentrations of components in preservation solutions<sup>a</sup>

Components (mM)	Preservation Solutions		
	EC	ECM	UW <sup>b</sup>
Na <sup>+</sup>	10.0	10.0	20.0
K <sup>+</sup>	115.0	115.0	140.0
Mg <sup>2+</sup>	0.0	0.0	5.0
Ca <sup>2+</sup>	0.5	0.5	0.5
Cl <sup>-</sup>	16.0	16.0	1.0
SO <sub>4</sub> <sup>2-</sup>	0.0	0.0	5.0
HPO <sub>4</sub> <sup>2-</sup>	42.5	42.5	0.0
H <sub>2</sub> PO <sub>4</sub> <sup>-</sup>	15.0	15.0	25.0
HCO <sub>3</sub> <sup>-</sup>	10.0	10.0	0.0
Glucose	180.0	5.5	0.0
Mannitol	0.0	174.5	0.0
HES (g/L)	0.0	0.0	50.0
Lactobionic acid	0.0	0.0	100.0
Raffinose	0.0	0.0	30.0
pH	7.2	7.2	7.4
Osm. (mOsm/L)	340	340	320

<sup>a</sup>ECM, EC-mannitol solution; HES, hydroxyethylstarch; Osm., osmolarity.

<sup>b</sup>Additional components of UW solutions are 5 mM adenosine, 1 mM allopurinol, 3 mM glutathione, 40 U/L insulin, and 16 mg/L dexamethasone.

injected into a Corning blood gas analyzer (Model 158, CIBA Corning Canada Inc.) to measure the  $P_{O_2}$ . The  $P_{O_2}$ 's of bath superfusate and lumen perfusate averaged  $3.9 \pm 1.3$  mmHg ( $n = 5$ ) and  $0.3 \pm 0.3$  mmHg ( $n = 4$ ), respectively. Except for the presence of Oxyrase<sup>TM</sup>, hypoxic Ringer had the same composition and pH (measured with pH-selective microelectrode in the bath<sup>1</sup>) as the standard Ringer. Since the electrolyte composition of the interstitial fluid has not been directly measured in an ischemic kidney, we adopted ischemic solutions used in cardiac ischemic models [111, 125, 209]. Aside from the low  $P_{O_2}$  maintained by the Oxyrase<sup>TM</sup>, the ischemic Ringer (Table 2.1) had higher concentrations of  $K^+$  and lactate<sup>-</sup>, and lower concentration of  $HCO_3^-$ , giving it a pH of 7.0 at 37°C when bubbled with 95%N<sub>2</sub>-5%CO<sub>2</sub>. Neither glucose nor alanine was present.

### 2.1.2 Preservation solutions

Euro-Collins' (EC) solution was prepared in our laboratory according to the manufacturer (Baxter Healthcare Corporation, Deerfield, IL, USA). Belzer UW-CSS (UW) solution was purchased from Du Pont Canada Inc. (Scarborough, Ont.), to which was added: 40 U/L of regular insulin (Novo Laboratories Ltd., Willowdale, Ont.) and 16 mg/L of dexamethasone (Organon Teknike Inc., Toronto, Ont.), as in clinical utilization of this solution. In addition,  $Ca^{2+}$  (0.5 mM  $CaCl_2$ ) was added to both the UW solution and the EC solution (including the ECM solution, see Table 2.2). Nominal  $Ca^{2+}$ -free solution has been documented to disrupt tight junction morphology [52]. It was also found in pilot studies that perfusion with nominal  $Ca^{2+}$ -free Ringer

---

<sup>1</sup>The manufacture and calibration of the pH-selective microelectrode are similar to those of  $Na^+$ -selective microelectrode, as described in detail in Section 2.3.2.

solution depolarized basolateral cell-membrane potential from  $-72 \pm 3$  to  $-20 \pm 7$  mV in  $12 \pm 4$  min ( $n = 6$ ,  $P < 0.001$ ).

## 2.2 Isolation and Perfusion of Tubules

Male Swiss white mice (16 to 25 g) were sacrificed by decapitation. Mid-cross-sections were cut from each kidney and immersed in ice-cold PVP solution (Table 2.1) less than 1.5 min after decapitation. Proximal straight tubules (0.2 to 1.5 mm) were isolated from the cortex by freehand dissection under a Wild Leitz dark-field dissection microscope (Model M5A, Wild Leitz Canada Ltd., Willowdale, Ont.). Tubules were then transferred to a temperature-controlled perfusion chamber and drawn into a holding pipette (Figure 2.1).

Solutions were delivered into the tubule lumen via an exchange pipette threaded down a perfusion pipette. The inner pipette at the collection end was omitted in most experiments, except for measuring transepithelial resistance, in which a tight electrical seal at the collection end is required (see Section 2.3.4). Tubules were also superfused with solutions flowing through the bath chamber at a rate of approximately 3 mL/min. Two circulators were used to control experimental temperatures. The perfusion chamber was connected, via two 3-way valves, to a 37°C-warm bath (Haake E3 circulator, Germany) and a cold bath (Lauda refrigerating circulator, Brinkmann Instrument, Rexdale, Ont.) set at either 22°C or 4°C. Temperature changes in the perfusion chamber were accomplished by switching from one water bath to the other. Half-times of cooling from 37°C to 22°C and from 37°C to 4°C were  $48 \pm 1$  sec ( $n = 6$ ) and  $50 \pm 1$  sec ( $n = 5$ ), respectively.

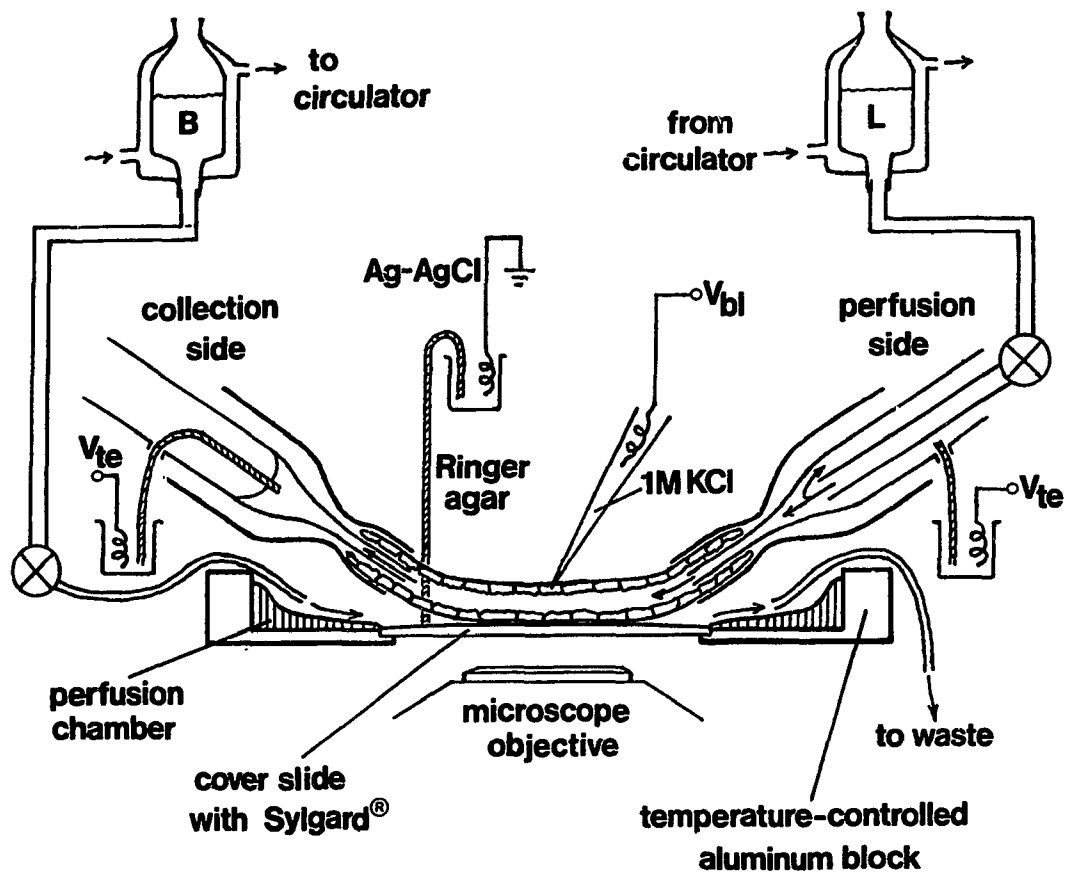


Figure 2.1: Schematic illustration of the tubular perfusion apparatus (not to scale). Arrows indicate the directions of solution or circulating water flow. *L* and *B* refer to the luminal perfusate and the bath superfusate, respectively (Modified from Figure 1 in reference [163]).

## 2.3 Electrophysiological Techniques

### 2.3.1 Potential difference measurements

Electrical connection to the lumen of the tubule was made with a Ag-AgCl half cell connected to either perfusion or collection pipette via a Ringer-agar bridge. Another Ag-AgCl half cell was connected to the bath via a second Ringer-agar bridge, serving as a common ground (refer to Figure 2.1). The interior of the cell was penetrated from the basolateral side with intracellular microelectrodes (Ling-Gerard fiber capillary). During the hypoxic/ischemic studies, the microelectrodes were backfilled with 3 M KCl, yielding electrode resistances ranging from 60 to 100 M $\Omega$ . Leakage of KCl into the interior of the cell (and subsequent cell swelling) was observed when tubules were exposed to lower temperatures (22°C and 4°C). The KCl concentration was therefore reduced to 1 M, increasing electrode resistance to 150 to 250 M $\Omega$ . Such a modification eliminated the problem of cell swelling. In addition,  $V_{bl}$  measured with the 1 M KCl-electrodes agreed completely with that measured with the 3 M KCl-electrodes.

Transepithelial potential difference ( $V_{te}$ ) and transmembrane potential difference ( $V_{bl}$ ) were recorded with the medium-impedance channel (10<sup>11</sup>  $\Omega$ ) of a WPI electrometer (Model Duo 777, World Precision Instruments, New Haven, CT, USA), and with the high-impedance channel (10<sup>15</sup>  $\Omega$ ) of another WPI electrometer (Model FD 223), respectively.

### 2.3.2 Intracellular Na<sup>+</sup>-activity measurement

Intracellular Na<sup>+</sup> activity ( $a_i^{\text{Na}}$ ) was determined by a Na<sup>+</sup>-microelectrode, manufactured as previously described [192]. Briefly, aluminosilicate capillary tubing (1.2mm OD/0.86mm ID, Federick Haer & Co., Brunswick, ME, USA) was pulled using a Flaming/Brown micropipette puller (Model 87, Sutter Instrument Company, Novato, CA, USA). The electrodes were then silanized in an 110°C oven twice for 90 sec each time, using tributylchlorosilan (Fluka Chemical Corp, St. Louis, MO, USA). After silanization, a small volume (100 to 200 nL) of Na<sup>+</sup>-selective resin (Natrium-ligand; Fluka, Ronkonkama, NY, USA) was introduced close to the tip of the electrode using a fine glass capillary (~ 100 μm in diameter) inserted into the back end. The electrode was then kept in a dark desiccator overnight to allow the Na<sup>+</sup>-resin to migrate to the tip. Finally, 100 mM NaCl solution was used as backfill. Care was taken to prevent the formation of air bubbles at the resin-NaCl solution interface. The electrode resistance was approximately 100 GΩ, and the reaction time was less than 5 sec.

The Na<sup>+</sup>-electrodes were calibrated using 100 mM NaCl, 10 mM NaCl, and 100 mM KCl solutions. Potential readings of Na<sup>+</sup>-electrodes in the above three solutions (recorded using the high-impedance channel of the FD223 electrometer, with a calomel as reference) were denoted as  $V^{100\text{Na}}$ ,  $V^{10\text{Na}}$  and  $V^{100\text{K}}$ , respectively. The slope and selectivity (of Na<sup>+</sup> over K<sup>+</sup>) were calculated according to

$$\text{Slope} = (V^{100\text{Na}} - V^{10\text{Na}})/0.94 \quad (2.1)$$

$$\text{Selectivity} = 10^{-(V^{100\text{Na}} - V^{100\text{K}})/\text{Slope}} \quad (2.2)$$

The number 0.94 in equation 2.1 is the logarithm (base 10) of the ratio of  $\text{Na}^+$  activity coefficients in 100 mM NaCl ( $\gamma^{100\text{Na}}$ ) and in 10 mM NaCl ( $\gamma^{10\text{Na}}$ ):  $\log_{10}(\gamma^{100\text{Na}}/\gamma^{10\text{Na}}) = 0.94$ . Average slope and selectivity of  $\text{Na}^+$ -electrodes used in this study were  $56.3 \pm 0.8$  mV/decade change in  $a_i^{\text{Na}}$  and  $(34 \pm 4):1$ , respectively ( $n = 9$  for both groups).

The potential difference of a  $\text{Na}^+$ -electrode inside a tubular cell ( $V_{\text{Na}}$ ) was recorded with the high impedance channel ( $10^{15} \Omega$ ) of the Duo 777 electrometer (WPI).  $a_i^{\text{Na}}$  was determined from the difference between  $V_{\text{Na}}$  and  $V_{\text{bl}}$ ; the latter was simultaneously recorded with a conventional microelectrode in an adjacent cell. Measurements of  $a_i^{\text{Na}}$  were corrected for  $\text{K}^+$  interference using the selectivity data and by assuming  $[\text{Na}^+]_i + [\text{K}^+]_i = 120$  mM.

### 2.3.3 Measurements of $\text{K}^+$ transference numbers of basolateral and apical cell membranes

Following a bath or a luminal application of 20- $\text{K}^+$  Ringer (Table 2.1), the  $t_{\text{K}(\text{bl})}$  and  $t_{\text{K}(\text{ap})}$  were calculated according to

$$t_{\text{K}(\text{bl})} = \Delta V_{\text{bl}} F Z_{\text{K}} / (RT \ln 4) \quad (2.3)$$

$$t_{\text{K}(\text{ap})} = \Delta V_{\text{ap}} F Z_{\text{K}} / (RT \ln 4) \quad (2.4)$$

where  $\Delta V_{\text{bl}}$  and  $\Delta V_{\text{ap}}$  are the magnitudes of the basolateral and apical membrane depolarization following the application of 20- $\text{K}^+$  Ringer, respectively.  $Z_{\text{K}}$  is the valence of  $\text{K}^+$  ( $Z_{\text{K}} = 1$ ) and  $F$ ,  $R$ ,  $T$  bear their usual meanings. The number 4 relates to the fourfold increase in  $[\text{K}^+]$  from 5 mM in control Ringer to 20 mM in 20- $\text{K}^+$  Ringer (20mM/5mM).

### 2.3.4 Tubular resistance measurements

#### Transepithelial resistance

Transepithelial resistance ( $R_{te}$ ) was measured using terminated luminal cable analysis as previously described [144, 163]. Briefly, DC-current pulses of 100 nA in amplitude and 2.5 sec in duration were injected into the tubular lumen through the perfusion pipette at frequencies of 0.02 to 0.04 Hz using a Grass S44 stimulator (Grass Instrument Co., Quincy, MA, USA). Voltage deflections at both perfusion ( $\Delta V_p$ ) and collection ( $\Delta V_c$ ) ends of the tubule were recorded.  $R_{te}$  was calculated according to

$$\lambda_l = X / \cosh^{-1}(\Delta V_p / \Delta V_c) \quad (2.5)$$

$$R_{te} = 2\sqrt{\pi \lambda_l^3 R_{input} \rho \tanh(X/\lambda_l)} \quad (2.6)$$

where  $\lambda_l$  is the length constant of the luminal cable,  $X$  is the tubule length,  $\rho$  is the specific resistivity of the Ringer solution, and  $R_{input}$  is the input resistance. Specific resistivity  $\rho$  was measured using YSI conductance meter (Model 32, Yellow Springs Instrument Co., Yellow Springs, OH, USA). Figure 2.2 shows the effect of temperature on  $\rho$ .  $R_{input}$  was calculated as  $\Delta V_p / 100$  nA.

#### Voltage divider ratio

The voltage divider ratio ( $\alpha$ ), defined as the ratio of deflections of apical ( $\Delta V_{ap}$ ) and basolateral ( $\Delta V_{bl}$ ) membrane potentials in response to a luminal current injection, was calculated according to [144, 163]

$$\alpha \equiv \Delta V_{ap} / \Delta V_{bl} = \frac{\Delta V_p}{\Delta V_{bl}} \{ \cosh[(X - x)/\lambda_l] / \cosh(X/\lambda_l) \} - 1 \quad (2.7)$$

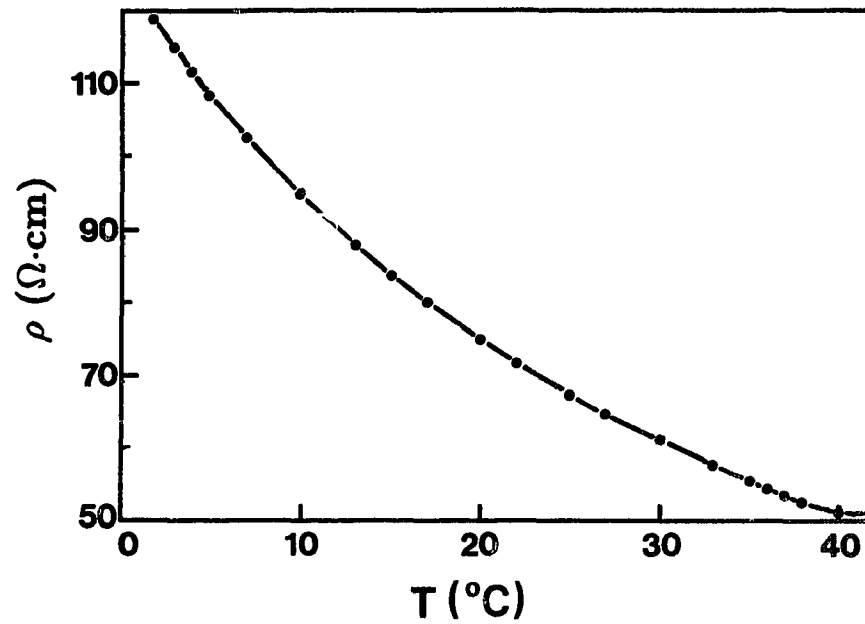


Figure 2.2: Effect of temperature on the resistivity of Ringer solution. Data shown here were from one of the two experiments, which yield identical results. Change in ionic composition in ischemic Ringer does not affect the resistivity of the solution.  $\rho$ , resistivity;  $T$ , temperature.

where  $\Delta V_{bl}$  was recorded using an intracellular voltage-electrode. The  $x$  denotes the distance between the electrode and the perfusion end. Other parameters were explained in Equations 2.5 and 2.6. The calculated  $\alpha$  was used as an estimate of the ratio of apical and basolateral membrane resistances ( $R_{ap}/R_{bl}$ ) (refer to Appendix A for details).

### Parallel resistance of $R_{ap}$ and $R_{bl}$

Parallel resistance of apical and basolateral membranes ( $R_z$ ) was measured with a modified cellular cable analysis for mammalian proximal tubules. Details of the method and the theory can be found in Appendix A.

Resistances of individual barriers [namely,  $R_{ap}$ ,  $R_{bl}$ , and shunt resistance ( $R_s$ )] were derived mathematically from  $R_{te}$ ,  $\alpha$ , and  $R_z$ :

$$R_{ap} = (\alpha + 1)R_z \quad (2.8)$$

$$R_{bl} = \frac{\alpha + 1}{\alpha} R_z \quad (2.9)$$

$$R_s = \frac{(\alpha + 1)^2 R_{te} R_z}{(\alpha + 1)^2 R_z - \alpha R_{te}} \quad (2.10)$$

## 2.4 Morphological Methods

### 2.4.1 Light microscopy

Photomicrographs of isolated perfused proximal tubules were taken at 200 $\times$  power under a Nikon inverted microscope (Model TMS-F, Nippon Kogaku K.K., Japan). Tubular cells, including their brush borders (BB) were clearly visible in the photograph (see Figure 4.4). Outer diameter (OD) and inner diameter (ID, exclusive of

the brush border) of proximal tubules were measured under the same magnification using a graticule inside the eyepiece. By modeling the tubule as a concentric cylinder [123, 124], the relative cell volume ( $R_v$ ) was determined according to

$$R_v = (OD_e^2 - ID_e^2)/(OD_c^2 - ID_c^2) \quad (2.11)$$

where subscripts  $e$  and  $c$  denote experimental and control data, respectively.

## 2.4.2 Electron microscopy

Proximal straight tubules were perfusion-fixed. Fixation was started by perfusing both the tubular lumen and the bath with paraformaldehyde-glutaraldehyde fixative (2% paraformaldehyde, 2.5% glutaraldehyde in 80 mM cacodylate buffer, 2 mM  $\text{CaCl}_2$ , pH 7.4). According to the study of Tripathi and colleagues using isolated perfused *Ambystoma* proximal tubules [191], either luminal or bath fixation alone was adequate to preserve the tubular ultrastructure. However, in a pilot study, addition of fixative to the bath alone produced a dramatic widening of the intercellular space, whereas luminal perfusion with the fixative alone resulted in empty spaces along the basal membrane (see Figure 4.6). It was found that in mouse proximal tubules, the ultrastructure is best preserved by introducing the fixative first to the lumen, immediately followed by rapid replacement of the bath solution with the same fixative. This fixation protocol has been used previously by Nielsen and colleagues in isolated perfused rabbit proximal tubules [149].

After 5 min of fixation in the perfusion chamber, the tubule was detached from the perfusion pipette and transferred to a micro test slide (single-well) filled with the same fixative for 10 min. The tubule was then washed with 80 mM cacodylate buffer

for 5 min, further fixed in 1% aqueous  $\text{OsO}_4$  solution for 15 min, and washed with distilled water for 5 min. The tubule was subsequently dehydrated by sequentially replacing distilled water with 50%, 70%, 90%, 95%, and 100% ethyl alcohol. Taab-Araldite resin (25 mL Taab 812, 15 mL Araldite, 55 mL DDSA, 2 mL DMP-30, Marivac Ltd, Halifax, NS) was added to the tubule overnight to allow complete infiltration. After the infiltration, the tubule was transferred to a droplet of fresh resin for 1 hour. Finally, the tubule was embedded in the same resin at  $65^\circ\text{C}$  for 24 hours. Ultrathin sections ( $\sim 60\text{--}80$  nm in thickness) were cut using a Reichert OMU3 ultramicrotome (C. Reichert AG, Austria). The sections were then collected on slotted copper grids ( $2 \times 1$  mm, coated with formvar) and viewed under a Zeiss transmission electron microscope (Model EM10B, Zeiss, Germany).

## 2.5 Measurement of Tubular ATP Content

The ATP content of isolated perfused tubules was measured using a luminometric method [211]. The protocol of tubule-ATP extraction was based on that developed by Beck and coworkers [18], with some modifications. Briefly, after tubule perfusion, the proximal straight tubule of 0.6 to 1.5 ( $1.04 \pm 0.04$ ,  $n = 26$ ) mm in length was released from the holding pipette and retrieved from the bottom of the perfusion chamber using a transfer pipette. The droplet ( $30 \mu\text{L}$ ) containing the tubule was deposited on a petri dish. Using a pair of fine forceps, the tubule was quickly transferred into a droplet of  $50 \mu\text{L}$  ice-cold perchloric acid (2%) for 4 min, during which time the image of the individual tubule was drawn using a camera lucida. The drawings of each tubule were later magnified and measured using a rotimeter.

After a 4-min extraction, the 50  $\mu\text{L}$  of perchloric acid was subsequently neutralized with 15.4  $\mu\text{L}$  of 1 M KOH. Finally, the mixture was diluted to 360  $\mu\text{L}$  using 25 mM tris(hydroxymethyl)aminomethane/acetate (Tris/acetate) buffer (pH 7.8) and stored at  $-80^{\circ}\text{C}$  for up to one week.

The ATP content of the tubule extract was measured using an ATP bioluminescent assay kit (Sigma Chemical Company, St. Louis, MO, USA). The assay was performed in 25  $\times$  60 mm glass vials at room temperature. First, 100  $\mu\text{L}$  of firefly luciferase-luciferin solution (ATP assay mix supplied in the assay kit) and 200  $\mu\text{L}$  of dilution buffer (supplied in the assay kit) were added to the reaction vials. The assay reaction was initiated by rapidly adding 200  $\mu\text{L}$  of tubule extract. The fluorescent intensity of the reaction solution was measured 20 to 30 sec after the initiation of the reaction in a custom-built luminometer (Institute of Marine Biosciences, National Research Council of Canada). The calibration curve was generated from  $\text{Na}_2\text{ATP}$  solutions of  $10^{-9}$ ,  $3 \times 10^{-9}$ ,  $10^{-8}$ ,  $3 \times 10^{-8}$  and  $10^{-7}$  M. To ensure that the assay conditions for the ATP standards were the same as those for the tubule samples, the reaction mixture for ATP standards contained 100  $\mu\text{L}$  of ATP assay mix, 200  $\mu\text{L}$  of tubule-free extraction mixture (2% perchloric acid, 1 M KOH and 25 mM Tris/acetate buffer mixed in the same proportions as used for tubule-ATP extraction), and 200  $\mu\text{L}$  of  $\text{Na}_2\text{ATP}$  in dilution buffer. Blanks were run with the assay, consisting of 100  $\mu\text{L}$  of ATP assay mix, 200  $\mu\text{L}$  of tubule-free extraction mixture, and 200  $\mu\text{L}$  of dilution buffer.

## 2.6 Experimental Protocols

### 2.6.1 Hypoxic and ischemic perfusion

Tubules were mounted on the perfusion apparatus 10 to 20 min after the animals were sacrificed. Transepithelial potential difference ( $V_{te}$ ) was recorded immediately after the onset of tubular perfusion with the control Ringer solution. Another 5- to 10-min period was required for stable cell impalement with conventional voltage microelectrode. In the case of cell impalement with  $\text{Na}^+$ -selective microelectrode, up to 30 min were required. Once all electrical potentials were stable for at least 2 min, a luminal 0-sub (organic substrate-free solution, see Table 2.1) pulse was applied to evaluate the quality of cell impalement<sup>2</sup>. The electrical potentials recorded immediately following the 0-sub pulse were regarded as controls. Tubules were then perfused bilaterally (lumen and bath) with the hypoxic or the ischemic solution for 20 min. After the 20-min hypoxic or ischemic perfusion, tubules were reperfused with the control Ringer. Two to three minutes were required for all electrical parameters to reach new steady levels (reperfusion period). At this time, a second luminal 0-sub pulse was applied to once again evaluate the quality of cell impalement.

$V_{bl}$ ,  $V_{te}$  and  $a_i^{\text{Na}}$  were continuously monitored during the entire course of the experimental protocol. However,  $t_{K(bl)}$ <sup>3</sup> and tubular resistance<sup>4</sup> ( $R_{te}$ ,  $R_{ap}$  and  $R_{bl}$ ) data were recorded only for the control period (control data) and post-hypoxic or

---

<sup>2</sup>Depolarization of cell membrane potential after luminal organic substrate deletion is an electrical response characteristic of the proximal tubule. See Section 1.3.2 for details.

<sup>3</sup>Measurement of  $t_{K(bl)}$  requires introduction of 20-K<sup>+</sup> Ringer to the bath (see Section 2.3.3). Such a solution change will inevitably introduce some oxygen into the bath during the hypoxia.

<sup>4</sup>Tubular cells can be damaged after a few intracellular current injections, rendering continuous monitoring impossible. To re-establish double impalement in a pair of new cells can require as long as 20 min.

post-ischemic reperfusion period (reperfusion data).

Cellular ATP content was measured in isolated perfused proximal tubules subjected to the following three conditions: 1) perfusion with oxygenated Ringer for 30 min (Control), 2) perfusion with oxygenated Ringer for 10 min, followed by perfusion with hypoxic Ringer for 20 min (Hypoxia), and 3) perfusion with oxygenated Ringer for 10 min, followed by perfusion with ischemic Ringer for 20 min (Ischemia). Comparison of ATP content between "Control" group and "Hypoxia" or "Ischemia" group may be complicated by the variability of tubule ATP content between animals or between tubules from different regions of the same kidney. To minimize these complications, pairs of proximal tubules that were next to each other were dissected and perfused simultaneously on two similar perfusion apparatus, with one tubule being treated as "Control" and the other as either "Hypoxia" or "Ischemia".

### **2.6.2 Temperature studies**

Electrophysiological and morphological parameters of proximal straight tubules were measured in control Ringer solution at 37°C, 22°C, and 4°C. In all experiments, except for tubular resistance measurements, tubules were initially perfused at 37°C during which time control electrophysiological data were collected. Characteristic electrical response to 0-sub was always tested at the beginning of each perfusion to ensure the presence of a functional proximal tubular segment. The system was then cooled down to either 22°C or 4°C. Changes in corresponding parameters were continuously monitored.

In tubular resistance measurements, one tubule was exposed to only one tem-

perature in each experiment. Data collected from three groups of tubules (for 37°C, 22°C and 4°C) were compared.

### **2.6.3 Preservative solution studies**

All tubules were initially perfused at 37°C with control Ringer solution during which time  $V_{te}$  was measured (control data). Tubules were then either kept at 37°C or cooled down to either 22°C or 4°C in Ringer-substrate solution. Once the new temperature had stabilized, control tubular diameters (OD and ID) were measured. Preservation solutions were then introduced to both lumen and bath sides (unless otherwise stated) for 10 min at 37°C, or 30 min at 22°C. Changes in tubular diameters during the perfusion of preservation solutions were monitored. At the end of experimental period, control Ringer solution was reintroduced for 6 to 15 min to completely remove residual preservation solutions and to allow recovery of cell volume. Finally, the tubule was rewarmed to 37°C, and a second  $V_{te}$  was recorded once the temperature and all electrical parameters had stabilized (reperfusion data).

## **2.7 Statistical Analysis**

All results are presented as mean values  $\pm$  S.E., followed by number of measurements ( $n$ ). Statistical comparisons were made with the paired Student's  $t$  test unless otherwise stated.  $P < 0.05$  was considered statistically significant.

## Chapter 3

# RESULTS I: Hypoxia and Ischemia

### 3.1 Electrophysiological Effects of Hypoxia

#### 3.1.1 Basolateral membrane and transepithelial potentials

When mouse proximal tubules were perfused (lumen and bath) with control Ringer solution at 37°C, the average  $V_{te}$  and  $V_{bl}$  were  $-1.62 \pm 0.06$  mV ( $n = 59$ ) and  $-69 \pm 1$  mV ( $n = 91$ ), respectively. These values are in agreement with published data [200]. Luminal removal of substrates (0-sub) hyperpolarized  $V_{bl}$  by  $6.2 \pm 0.2$  mV ( $n = 89$ ,  $P < 0.001$ ), and depolarized  $V_{te}$  to values approaching 0 mV. This characteristic electrical response to 0-sub was seen in all tubules that were successfully perfused, confirming that proximal tubules were obtained.

When control Ringer (lumen and bath solutions) was replaced with the hypoxic Ringer (see Table 2.1), there was an immediate 1- to 2-mV depolarization of  $V_{bl}$  (Figure 3.1a). This depolarization of  $V_{bl}$  was accounted for by non-specific effects of Oxyrase™ on the glass microelectrodes, because such a response to solution change from control to hypoxic Ringer was observed when the voltage-electrode was placed in the bath. For the majority of tubules studied (11 out of 15),  $V_{bl}$ , once corrected

for the effect of Oxyrase<sup>TM</sup> was not affected by the hypoxic solution perfusion over the 20-min period (Figure 3.1a). In four tubules,  $V_{bl}$  did depolarize after  $14 \pm 1$  min of hypoxic solution perfusion at a rate of  $1.5 \pm 0.2$  mV/min (Figure 3.1a, *insert*). This depolarization of  $V_{bl}$  was reversed at 20 min by reperfusion with control Ringer in both the lumen and the bath. In all fifteen tubules studied,  $V_{bl}$  returned to control level during the reperfusion period ( $-72 \pm 1$  mV control and reperfusion,  $n = 15$ ). These results are summarized in Figure 3.2a.

With the onset of hypoxic Ringer perfusion, there was a depolarization of  $V_{te}$  by  $0.23 \pm 0.04$  mV ( $n = 27$ , Figure 3.1b). This depolarization can not be explained by the interference of Oxyrase<sup>TM</sup>, because Oxyrase<sup>TM</sup> did not affect baseline  $V_{te}$  in the absence of tubules. The magnitude of the tubule  $V_{te}$  depolarization after the onset of hypoxia increased with time, reaching  $0.90 \pm 0.08$  mV ( $n = 24$ ) at the end of 20-min hypoxia period (Figure 3.1b). Reperfusion with control Ringer only partially restored the  $V_{te}$  (Figure 3.1b), so that the  $V_{te}$  recorded during reperfusion ( $-1.1 \pm 0.1$  mV,  $n = 30$ ) was significantly lower ( $P < 0.001$ ) than the  $V_{te}$  recorded in the control period ( $-1.7 \pm 0.1$  mV,  $n = 30$ , Figure 3.2b). To eliminate the possibility that  $V_{te}$  might have deteriorated with time, a time control experiment was conducted in which tubules were perfused continuously with control Ringer for 20 min or longer. The results indicated that the  $V_{te}$  was stable for at least 20 min under these control conditions ( $\Delta V_{te} = -0.01 \pm 0.03$  mV between 0-min group and 20-min group,  $n = 12$ , Figure 3.2c).

These data indicated that the majority of tubular cells were capable of maintaining the transmembrane electrical gradient at a  $P_{O_2}$  level of 4 mmHg. However,

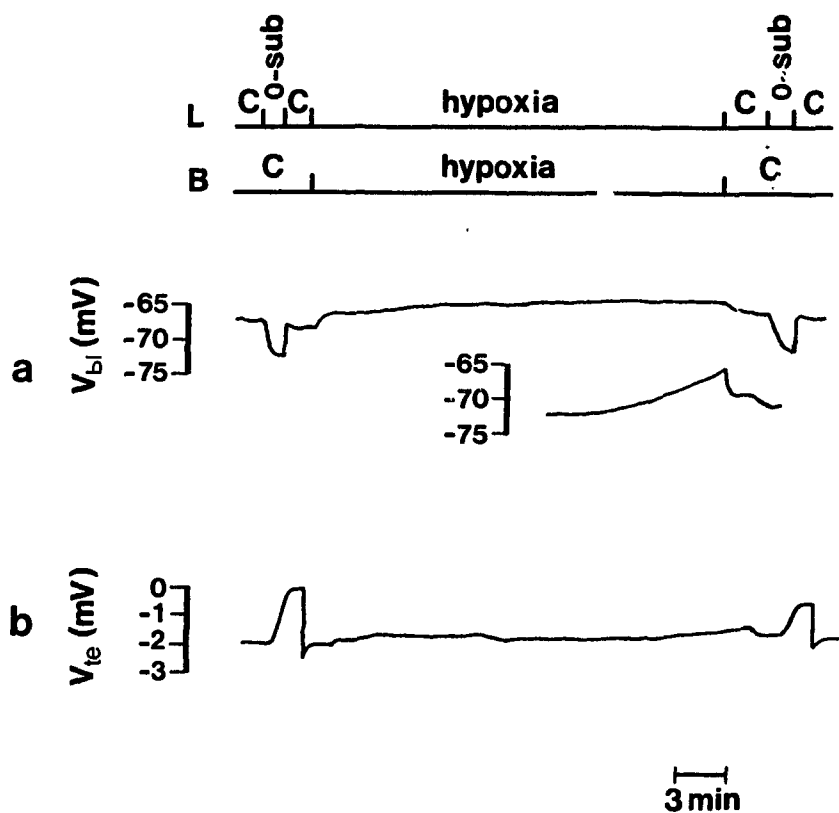


Figure 3.1: Representative tracings of basolateral membrane potential ( $V_{bl}$ ) and transepithelial potential ( $V_{te}$ ) in response to luminal substrate removal (0-Sub) and to 20-min bilateral hypoxic perfusion (hypoxia) at 37°C. *Insert* illustrates a representative tracing from a few tubules which depolarized at the end of the hypoxic perfusion period. Compositions of luminal perfusate (L) and bath superfusate (B) are given at the top of the tracings. C represents perfusion with control Ringer.

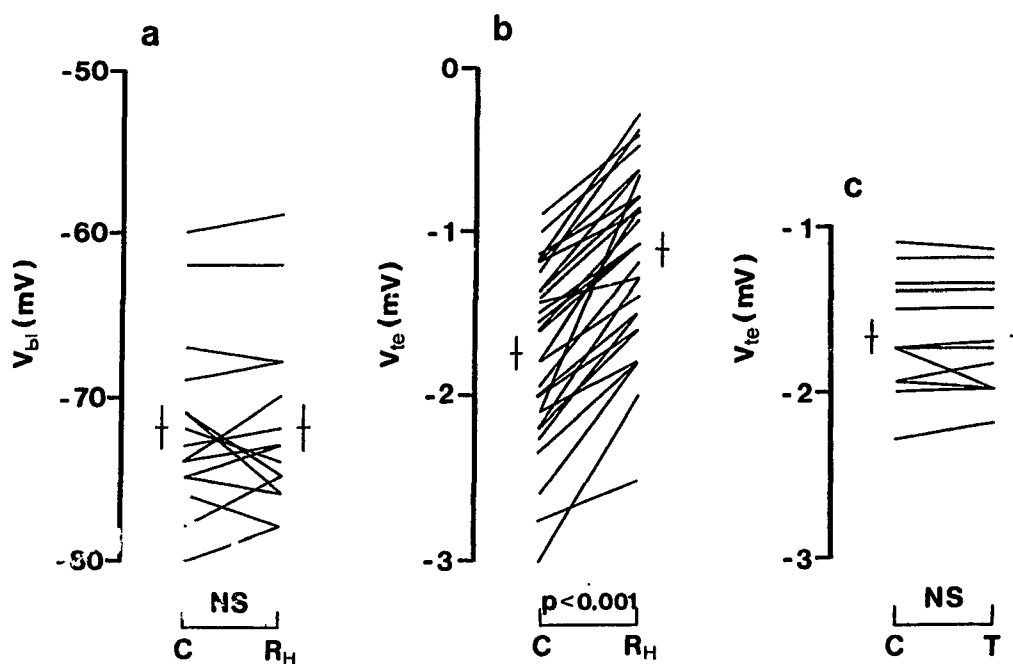


Figure 3.2: Effects of 20-min hypoxic perfusion at 37°C on  $V_{bl}$  (a) and  $V_{te}$  (b), and time control of  $V_{te}$  (c). Each line connects a pair of datum points from one tubule measured under different experimental conditions. Horizontal bars represent the means, and vertical bars represent the S.E. Comparisons were made using paired  $t$  test. Abbreviations: C, control perfusion;  $R_H$ , control reperfusion following hypoxia; T, 20-min or longer time-control perfusion; NS, not significant. See Section 2.6.1 for details.

the observed change in  $V_{te}$  would suggest a compromised transepithelial electrogenic  $\text{Na}^+$  transport shortly after the exposure to the hypoxic environment.

### 3.1.2 Basolateral $\text{K}^+$ transference number and intracellular $\text{Na}^+$ activity

Basolateral membrane potential is mainly determined by the transmembrane  $\text{K}^+$  gradient and the  $\text{K}^+$  permeability across the membrane (see Section 1.3). To further support the finding that  $V_{bl}$  was well maintained in 70% of tubule cells during 20-min hypoxia and in all tubule cells during reperfusion (see Section 3.1.1), we set out to show that hypoxia did not affect the  $\text{K}^+$  gradient nor  $\text{K}^+$  permeability ( $t_{K(bl)}$ ) across the basolateral membrane.

Intracellular  $\text{Na}^+$  activity ( $a_i^{\text{Na}}$ ) rather than intracellular  $\text{K}^+$  activity ( $a_i^{\text{K}}$ ) was measured in these experiments. According to previous studies, a decrease in  $a_i^{\text{K}}$  was always accompanied by an increase in  $a_i^{\text{Na}}$  when  $\text{Na}^+, \text{K}^+$ -ATPase was inhibited during warm ischemia [132] or cooling [127]. The monitoring of  $a_i^{\text{Na}}$  was continuous throughout the experiment. The measurements of  $t_{K(bl)}$  were performed twice for each experiment, first before hypoxia and then after hypoxia (see Section 2.6.1).

Figure 3.3 illustrates a representative tracing of  $a_i^{\text{Na}}$  and  $t_{K(bl)}$  measurements. Once the  $\text{Na}^+$ - and voltage-electrodes were inside two adjacent cells (refer to Section 2.3.2 for technical details), a luminal 0-sub (see Table 2.1) pulse was used to evaluate the quality of the cell impalements. It is well documented that removal of substrates from the luminal perfusate inactivates apical  $\text{Na}^+$ -substrate cotransporters and reduces  $a_i^{\text{Na}}$  [143]. All  $\text{Na}^+$ - and voltage-electrodes used in the experiments responded to luminal organic substrate deletion (0-sub), with a decrease in  $a_i^{\text{Na}}$  from  $14.2 \pm$

1.1 mM in control to  $8.7 \pm 1.0$  mM in 0-sub ( $n = 6$ ,  $P < 0.001$ ). Following the luminal 0-sub pulse, hypoxic Ringer was introduced to both the luminal and the bath sides for 20 min. In all six experiments, 20-min hypoxia had no effect on  $a_i^{\text{Na}}$ , and  $a_i^{\text{Na}}$  remained unchanged during the reperfusion period ( $14.2 \pm 1.1$  mM control versus  $14.3 \pm 1.3$  mM reperfusion,  $n = 6$ ,  $P > 0.5$ ). In addition,  $t_{\text{K(bi)}}$  was measured by applying two 20-K<sup>+</sup> pulses, one before and the other after hypoxia (Figure 3.3). This parameter was found to remain unaltered after 20 min of hypoxia ( $0.69 \pm 0.02$  before and after hypoxia,  $n = 9$ ,  $P > 0.5$ ).

These data would suggest that ionic gradients and permeabilities across the basolateral membrane remained intact after 20-min exposure to  $P_{\text{O}_2}$  of 4 mmHg.

### 3.1.3 Transepithelial resistance

Transepithelial resistance ( $R_{te}$ ) was measured to assess the electrical tightness of the epithelium. Twenty minutes of hypoxia decreased  $R_{te}$  from  $14.3 \pm 1.2 \Omega \cdot \text{cm}^2$  in control to  $9.2 \pm 1.1 \Omega \cdot \text{cm}^2$  during reperfusion ( $n = 7$ ,  $P < 0.005$ , Figure 3.4a). A time control experiment showed no significant change in  $R_{te}$  after a 20-min control perfusion ( $13.4 \pm 1.2 \Omega \cdot \text{cm}^2$  versus  $13.2 \pm 1.3 \Omega \cdot \text{cm}^2$ ,  $n = 7$ ,  $P > 0.2$ , Figure 3.4b). Therefore, the decrease in  $R_{te}$  during hypoxia could not be attributed to a natural deterioration of the preparation with time. The data indicate that the proximal tubule may become more leaky after the hypoxic insult.

In summary, hypoxia led to a minimal disturbance of  $V_{bi}$ ,  $a_i^{\text{Na}}$ , and  $t_{\text{K(bi)}}$ . However, there was a significant decrease in both  $V_{te}$  and  $R_{te}$ . In fact, a good correlation between the percentage reduction in  $V_{te}$  and  $R_{te}$  following the hypoxic perfusion was

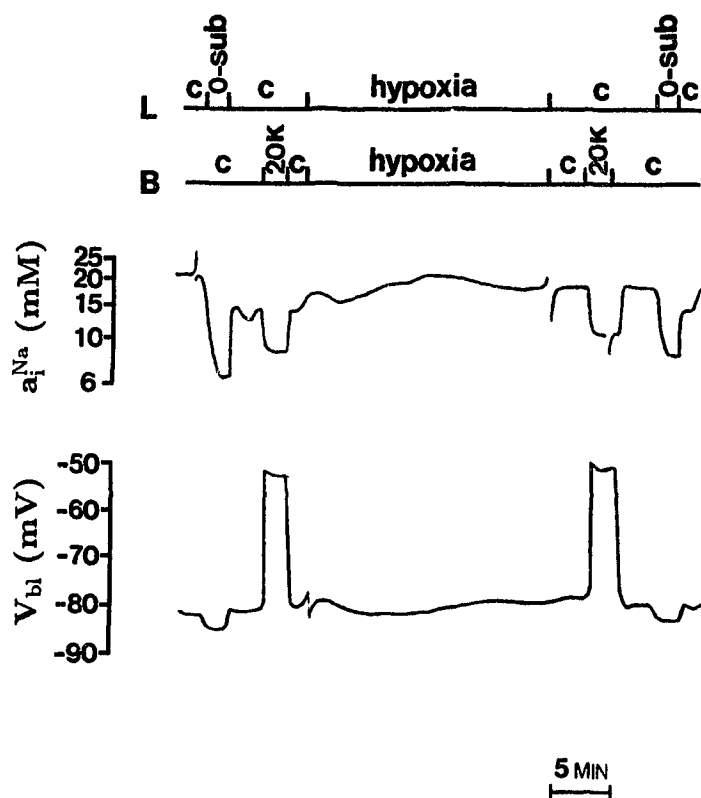


Figure 3.3: Effects of 20-min hypoxic perfusion at 37°C on  $K^+$  transference number  $[t_{K(b1)}]$  and intracellular  $Na^+$  activity ( $a_i^{Na}$ ): representative tracings from one of the six measurements. Compositions of luminal perfusate (L) and bath superfusate (B) are given at the top of the tracings (C, control perfusion). The  $t_{K(b1)}$  was estimated from the depolarization of  $V_{b1}$  (lower tracing) following bath perfusion of 20-K Ringer (20K). The  $a_i^{Na}$  (upper tracing) was measured using an intracellular  $Na^+$ -selective microelectrode. See Sections 2.3.2 and 2.3.3 for details.

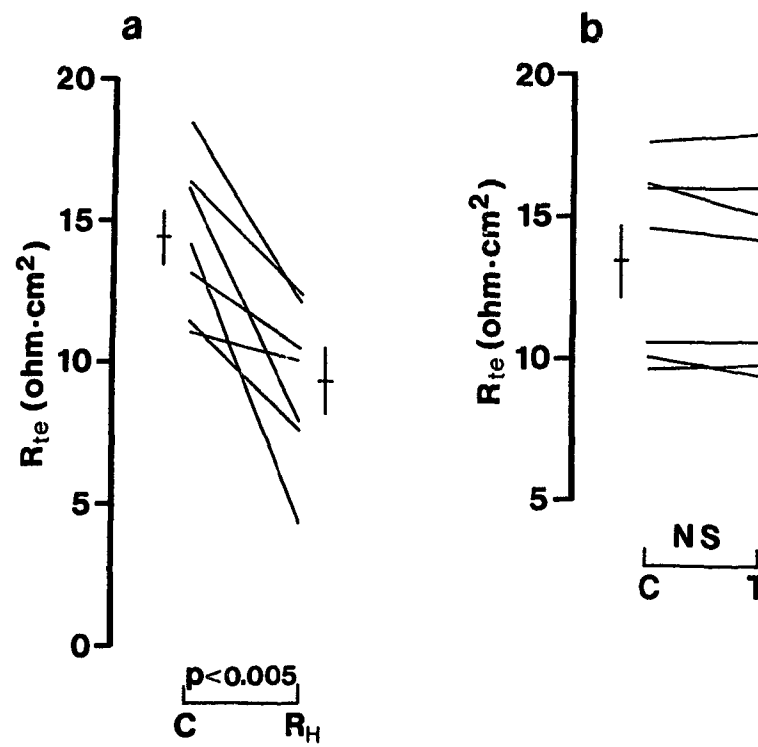


Figure 3.4: Effect of 20-min hypoxic perfusion (a) and time-control perfusion (b) on the transepithelial resistance ( $R_{te}$ ). Refer to legend to Figure 3.2 for abbreviations.

observed (see Figure 3.9). Implications of this correlation will be discussed in Section 5.2.3.

## 3.2 Electrophysiological Effects of Ischemia

### 3.2.1 Basolateral membrane and transepithelial potentials

An artificial ischemic solution was prepared to simulate hypoxia, acidosis,  $K^+$  and lactate accumulation, and substrate deprivation (refer to the last column in Table 2.1). The effects of ischemic perfusion on  $V_{bl}$  and  $V_{te}$  were monitored.

As shown in Figure 3.5, ischemic perfusion resulted in a depolarization of  $V_{bl}$  by  $27.6 \pm 0.9$  mV ( $n = 20$ ,  $P < 0.001$ ) and a depolarization of  $V_{te}$  to zero. The depolarization of  $V_{bl}$  was most likely related to the high  $K^+$  and low pH of the ischemic Ringer and not an indication of cell damage [30, 143, 169]. Indeed,  $V_{bl}$  repolarized back to the preischemic levels during reperfusion with control Ringer solution ( $-70 \pm 1$  mV during control and reperfusion periods,  $n = 20$ ,  $P > 0.5$ , Figure 3.6b). In contrast to  $V_{bl}$ , the depolarization of  $V_{te}$  was not completely reversed upon reperfusion with control Ringer solution ( $-1.4 \pm 0.1$  mV control versus  $-0.82 \pm 0.05$  mV reperfusion,  $n = 17$ ,  $P < 0.001$ , Figure 3.6a).

These data suggest that ischemia may be no more damaging than hypoxia to tubular cells. However, similar to the findings during hypoxia, the decrease in  $V_{te}$  would suggest that certain irreversible changes occurred to the transepithelial electrogenic  $Na^+$  transport.

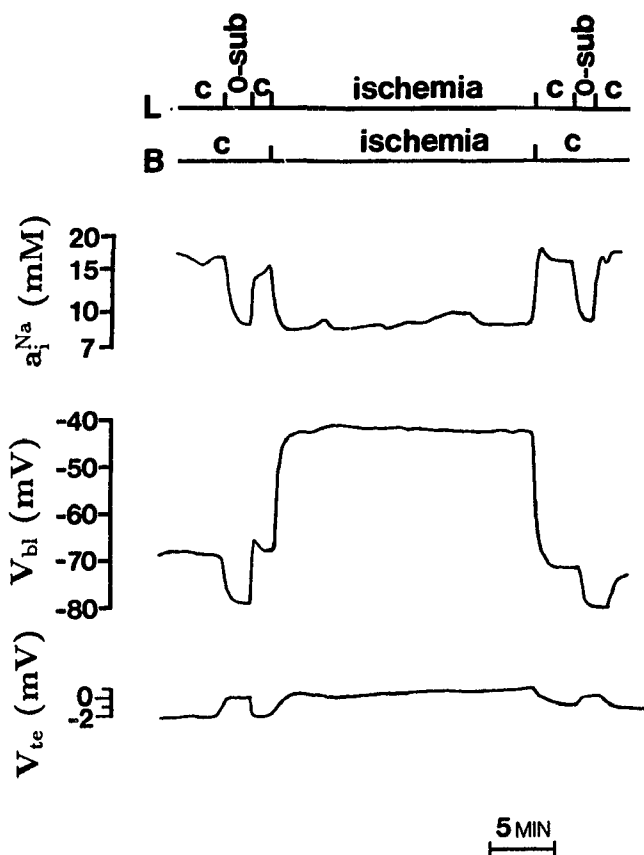


Figure 3.5: Representative tracings of  $a_i^{\text{Na}}$ ,  $V_{bl}$  and  $V_{te}$  in response to 0-sub (lumen) and ischemic Ringer (lumen and bath) perfusion at 37°C. Compositions of luminal perfusate (L) and bath superfusate (B) are given at the top of the tracings. C refers to perfusion with control Ringer. See legend to Figure 3.3 for details.

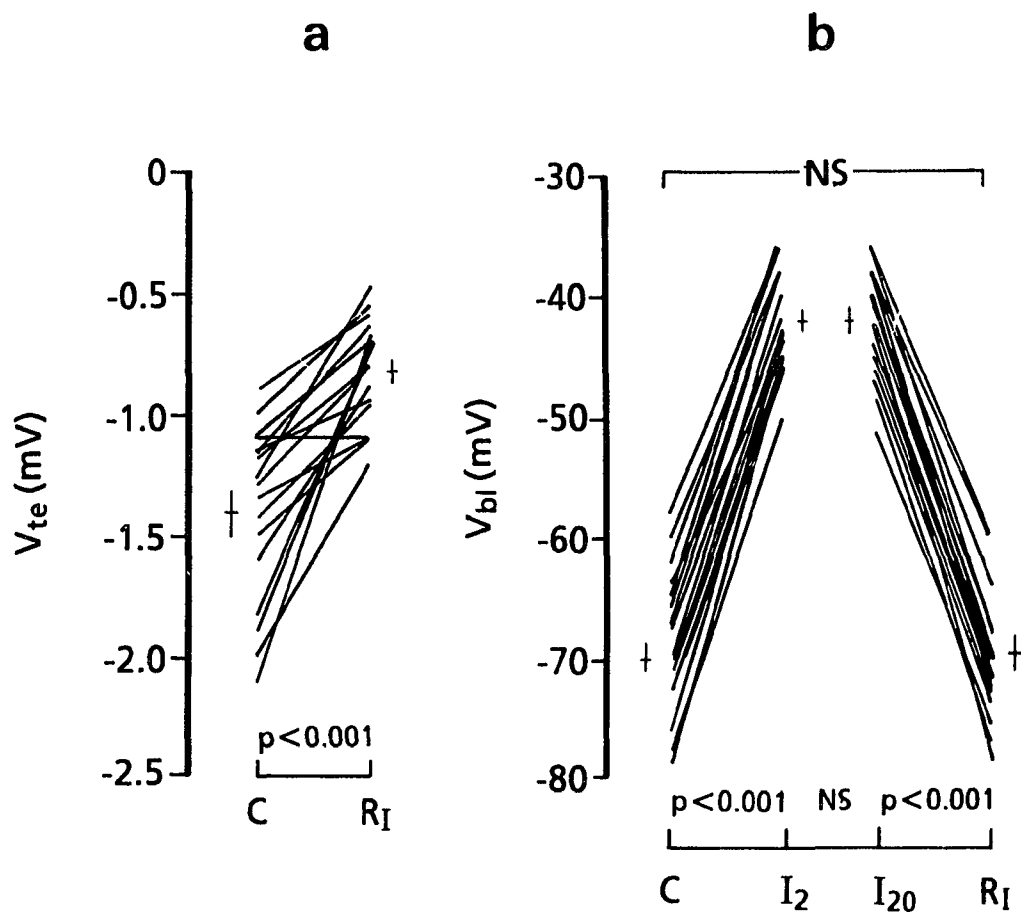


Figure 3.6: Effects of 20-min ischemic perfusion on  $V_{te}$  (a) and  $V_{bl}$  (b). Each line connects a paired datum points from one tubule measured under different experimental conditions. Horizontal bars represent means and vertical bars represent S.E. Abbreviations: C, control perfusion;  $I_2$ , 2 min of ischemic perfusion;  $I_{20}$ , 20 min of ischemic perfusion;  $R_I$ , control reperfusion following ischemia; NS, not significant. See Section 2.6.1 for details.

### 3.2.2 Basolateral $K^+$ transference number and intracellular $Na^+$ activity

The  $a_i^{Na}$  and  $t_{K(b)}$  were also measured in the ischemic-perfused tubule preparation. Bilateral perfusion of the ischemic Ringer led to a decrease in  $a_i^{Na}$  (Figure 3.5) from  $15.8 \pm 0.6$  mM to  $9.0 \pm 0.6$  mM ( $n = 3$ ,  $P < 0.002$ ). This decrease in  $a_i^{Na}$  was likely caused by the huge depolarization of cell membrane potential induced by the high- $K^+$  content (20 mM) of the ischemic Ringer. As pointed out by Morgunov and colleagues [143], membrane depolarization inhibits the substrate-coupled apical  $Na^+$  entry because of the reduction in transmembrane  $Na^+$  electrochemical gradient. During the reperfusion period following the 20-min ischemia,  $a_i^{Na}$  returned to preischemic level ( $15.8 \pm 0.6$  mM control versus  $15.9 \pm 0.8$  mM reperfusion,  $n = 3$ ,  $P > 0.4$ ). In addition, no significant difference was found between the  $t_{K(b)}$  recorded before and after (reperfusion) ischemia ( $0.73 \pm 0.01$  control versus  $0.75 \pm 0.01$  reperfusion,  $n = 6$ ,  $P > 0.1$ ). These results are in agreement with our previous findings that there was no significant alteration in  $V_{bl}$  following 20 min of ischemia (see Section 3.2.1), and confirm that the functional integrity of proximal tubule cells was well maintained after the 20-min ischemic insult.

### 3.2.3 Tubular resistances

Resistances of apical and basolateral membranes as well as the transepithelial resistance were measured before and after the ischemic perfusion. Electrical resistance of a barrier reflects the overall ionic permeability across that barrier. Knowledge of such electrical data is important for assessment of ionic transport across the barrier.

Figure 3.7 illustrates that 20 min of ischemia led to a decrease in  $R_{te}$  from  $12.6 \pm 1.2 \Omega \cdot \text{cm}^2$  in control to  $8.1 \pm 1.0 \Omega \cdot \text{cm}^2$  during reperfusion ( $n = 6$ ,  $P < 0.05$ ). Similar findings were reported following hypoxia (see Section 3.1.3). This decrease in  $R_{te}$  could not be attributed to the natural deterioration of the perfused tubule preparation, as indicated by the time control experiment summarized in Figure 3.4b.

In a tubular epithelium, the transepithelial resistance consists of two parallel components, the resistance across tubular cells (equal to the sum of apical and basolateral membrane resistances) and the shunt resistance (the tight junction). To clarify which component(s) of  $R_{te}$  were altered by ischemia, resistances of the apical ( $R_{ap}$ ) and basolateral ( $R_{bl}$ ) membranes as well as shunt resistance ( $R_s$ ) were determined before and after the ischemic perfusion, using electrical cable analysis (refer to Section 2.3.4 and Appendix A for details).

In this experiment, double impalements with two voltage-electrodes into two adjacent cells a certain distance ( $x$ ) apart were established, and the voltage deflection ( $\Delta V_{bl}$ ) was recorded by one electrode when a DC current was injected via the other electrode. The  $\Delta V_{bl} \sim x$  relationship was determined and used to calculate the parallel resistance of apical and basolateral membrane ( $R_x$ ), which was then combined with the result from luminal cable analysis to yield individual membrane resistances (see Equations 2.8 to 2.10). As shown in Figure 3.8, the  $\Delta V_{bl}$  attenuated exponentially with the increase in distance ( $x$ ). No difference in the  $\Delta V_{bl} \sim x$  relationship between control (filled circles) and reperfusion groups (empty circles) was observed (control:  $n = 63$ ; reperfusion:  $n = 21$ ,  $P > 0.4$  with pooled  $t$  test).

Table 3.1 summarizes the resistance data derived from both luminal and cellular

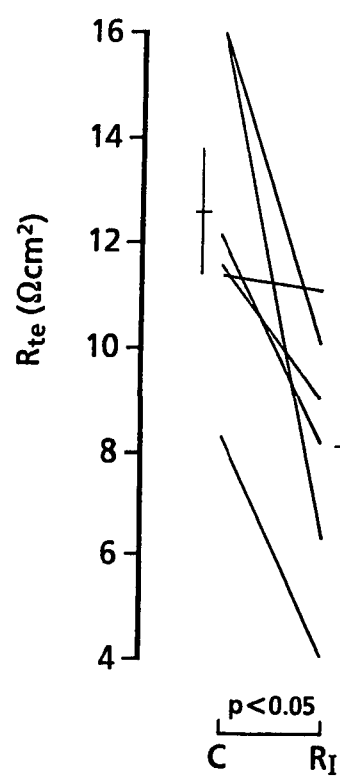


Figure 3.7: Effect of 20-min ischemic perfusion on  $R_{te}$ . Refer to legend in Figure 3.6 for abbreviations.

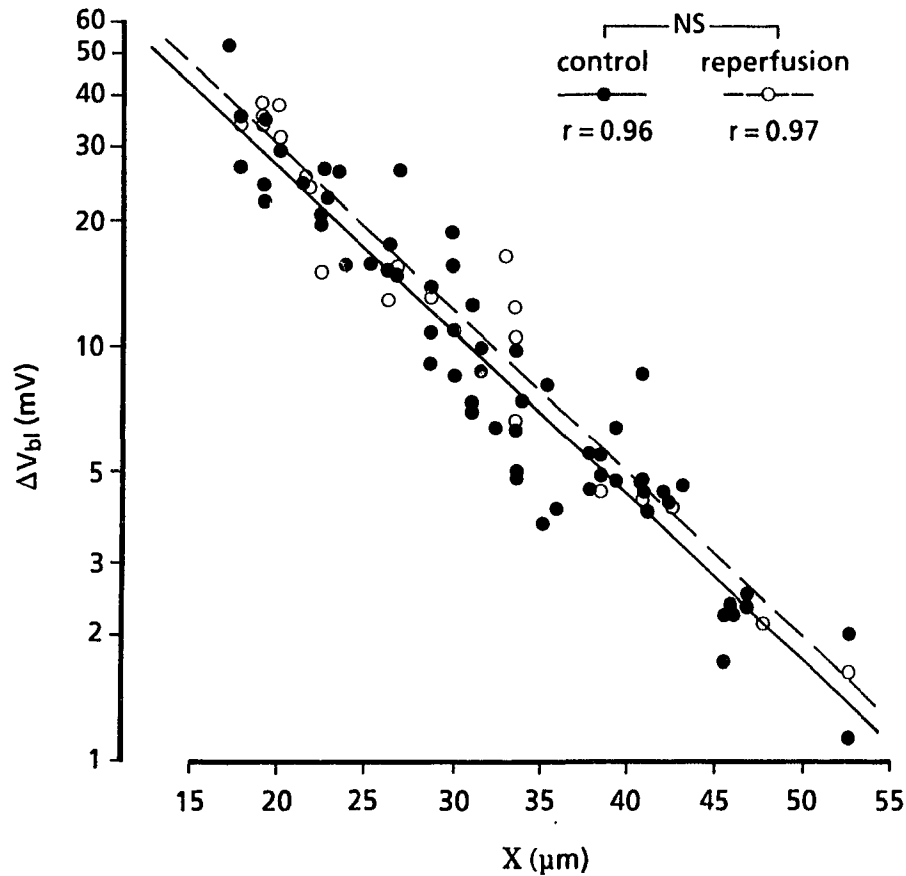


Figure 3.8: Attenuation of basolateral voltage deflection ( $\Delta V_{bl}$ ) along the tubules in cellular cable analysis. The  $\Delta V_{bl}$ -axis is drawn in the logarithmic scale. The  $x$  is the distance between current-injection and sensing microelectrodes. Straight lines were fitted to data by least square regression analysis;  $r$ , correlation coefficient. Control (solid line and filled circles) and reperfusion following 20-min ischemia (broken line and empty circles) were compared by pooled  $t$  test; NS, not significant. See Appendix A for details.

Table 3.1: Effects of ischemia on tubular resistances<sup>a</sup>

	$R_z$	$\alpha$	$R_{ap}$	$R_{bl}$	$R_s$
Control	$74 \pm 9$	$3.6 \pm 0.2$	$369 \pm 48$	$92 \pm 11$	$13 \pm 1$
<i>n</i>	63	6	63	63	6
Post-ischemia	$83 \pm 13^b$	$3.8 \pm 0.4^c$	$454 \pm 88^b$	$101 \pm 16^b$	$8 \pm 1^d$
<i>n</i>	21	6	21	21	6

<sup>a</sup>Abbreviations:  $R_z$ , parallel resistance of apical and basolateral membranes;  $\alpha$ , voltage divider ratio;  $R_{ap}$ , apical membrane resistance;  $R_{bl}$ , basolateral membrane resistance;  $R_s$ , shunt resistance. Values are means  $\pm$  S.E. in  $\Omega \cdot \text{cm}^2$ , but  $\alpha$  is dimensionless. *n*, number of measurement.

<sup>b</sup> $P > 0.3$  versus control, compared with pooled *t* test.

<sup>c</sup> $P > 0.6$  versus control, compared with paired *t* test.

<sup>d</sup> $P < 0.05$  versus control, compared with paired *t* test.

cable analyses. These results indicated that the change in  $R_{te}$  was solely due to the decrease in shunt resistance. The cell membrane resistances remained unchanged.

In summary, although perfusion with ischemic Ringer depolarized  $V_{bl}$  and decreased  $a_i^{\text{Na}}$ , the changes in electrophysiological parameters pertaining to cell integrity and function ( $V_{bl}$ ,  $a_i^{\text{Na}}$ ,  $t_{K(bl)}$ ,  $R_{ap}$  and  $R_{bl}$ ) were transient and returned to control values immediately after the ischemic insult. However, the decreases in  $V_{te}$  and  $R_{te}$  persisted into the reperfusion period. Changes in  $V_{te}$  and  $R_{te}$  appear to be tightly coupled, because an examination of the six tubules studied during ischemia (filled circles) and the seven tubules studied during hypoxia (empty circles) indicated that for each individual tubule, there was a good correlation between the percentage decrease in  $V_{te}$  and the percentage decrease in  $R_{te}$  (Figure 3.9). This high degree of

correlation would suggest that the decrease in  $V_{te}$  is in fact the result of a decrease in  $R_{te}$ .

### 3.3 Electrophysiological Effects of Ouabain

The  $\text{Na}^+, \text{K}^+$ -ATPase was blocked by bath perfusion of control Ringer containing  $10^{-4}$  M ouabain. Changes in electrophysiological parameters associated with the inhibition of  $\text{Na}^+, \text{K}^+$ -ATPase were recorded. As shown in Figure 3.10,  $10^{-4}$  M ouabain depolarized  $V_{bl}$  by  $16.3 \pm 1.1$  mV ( $n = 6, P < 0.001$ ) and depolarized  $V_{te}$  from  $-1.7 \pm 0.2$  mV to  $-0.1 \pm 0.1$  mV ( $n = 7, P < 0.001$ ). Intracellular  $\text{Na}^+$  activity ( $a_i^{\text{Na}}$ ) increased from  $16.7 \pm 2.3$  mM to  $55.7 \pm 3.3$  mM ( $n = 3, P < 0.01$ ). Changes in  $V_{bl}$ ,  $V_{te}$  and  $a_i^{\text{Na}}$  occurred immediately following the application of ouabain to the bath, and reached their maximal values in 5 to 6 min. These results are in agreement with previous reports of the effects of ouabain on membrane potential [200] and intracellular  $\text{Na}^+$  activity [157] in the mouse and the rat kidney tubules, respectively.

### 3.4 Hypoxia/Ischemia and Proximal Tubular Ultrastructure

Effects of hypoxia and ischemia on the ultrastructure of perfusion-fixed proximal straight tubules were studied. The morphological structure of proximal straight tubules perfused with control Ringer solution was well preserved (Figure 3.11a). The brush border and the basal membrane remained intact, endocytic vacuoles were small and located close to the apical membrane surface. Although some mitochondria

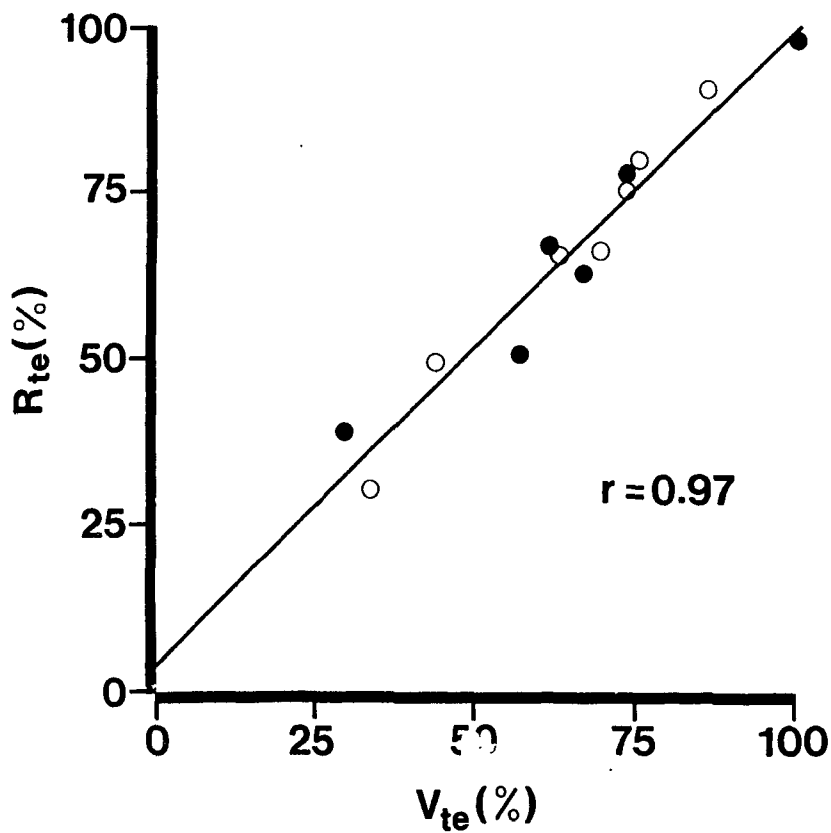


Figure 3.9: Correlation between the effects of 20-minute hypoxic (empty circles) and ischemic (filled circles) perfusion on  $V_{te}$  and  $R_{te}$ .  $V_{te}$  (%) and  $R_{te}$  (%) refer to the ratios of  $V_{te}$  and  $R_{te}$  during reperfusion to the initial control values of these parameters. Each point represents a simultaneous measurement of both  $V_{te}$  and  $R_{te}$  in a single tubule;  $r$ , correlation coefficient.

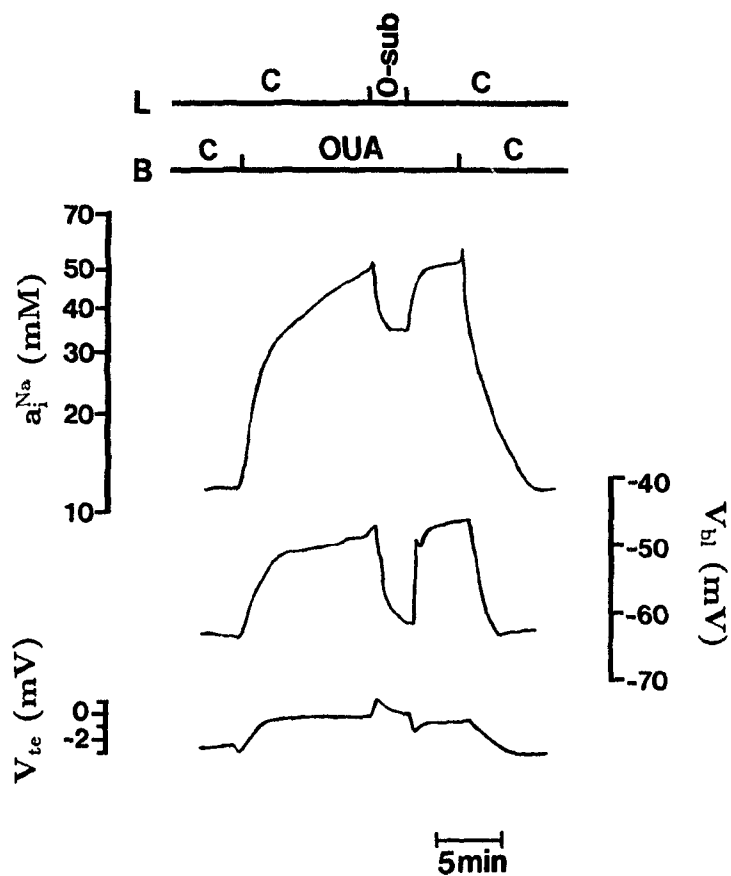


Figure 3.10: Representative tracings of  $a_i^{\text{Na}}$ ,  $V_{\text{bl}}$  and  $V_{\text{te}}$  in response to bath perfusion of  $10^{-4}\text{M}$  ouabain (OUA) at  $37^\circ\text{C}$ . Compositions of luminal perfusate (L) and bath superfusate (B) are given at the top of the tracings. C, control perfusion. See legend to Figure 3.3 for details.

appeared elongated, the majority of these structures were rounded in appearance, and randomly distributed in the cytoplasm. After 60 min of perfusion with control Ringer at 37°C, there were more numerous lysosome-like structures associated with the Golgi apparatus (Figure 3.11b). However, other cellular ultrastructures appeared to be intact. The ultrastructure of mouse proximal straight tubule described above is similar to those described in rabbit proximal straight tubules [149], fixed by either *in vivo* or *in vitro* perfusion.

Figure 3.12 compares the ultrastructures of proximal tubules perfused with control Ringer (a) with those perfused with either hypoxic (b,d) or ischemic (c) solutions. Twenty minutes of hypoxia or ischemia followed by 5 min of reperfusion had little effect on the overall cellular structure of the proximal tubule. The brush borders were mainly intact and approximately the same height after the hypoxic or ischemic insults. The nuclei had similar appearance, and the mitochondria were similar in density and shape in all tubules. However, there appeared to be an increase in the number and size of autophagosomes and myeloid bodies in both hypoxic and ischemic tubules (Figure 3.12d).

### **3.5 Hypoxia/Ischemia and Intracellular ATP Content**

Reduction in intracellular ATP content is a hallmark of ischemia. It was therefore of interest to investigate the effects of hypoxia and ischemia on tubule ATP content in the present model system. In freshly isolated proximal straight tubules, intracellular ATP content was  $6.64 \pm 0.58$  pmoles/mmTL ( $n = 14$ ), approximately 7 mM as

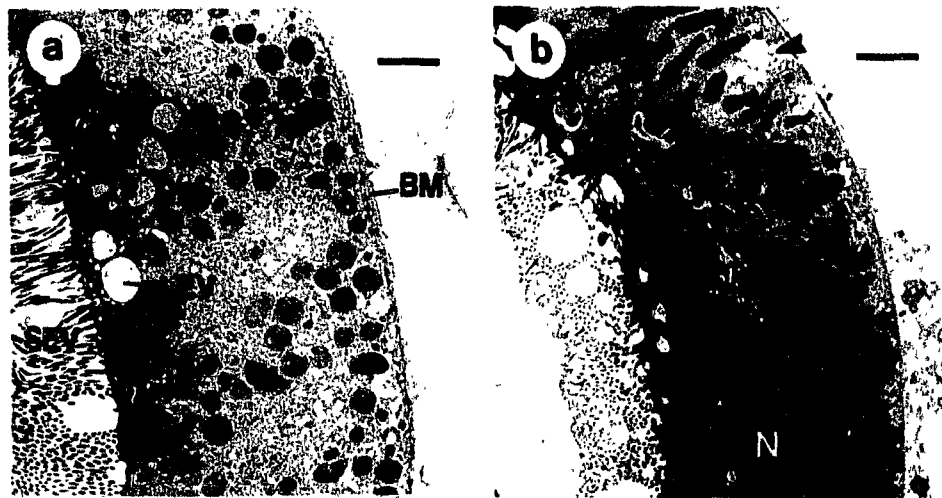
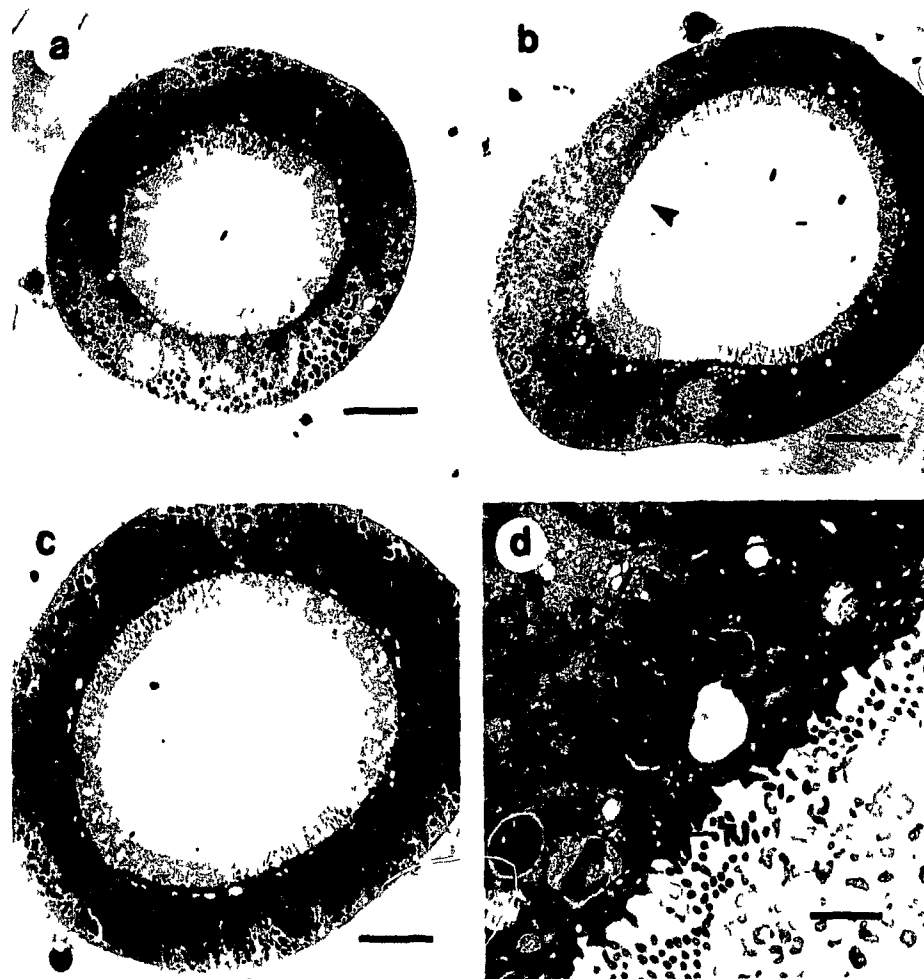


Figure 3.11: (a) Ultrastructural appearance of proximal straight tubule cells under control conditions. The tubule was isolated and perfused bilaterally with control Ringer for 15 min at 37°C before it was fixed by bilateral perfusion of the paraformaldehyde-glutaraldehyde solution (Section 2.4.2). (b) The ultrastructure of a proximal tubule fixed after 60 min of perfusion with control Ringer at 37°C. Arrowhead in (b) indicates the basal empty space resulted from the fixation (see Section 2.4.2 for details). Abbreviations: M, mitochondrion; D, dense body (lysosome); G, Golgi apparatus; LEV, large endocytic vacuole; SEV, small endocytic vacuole; N, nucleus; BM, basement membrane. Bars represent 2  $\mu$ m.



**Figure 3.12:** Proximal tubules were fixed after 15 min of perfusion with control Ringer at 37°C (a), after 20 min of hypoxic perfusion followed by 5 min of control reperfusion at 37°C (b), or after 20 min of ischemic perfusion followed by 5 min of control reperfusion at 37°C. Arrowhead in (b) indicates focal damage to the microvilli, an enlarged view of which is shown in (d). Abbreviations: AU, autophagosome; MB, myeloid body; MV, multivesicular endosome; G, Golgi apparatus; TJ, tight junction. Bars represent 10  $\mu\text{m}$  in (a) to (c), and 1  $\mu\text{m}$  in (d).

calculated according to the outer and inner diameters of the tubule. This value is comparable to that reported by Uchida in S<sub>3</sub> segments of microdissected mouse proximal tubules [196]. Thirty-minute perfusion with control Ringer significantly increased the intracellular ATP content to  $8.34 \pm 0.68$  pmoles/mmTL ( $n = 14$ ,  $P < 0.005$  compared with freshly dissected group). Figure 3.13 compares the cellular ATP levels between control perfused tubules and those subjected to 20 min of either hypoxic or ischemic perfusion at 37°C. At the end of the 20-min hypoxia, tubule ATP content was 47% of control perfused tubules ( $8.69 \pm 0.90$  versus  $4.06 \pm 0.33$  pmoles/mmTL,  $n = 8$ ,  $P < 0.001$ ). On the other hand, the decrease in tubule ATP content following the 20-min ischemia was not statistically significant ( $7.07 \pm 0.91$  versus  $5.59 \pm 0.48$  pmoles/mmTL,  $n = 5$ ,  $P > 0.1$ ). These data would suggest that the energy metabolism of proximal tubule cells was compromised due to the low  $P_{O_2}$  in the hypoxic Ringer. However, some components in the ischemic Ringer solution appeared to prevent tubular ATP depletion in the face of a low  $P_{O_2}$  environment. The effects of these components in the ischemic solution will be discussed in Section 6.1.2.

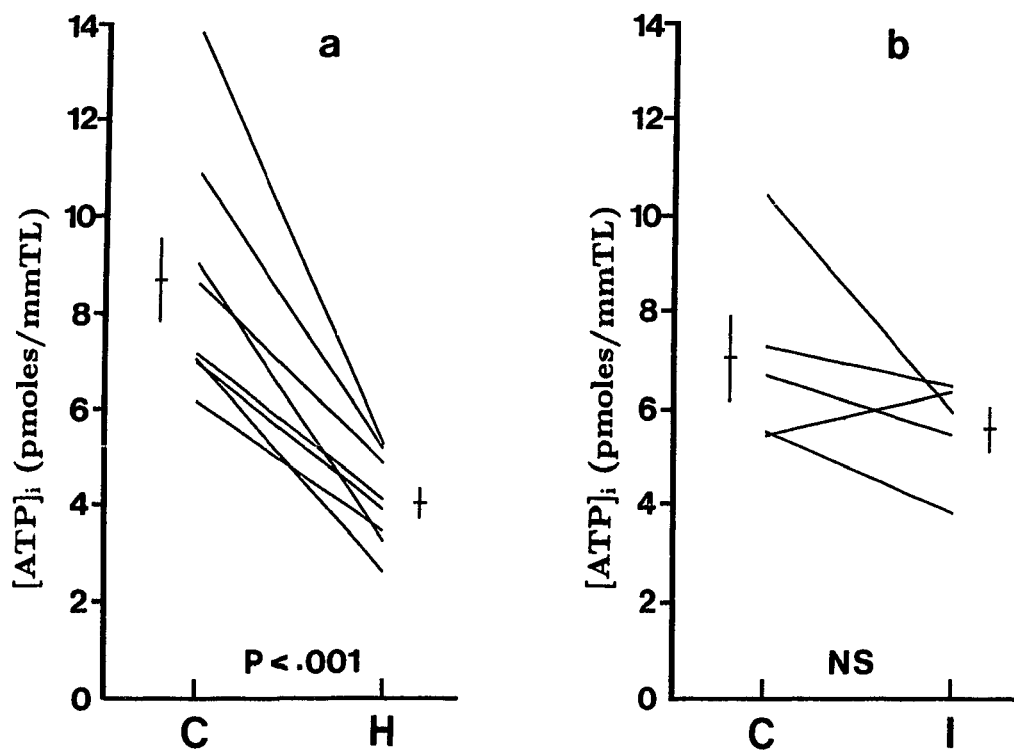


Figure 3.13: Effects of 20-min hypoxic (a) and ischemic (b) perfusion at 37°C on tubular ATP content. Each pair of data were obtained from a pair of tubules isolated from the same kidney, one perfused with control Ringer (C) and the other perfused with either hypoxic (H) or ischemic Ringer (I). See Section 2.6.1 for details.

## Chapter 4

# RESULTS II: Temperature and Preservation Solutions

### 4.1 Effects of Cooling

In this section, the effects of cooling from 37°C to either 4°C or 22°C on electrophysiological parameters and cell volume were studied. Previous studies have documented that exposure of proximal tubule cells to reduced temperatures leads to inhibition of the Na<sup>+</sup>,K<sup>+</sup>-ATPase and disturbance of cellular ionic balance, similar to the effect of ouabain [127].

Figure 4.1 illustrates the effects of cooling from 37°C to 4°C on  $V_{te}$ ,  $V_{bl}$ , and  $t_{K(bl)}$  in mouse proximal straight tubules, perfused bilaterally with control Ringer solution. Cooling to 4°C rapidly depolarized  $V_{te}$  from  $-1.72 \pm 0.26$  mV to  $+0.03 \pm 0.12$  mV ( $n = 5$ ,  $P < 0.001$ ). Despite the rapid change in solution temperature (half time of cooling from 37°C to 4°C was within one minute, see Section 2.2), the depolarization of  $V_{bl}$  was gradual, reaching  $-16.9 \pm 2.0$  mV after 60 min from control values of  $-73.9 \pm 1.6$  mV ( $n = 5$ ,  $P < 0.001$ ). Associated with this depolarization of  $V_{bl}$  was a 55% decrease in  $t_{K(bl)}$  from  $0.72 \pm 0.02$  to  $0.32 \pm 0.05$  after 60 min

( $n = 5$ ,  $P < 0.001$ ). The recovery of all parameters was completed within 30 min of rewarming to 37°C. These results extend the observation previously reported by Völkl and colleagues that cooling led to a depolarization of  $V_{bl}$  and a decrease in  $t_{K(bl)}$  [200].

In Figure 4.2, cooling to 22°C rapidly depolarized  $V_{te}$  from  $-2.30 \pm 0.27$  to  $-0.62 \pm 0.14$  mV ( $n = 5$ ,  $P < 0.005$ ). Changes in  $V_{bl}$  and  $t_{K(bl)}$  were not as dramatic as those recorded at 4°C. Thirty minutes of perfusion with Ringer solution at 22°C depolarized  $V_{bl}$  by  $7.2 \pm 1.3$  mV ( $n = 5$ ,  $P < 0.005$ ) and reduced  $t_{K(bl)}$  from  $0.67 \pm 0.03$  to  $0.54 \pm 0.04$  ( $n = 5$ ,  $P < 0.01$ ). The recovery of all parameters was completed within 30 min of rewarming to 37°C.

Cooling to 22°C for 30 min did not significantly affect the intracellular  $\text{Na}^+$  content ( $a_i^{\text{Na}}$ ), whereas cooling to 4°C significantly increased  $a_i^{\text{Na}}$  from  $13.2 \pm 2.0$  to  $42.6 \pm 2.7$  mM ( $n = 6$ ,  $P < 0.001$ ) over a 40-min period (Figure 4.3).

Table 4.1 compares apical membrane resistance ( $R_{ap}$ ), basolateral membrane resistance ( $R_{bl}$ ), and shunt resistance ( $R_s$ ) at 37°C, 22°C and 4°C. Resistances of all tubule-barriers increased dramatically at 22°C. Cooling to 4°C further increased  $R_{bl}$  and  $R_s$ . However, no further significant increase in  $R_{ap}$  was observed.

Cooling from 37°C to 4°C led to a sustained decrease in cell volume of approximately 20% of the 37°C-control value, as measured with morphometric method described in Section 2.4.1. This decrease in cell volume persisted for the duration (60 min) of perfusion at 4°C ( $n = 4$ ,  $P < 0.005$ , Figures 4.4c and 4.5). These results obtained from light microscopy were confirmed using electron microscopy (Figure 4.6). As shown in Figure 4.6, although a decrease in cell volume at 4°C

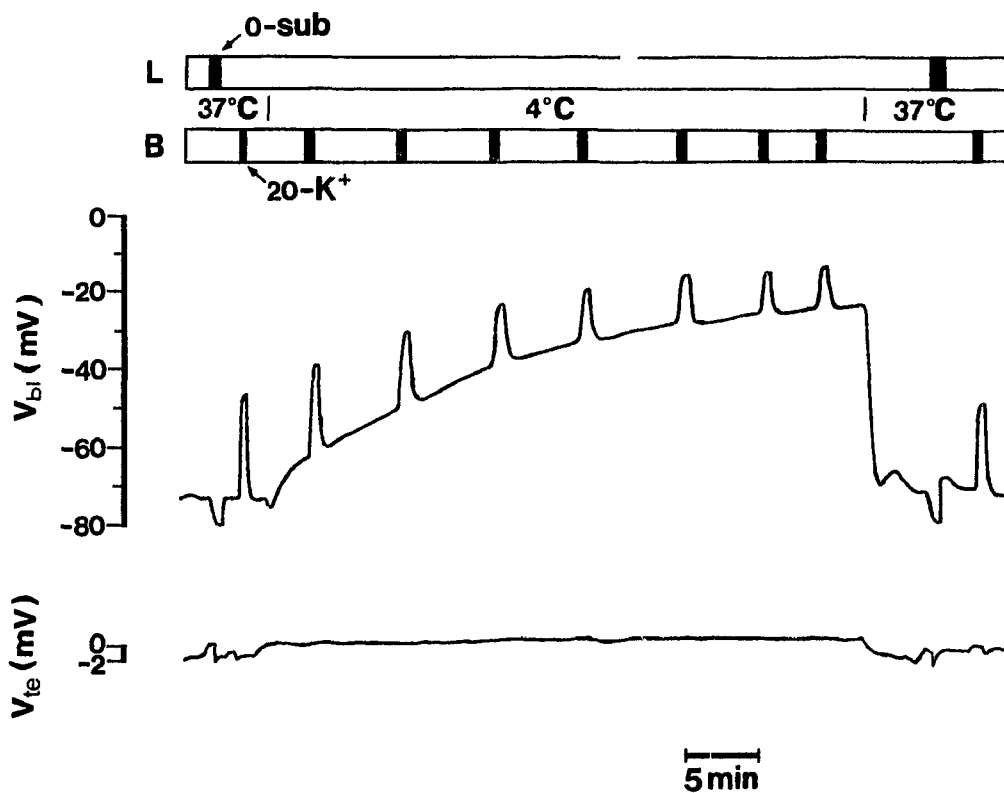


Figure 4.1: Representative tracings of basolateral cell membrane potential ( $V_{bl}$ ) and transepithelial potential ( $V_{te}$ ) in response to cooling to 4°C. Tubular lumen (L, upper bar) was continuously perfused with control Ringer solution, except for two substrate-free Ringer (0-sub) pulses (solid areas) at the beginning and the end of the experimental protocol. Bath perfusate (B, lower bar) was periodically switched between control and 20-K<sup>+</sup> (solid areas) solutions to evaluate the change in basolateral K<sup>+</sup> transference number [ $t_{K(bl)}$ ] with the cooling. Temperature changes were indicated between two bars. See Section 2.6.2 for details.

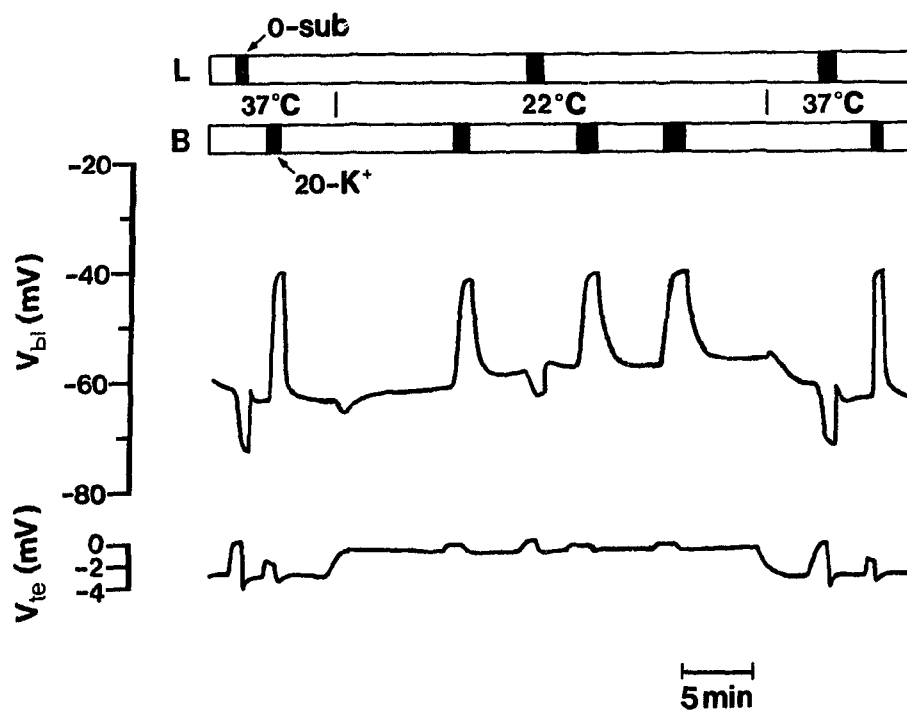


Figure 4.2: Representative tracings of  $V_{bl}$  and  $V_{te}$  in response to cooling to 22°C. Tubular lumen (L, upper bar) was continuously perfused with control solution, with interruption by three 0-sub pulses (solid areas). Bath perfusate (B, lower bar) was periodically switched between control and 20-K<sup>+</sup> (solid areas) solutions to evaluate the change in  $t_{K(bl)}$  with the cooling. Temperature changes were indicated between two bars.

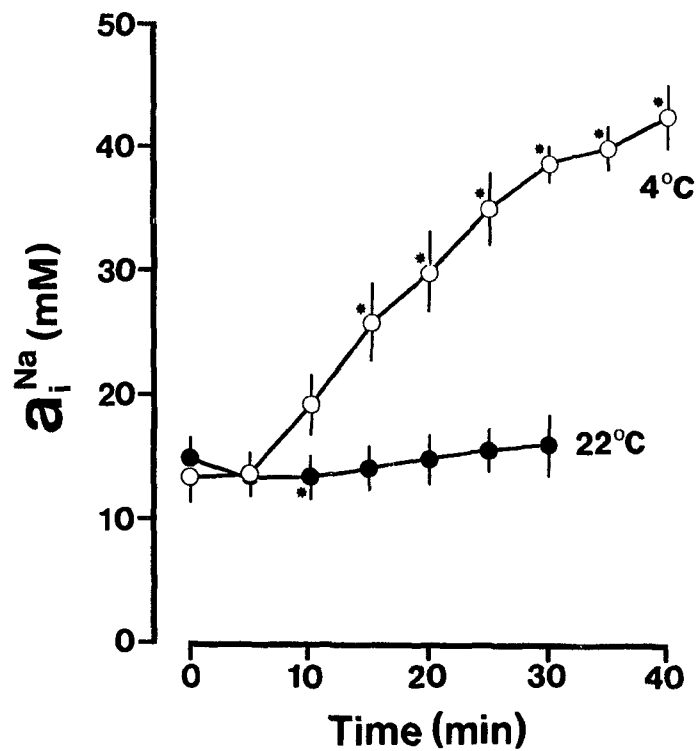


Figure 4.3: Effects of cooling from 37°C to 4°C and 22°C on intracellular Na<sup>+</sup> activity ( $a_i^{\text{Na}}$ ): time courses. Rapid cooling from 37°C to 4°C (open circles) and 22°C (closed circles) started at 0 min, and continued for 40 min (4°C) and 30 min (22°C), respectively. Averages of five and six experiments for closed and open circles, respectively. \*  $P < 0.05$  versus control.

Table 4.1: Effects of temperature on tubular resistances<sup>a</sup>.

Temp.	$R_{ap}$	$R_{bl}$	$R_s$
37°C	369 ± 48 (63)	92 ± 11 (63)	13 ± 1 (6)
22°C	1415 ± 165 <sup>b</sup> (44)	447 ± 44 <sup>b</sup> (44)	22 ± 1 <sup>b</sup> (9)
4°C	1952 ± 204 <sup>c</sup> (26)	2012 ± 168 <sup>d</sup> (26)	53 ± 4 <sup>d</sup> (6)

<sup>a</sup>Values are means ± S.E. in  $\Omega \cdot \text{cm}^2$ . Numbers of measurements are indicated in parentheses. See legend to Table 3.1 for abbreviations.

<sup>b</sup> $P < 0.05$  versus 37°C control.

<sup>c</sup> $P < 0.05$  versus 37°C control,  $P > 0.05$  versus 2°C data.

<sup>d</sup> $P < 0.05$  versus 37°C control and 22°C data.

is evident, the structural integrity of the cells appears to be well maintained and similar to control. Cooling from 37°C to 22°C resulted in a decrease in cell volume of approximately 10% of 37°C-control value. Such a cell shrinkage was sustained for up to 30 min at 22°C (Figures 4.4d and 4.5).

In summary, exposure of proximal tubules to 4°C led to a depolarization of membrane and transepithelial potentials, an increase in intracellular  $\text{Na}^+$  content, and a decrease in membrane ionic conductances. In contrast, exposure to 22°C did not affect intracellular  $\text{Na}^+$  content and caused only a slight depolarization of membrane potential, but it dramatically decreased the transepithelial potential and the membrane ionic conductances. Exposure to both temperatures also caused cell shrinkage.

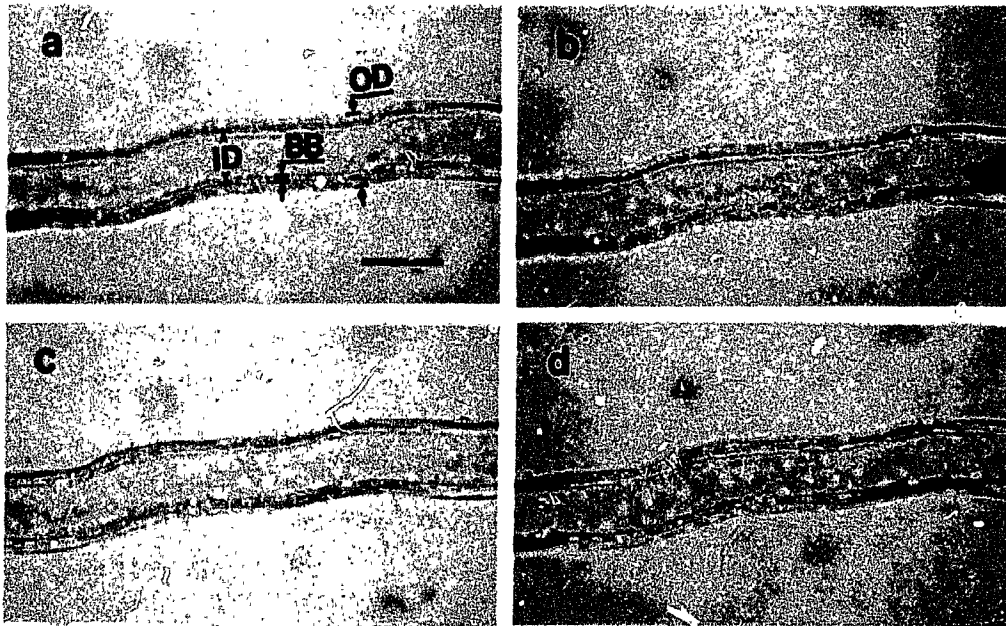


**Figure 4.4:** Effects of temperature on cell volume in isolated mouse proximal straight tubules perfused with control Ringer solution. All photomicrographs were taken at 200 $\times$  power. (a) 5 min after perfusion at 37°C, (b) 60 min after perfusion at 37°C, (c) 60 min after cooling to 4°C, (d) 30 min after cooling to 22°C. Abbreviations: ID, inner diameter; OD, outer diameter; BB, brush borders. Bar represents 50  $\mu$ m and applies to all photographs.

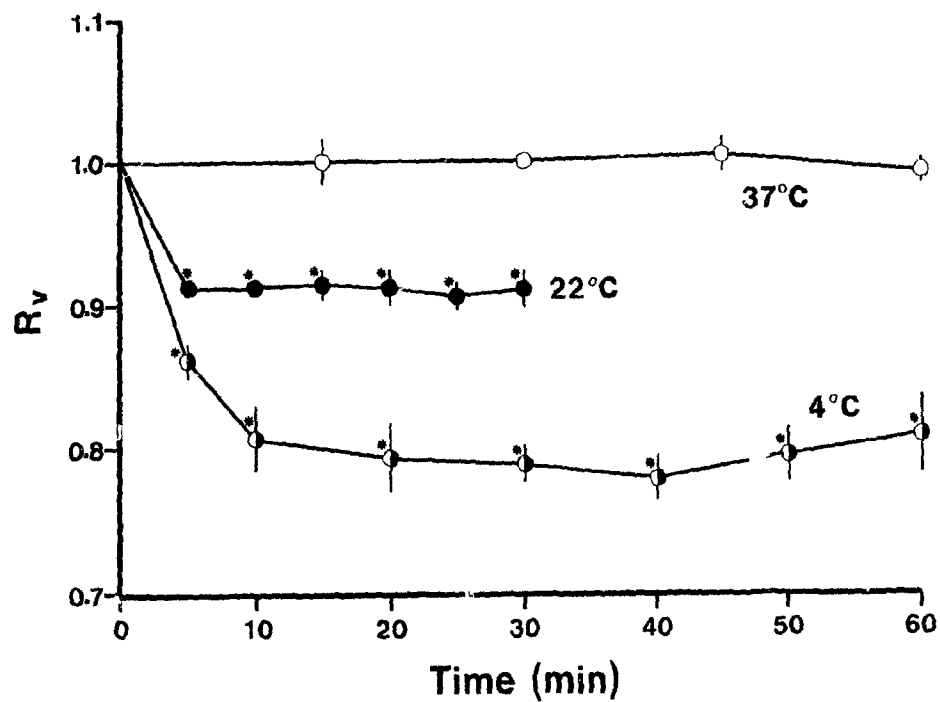


Figure 4.5: Time courses of cell volume changes following cooling from 37°C to 4°C (half-closed circles) and to 22°C (closed circles). Relative cell volume ( $R_v$ ) was calculated according to Equation 2.11. Cooling from 37°C to 22°C and 4°C was initiated at 0 min. A time control of  $R_v$  in tubules perfused at 37°C was also shown (open circles). Averages of four (4°C and 22°C) and three (37°C) experiments. Error bars are not shown when they are equal to or smaller than the size of the symbols. \*  $P < 0.05$  versus control.

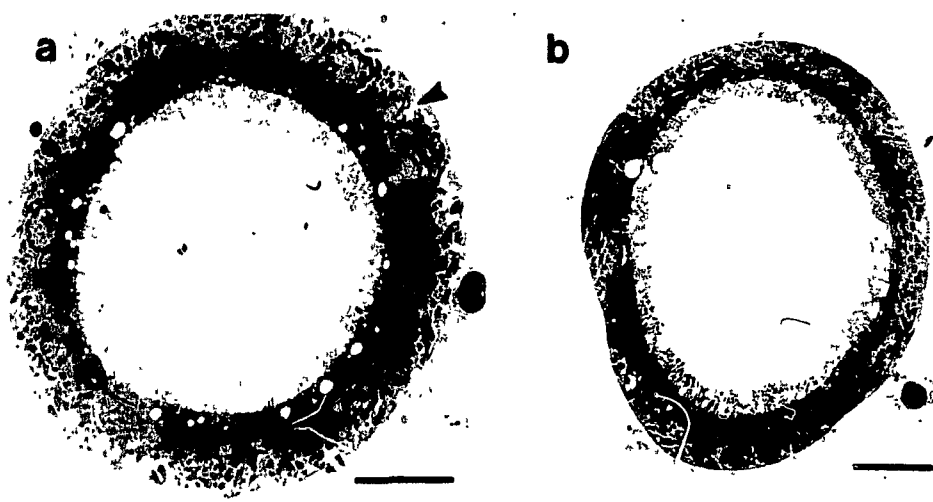


Figure 4.6: Effects of temperature on cell ultrastructures in isolated mouse proximal straight tubules perfused with control Ringer solution. Tubules were perfusion fixed after 10 min of perfusion at 37°C (a), or after 60 min of perfusion at 4°C (b). The basal empty space (arrowhead) seen in (a) may be due to the fixation artifact (see Section 2.4.2). Bars represent 10  $\mu\text{m}$ .

## **4.2 Comparison of EC and UW Solutions at 22°C and 37°C**

Preservation solutions are designed to preserve kidneys for transplantation at temperatures close to 0°C. Pilot studies were conducted to test the abilities of EC and UW solutions to preserve single perfused tubules at reduced temperature. EC and UW solutions were introduced both to the lumen and the bath sides of the tubules for up to 60 min at 4°C, followed by reperfusion with control Ringer and rewarming to 37°C. It was found that tubules were able to survive this experimental manoeuvre with no significant change in their morphological and electrophysiological parameters. In fact, isolated perfused proximal tubule can survive 60 min of 4°C perfusion with control Ringer solution. Indeed, preservation of kidney function for up to 12 hours using Ringer solution has been reported in some early studies.

Although EC and UW solutions are not designed for preservation at temperatures substantially higher than 0°C, renal tubules could be exposed to these solutions when kidneys are rewarmed to room temperature or even body temperature during the anastomosis (see Section 1.4.2). The effects of EC and UW perfusion at 22°C and 37°C were therefore studied on single perfused tubules.

### **4.2.1 Effects of EC and UW solutions at 22°C**

Perfusion with EC solution at 22°C resulted in a significant increase in cell volume after a 10-min delay. The increase in cell volume was completely reversed following a 6- to 12-min washout of EC solution using control Ringer solution (Figure 4.7). On the other hand, the increase in cell volume was minimal when tubules were exposed

to UW solution at 22°C (Figure 4.8). The changes in cell volume during EC and UW perfusion at 22°C are summarized in Figure 4.9.

In order to document if the morphological changes attributed to the 20-min EC exposure described above brought about any irreversible deterioration in tubular transport function,  $V_{te}$  was measured at the end of the 6- to 12-min washout period and compared with control values (Figure 4.10). A significant deterioration of  $V_{te}$  was recorded in tubules previously exposed to the EC solution, even though the cell volume had returned to the control value. In contrast,  $V_{te}$  was not affected by the 20-min UW exposure/perfusion. These data suggest that the initial cell swelling during EC perfusion may have a more permanent damaging effect on proximal tubule transport.

#### **4.2.2 Effects of EC and UW solutions at 37°C**

The effects of EC and UW perfusion on cell morphology and transepithelial potential at 37°C were also investigated. A significant increase in cell volume was observed after 3 min of EC perfusion (Figure 4.11). Increases in cell volume in EC solution reached their maximum value between 6 and 12 min. Following 12 min, the height of the cell layer decreased, which may be explained by a disruption of cellular structure (Figure 4.11e). On the other hand, no cell swelling was observed in UW solution (Figure 4.12). The data on cell volume are summarized in Figure 4.13.

The electron micrographs confirmed the cell volume changes observed using light microscopy. In Figure 4.14a, after 10 min of EC perfusion at 37°C, considerable cell swelling resulted in partial occlusion of the tubular lumen. Blebbing of cytoplasmic

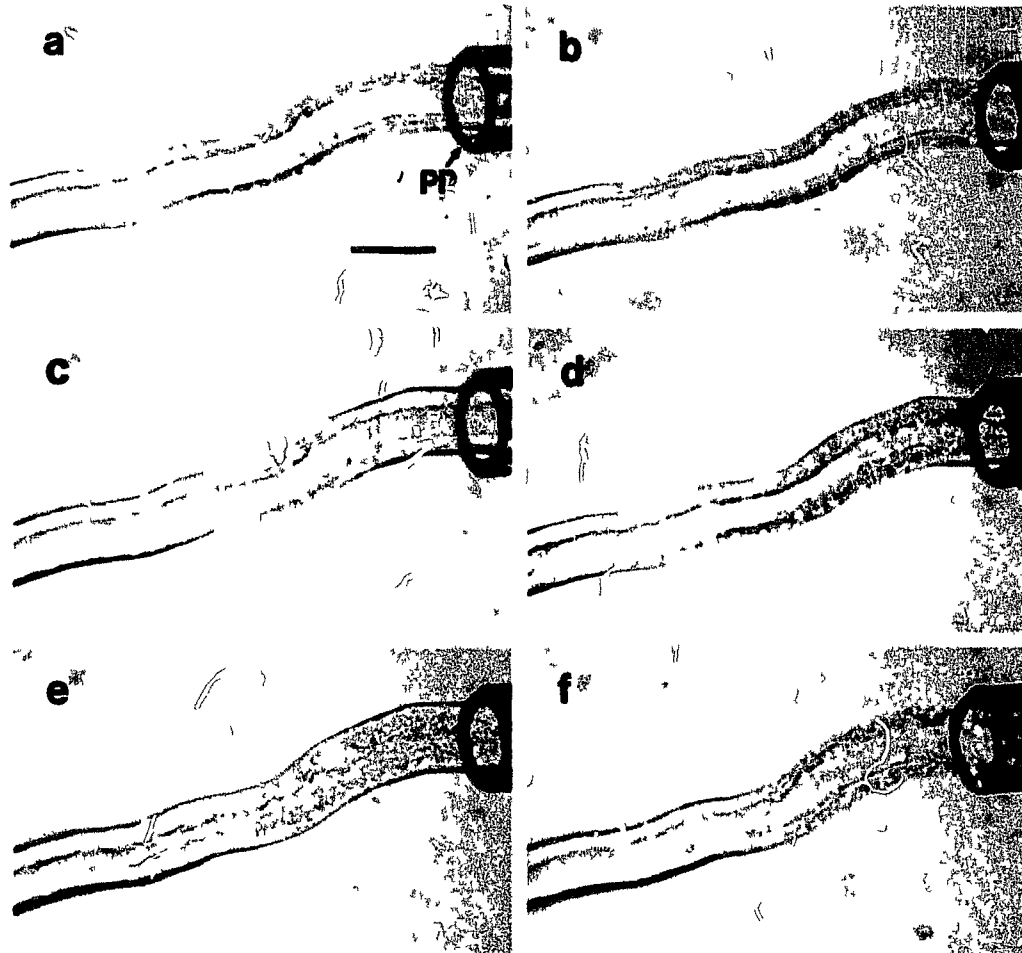


Figure 4.7: Effects of EC perfusion on tubular morphology at 22°C. The proximal tubule was initially perfused with control Ringer solution (a), followed by a 20-min EC perfusion [(b) 5 min, (c) 10 min, (d) 15 min, (e) 20 min], and a 10-min washout of the EC solution with control Ringer (f). The tip of the perfusion pipette (PP) is seen on the right in each photograph. Bar represents 50  $\mu\text{m}$  and applies to all photographs. See Section 2.6.3 for the detailed experimental protocol.

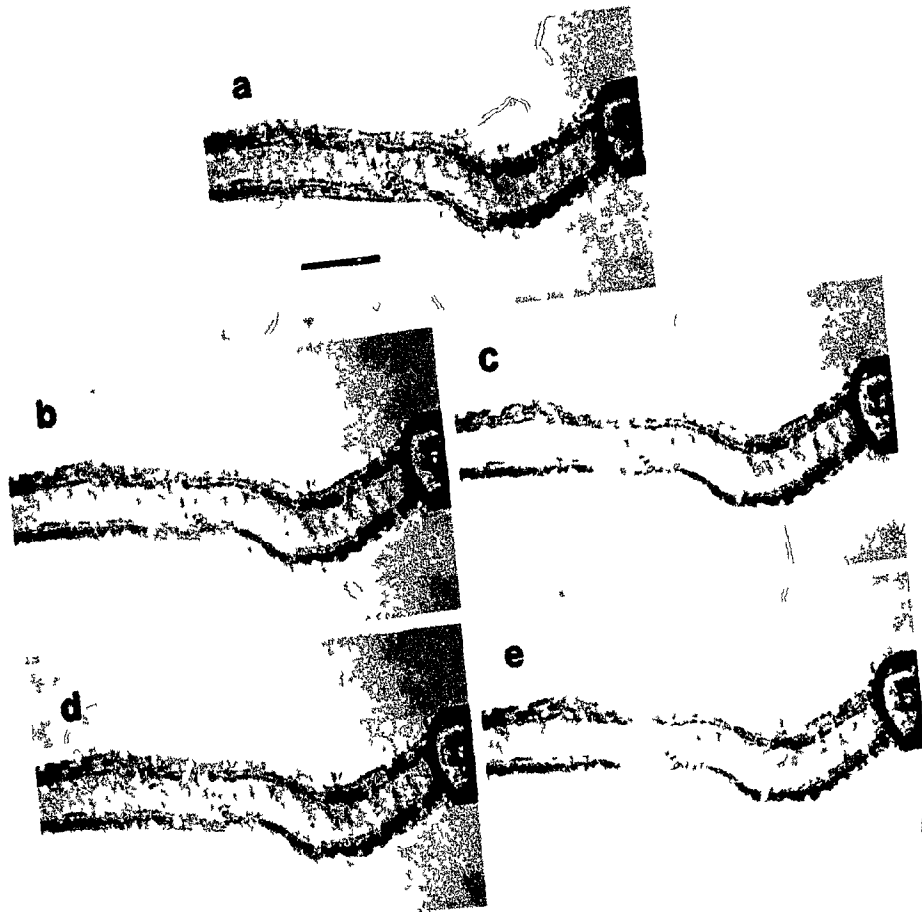


Figure 8. Effects of UW perfusion on tubular morphology at 22°C. The proximal tubule was initially perfused with control Ringer solution (a), followed by a 20-min UW perfusion [(b) 5 min, (c) 10 min, (d) 15 min, (e) 20 min] Bar represents 50  $\mu$ m and applies to all photographs.

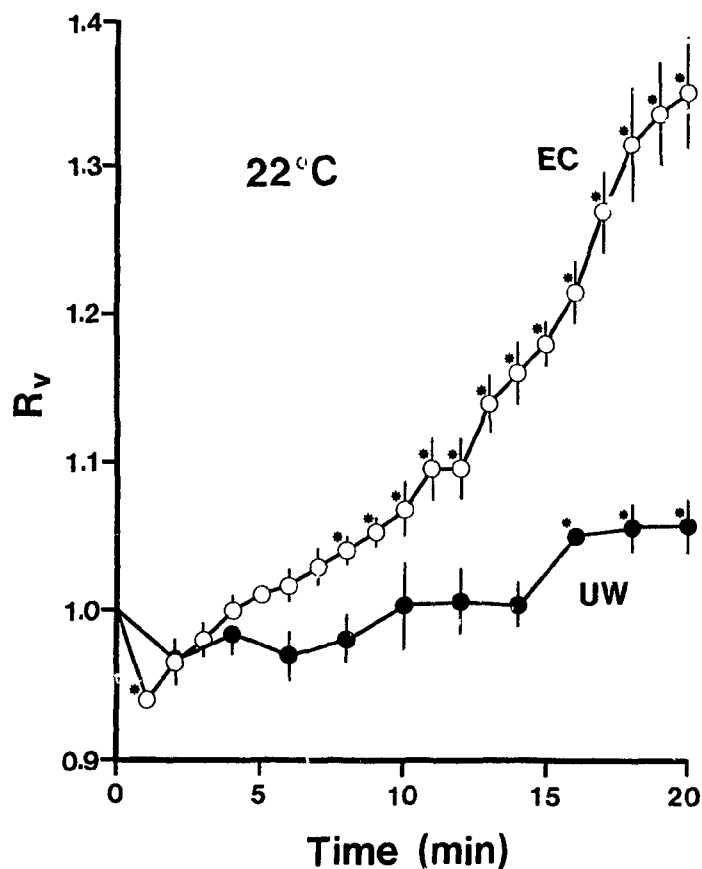


Figure 4.9: Effects of EC perfusion (open circles) and UW perfusion (closed circles) at 22°C on cell volume. EC and UW perfusion was initiated at 0 min. Relative cell volume ( $R_v$ ) was determined according to Equation 2.11, in which subscript  $c$  denotes tubular diameters in control Ringer at 22°C (see Section 2.6.3). Error bars are not shown when they are equal to or smaller than the size of the symbols. Averages of four experiments for each preservation solution. \*  $P < 0.05$  versus control (time zero).

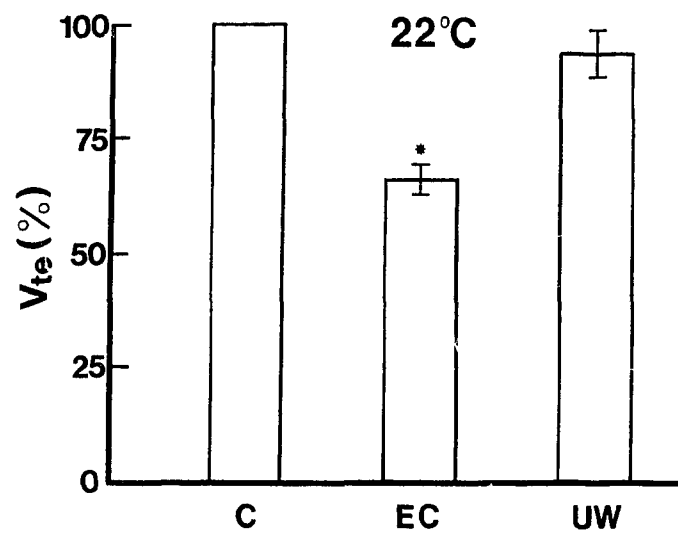


Figure 4.10: Recovery of  $V_{te}$  following a 20-min EC perfusion (EC) and a 20-min UW perfusion (UW) at 22°C. Changes in  $V_{te}$  were expressed as a percentage of control (C), the latter being set at 100%. Control data refer to the  $V_{te}$  measured in control Ringer before EC or UW perfusion at 37°C. Recovery data were also measured in control Ringer at 37°C, but after the 20 min of EC or UW perfusion at 22°C. Averages of four experiments for each preservation solution. \*  $P < 0.05$  versus control. See Section 2.6.3 for the detailed experimental protocol.

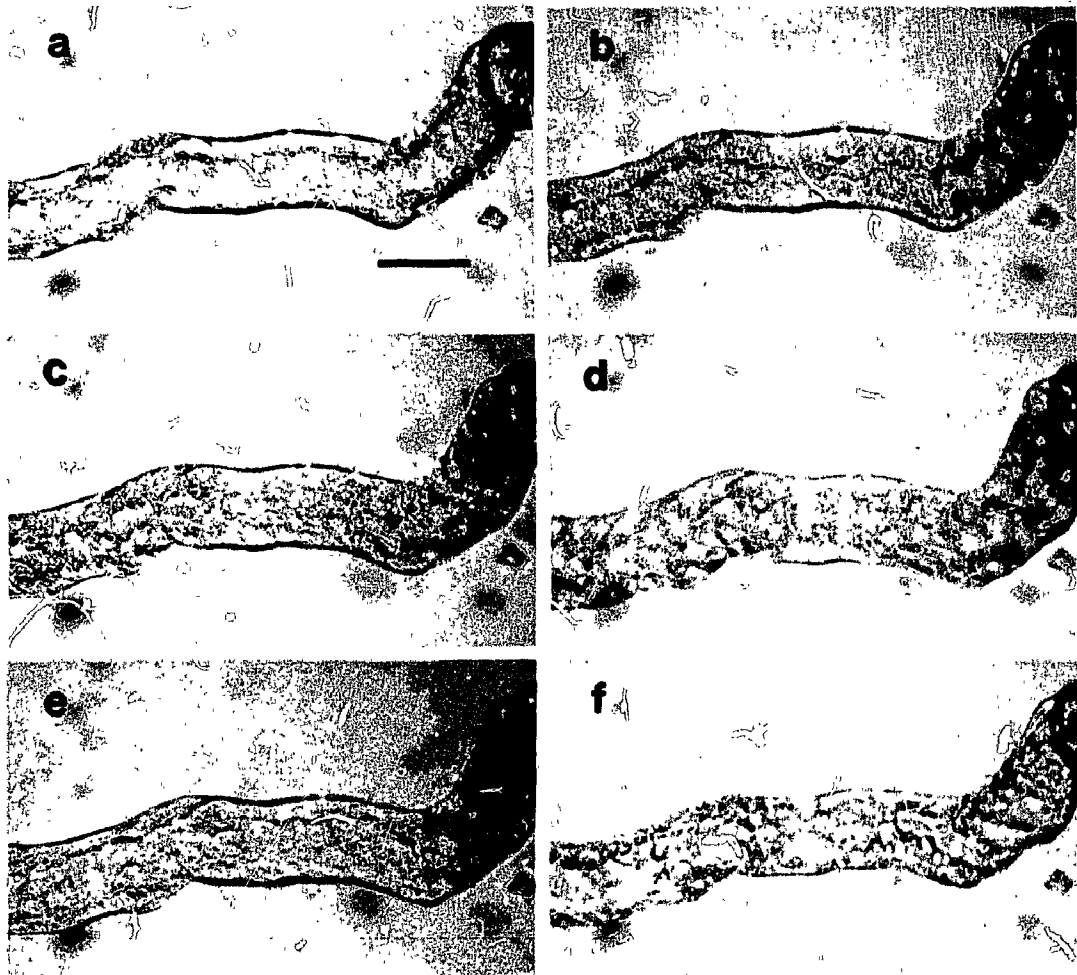


Figure 4.11: Effects of EC perfusion on tubular morphology at 37°C. The proximal tubule was initially perfused with control Ringer solution (a), followed by a 20-min EC perfusion [(b) 3 min, (c) 6 min, (d) 12 min, (e) 20 min], and a 10-min washout of the EC solution with control Ringer (f). Bar represents 50  $\mu\text{m}$  and applies to all photographs.

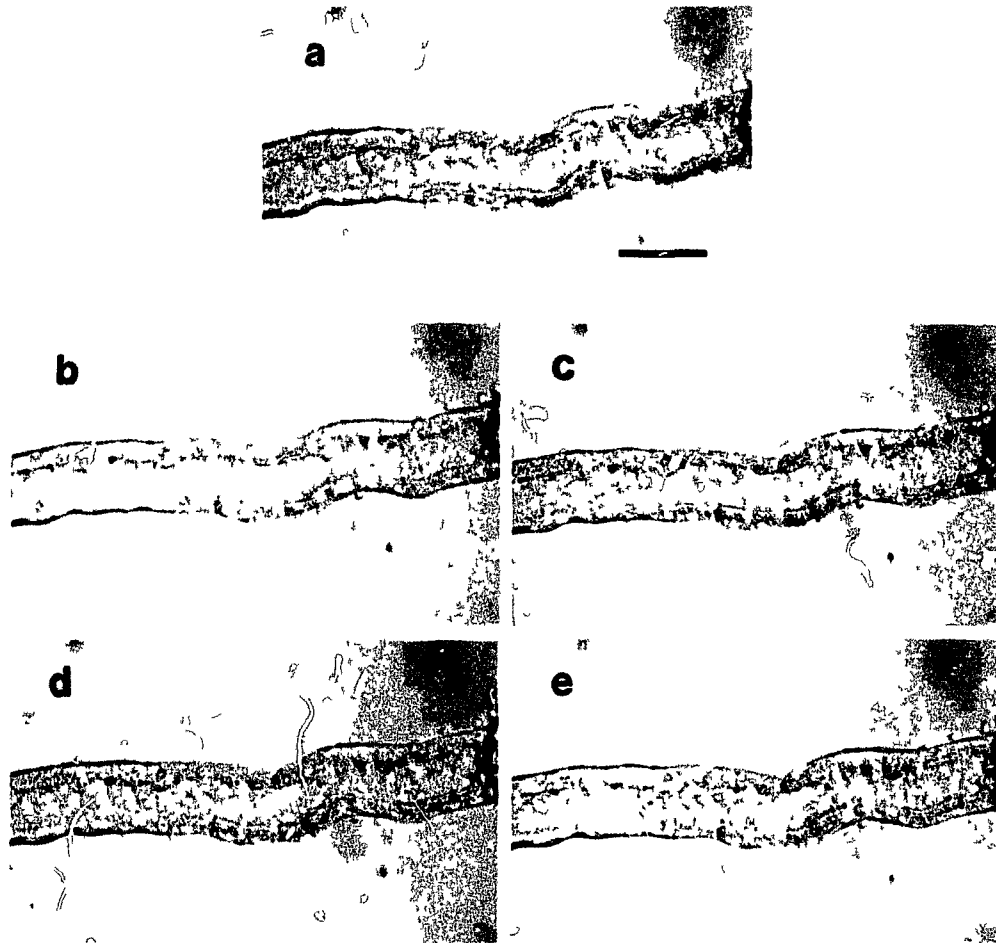


Figure 4.12: Effects of UW perfusion on tubular morphology at 37°C. The proximal tubule was initially perfused with control Ringer solution (a), followed by a 20-min UW perfusion [(b) 5min, (c) 10 min, (d) 15 min, (e) 20 min]. Bar represents 50  $\mu\text{m}$  and applies to all photographs.

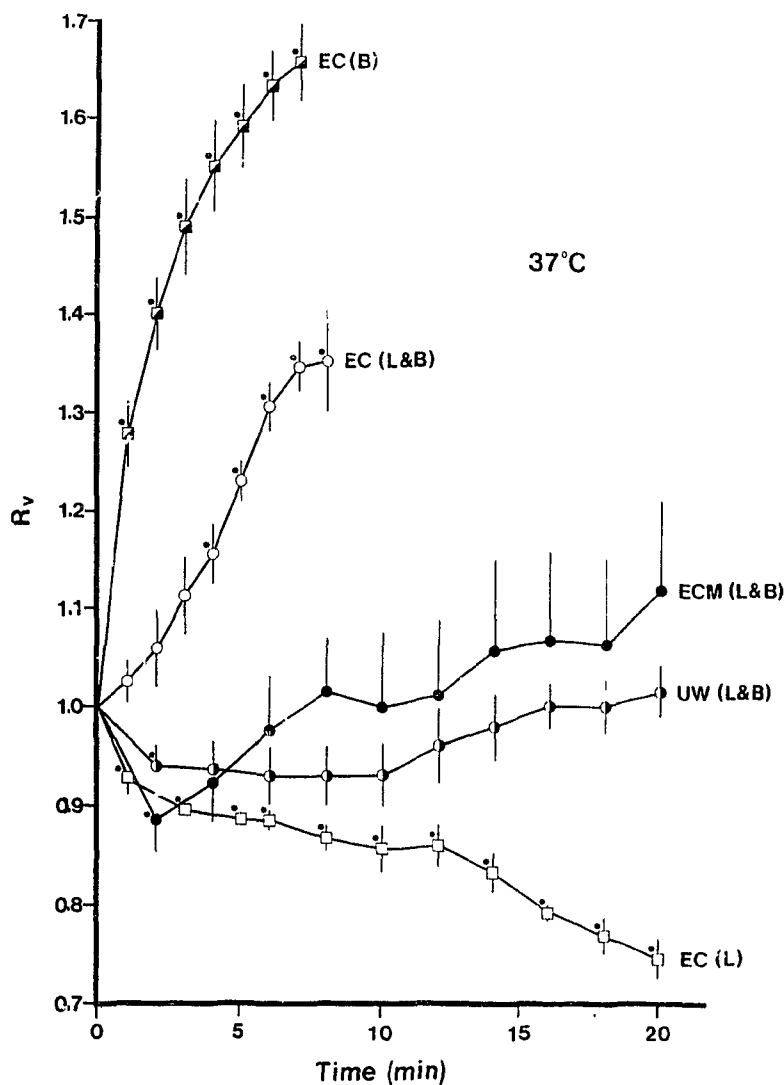


Figure 4.13: Effect of EC perfusion (open circles, open squares, and half-closed squares), EC-mannitol (ECM) perfusion (closed circles,  $n = 6$ ) and UW perfusion (half-closed circles,  $n = 6$ ) at 37°C on relative cell volume ( $R_v$ ). Open circles, EC perfusion on both the luminal and the basolateral sides [EC(L&B),  $n = 5$ ]. Half-closed squares, EC perfusion on the basolateral side only [EC(B),  $n = 7$ ]. Open squares, EC perfusion on the luminal side only [EC(L),  $n = 4$ ]. Error bars are not shown when they are equal to or smaller than the size of the symbols. \*  $P < 0.05$  versus control (time zero).

contents into the lumen was also seen. In contrast, perfusion with UW solution at 37°C did not result in cell swelling, even though the perfusion time was doubled to 20 min (Figure 4.14b). In Figure 4.14b, the apical surface of the tubule cell was essentially intact, although it appeared that, compared to control, there was an increase in the number of endocytic vacuoles. Large empty spaces along the basal surface of the cells may be artifacts of fixation. Such an artifact was especially noticeable under this experimental condition because fast exchange of bath UW solution with the fixative was impossible owing to the high viscosity of the UW solution.

The recovery of electrogenic transport function following EC and UW perfusion at 37°C was assessed by measuring  $V_{te}$ . Tubule reperfusion with control Ringer following a 9-min EC perfusion at 37°C recovered only one third of the original  $V_{te}$ . After a 10-min UW perfusion at 37°C, the  $V_{te}$  recorded during reperfusion with control Ringer was not significantly different from the control value (Figure 4.15).

The deterioration of  $V_{te}$  during the reperfusion period after a 9-min EC perfusion may be correlated with the ultrastructural changes seen under this experimental condition. In Figures 4.16a and 4.16d, cell swelling during the EC perfusion led to some cellular damage upon reperfusion, although the cell volume appeared to return to normal. In contrast, proximal tubule cells recovering from UW perfusion were better preserved, as judged by the overall ultrastructural appearance of the cells, although some large vacuoles were seen (Figure 4.16b). Figure 4.16c also illustrates the ultrastructure of a proximal tubule perfused with EC-mannitol solution followed by control reperfusion. Compared with Figure 4.16b, it appeared that ECM solution

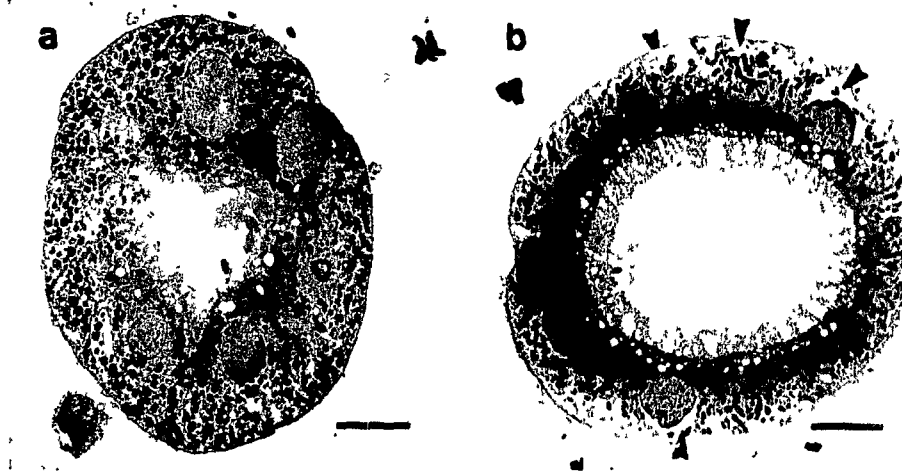


Figure 4.14: Effects of EC & UW perfusion on cellular ultrastructures. Tubules were perfusion-fixed immediately after either a 10-min EC perfusion (a) or a 20-min UW perfusion (b) at 37°C. Arrowheads indicate basal empty spaces. Bars represent 10  $\mu\text{m}$ .

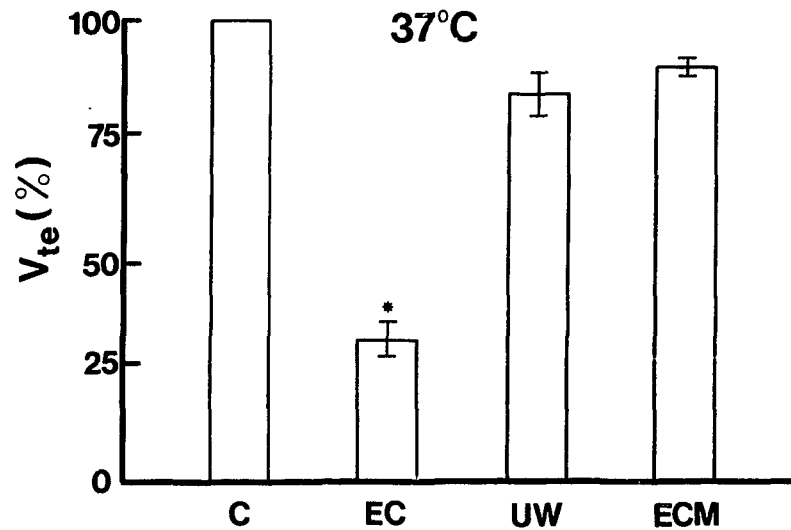


Figure 4.15: Recovery of  $V_{te}$  following a 9-min EC perfusion (EC), a 10-min EC-mannitol perfusion (ECM), and a 10-min UW perfusion (UW) at 37°C. Changes in  $V_{te}$  were expressed as a percentage of control, the latter being set at 100%. Control data (C) refer to the  $V_{te}$  measured when tubules were perfused with control Ringer solution before the EC, ECM, or UW perfusion. Recovery data were also measured in Ringer solution, but after the EC, ECM, or UW perfusion. Averages of three (UW and ECM) and four (EC) experiments. \*  $P < 0.05$  versus control. See Section 2.6.3 for the detailed experimental protocol.

was as effective, if not better than, the UW solution in this model system. The electrophysiological assessment of the effectiveness of ECM solution will be described in the following section.

### 4.3 Further Investigation of Osmotic Effects of EC solution at 37°C

Epithelial cells, such as proximal tubule cells, possess characteristic apical and basolateral membranes, which differ in their protein and lipid content from each other. Each membrane surface has unique transport systems and ionic permeabilities (see Section 1.1.3). Because of the structural and functional differences between the apical and the basolateral membranes, one would predict that the EC solution might affect cell volume differently when perfused in the lumen as opposed to the bath.

The sidedness effect of the EC solution on cell volume was studied. When perfused on the luminal side only, the EC solution [EC(L)] significantly decreased rather than increased the cell volume (Figure 4.13). In contrast, when perfused via the bath only, the EC solution increased the cell volume at a higher rate than in bilateral perfusion experiments [compare EC(B) and EC(L&B) curves in Figure 4.15]. The data would suggest that the osmotic threat of the EC solution originated from its interaction with the basolateral membrane.

The effectiveness of mannitol as a membrane impermeant was tested by substituting glucose in EC solution with mannitol (ECM solution, see Table 2.2). Compared with the original EC solution, ECM solution abolished the increase in cell volume, as shown in Figure 4.13. In addition,  $V_{te}$  was well preserved after a 10-min ECM

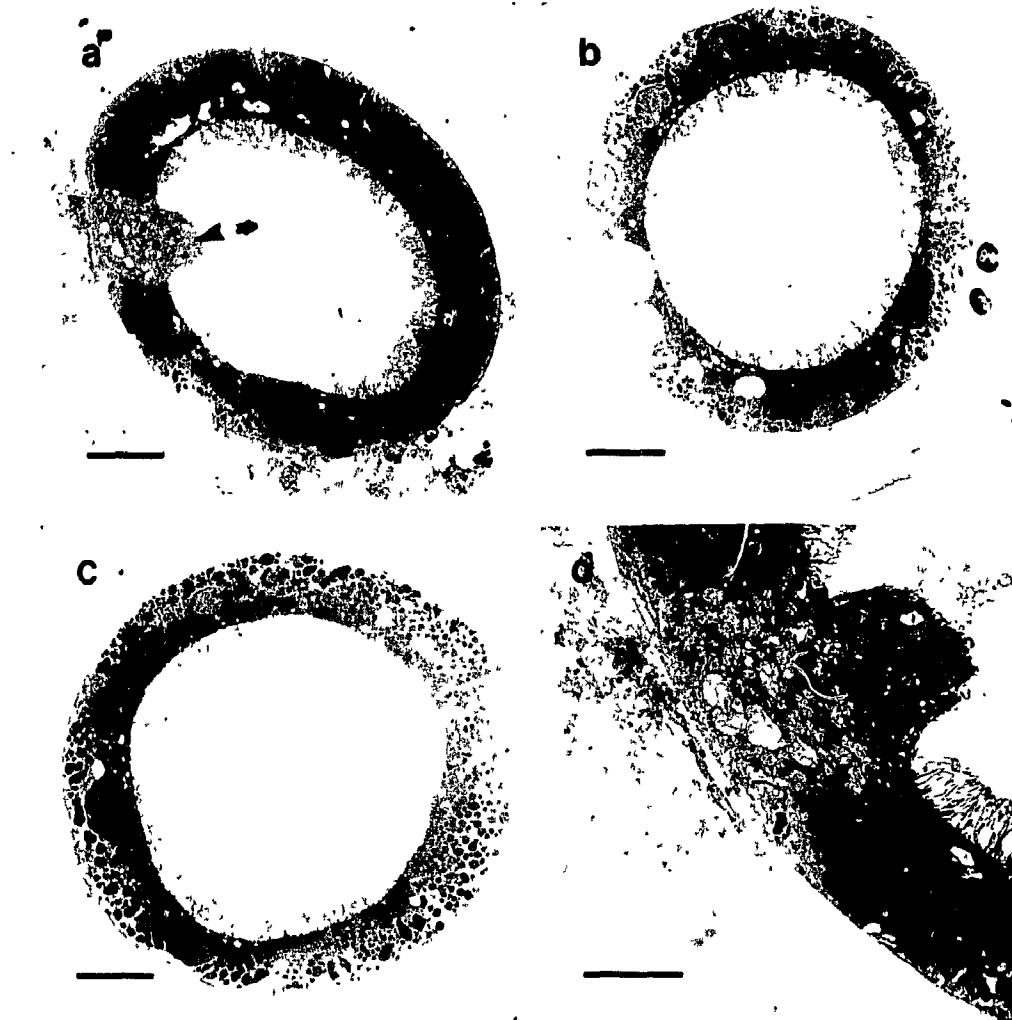


Figure 4.16: Cell ultrastructures during control reperfusion following EC, ECM or UW perfusion at 37°C. Proximal tubules were fixed following a 9-min EC perfusion and a 6-min control reperfusion (a), following a 10-min UW perfusion and a 15-min control reperfusion (b), and following a 10-min ECM perfusion and a 6-min control reperfusion (c). Arrowhead in (a) indicates a damaged cell, a close-up view of which is given in (d). Bars represent 10  $\mu\text{m}$  in (a) to (c), and 5  $\mu\text{m}$  in (d).

perfusion at 37°C (Figure 4.15). This result is consistent with the well preserved tubular ultrastructure seen under this experimental condition (see Figure 4.16c), and suggests that the choice of an effective osmotic agent in preservation solutions is crucial in the prevention of cell swelling at 37°C.

## Chapter 5

# DISCUSSION I: Electrophysiology of Proximal Tubular Transport

The model system of amphibian proximal tubules was developed in the 1970's and 1980's so that ionic gradients and permeabilities could be easily studied using electrophysiological methods [5, 31, 33, 96]. Such analysis has proven to be an effective way to assess the transport function in amphibian proximal tubules. The mammalian proximal tubular cell is smaller than its amphibian counterpart, rendering some electrophysiological measurements (e.g. cell cable analysis described in Appendix A) difficult. Let us begin with a discussion on the analysis of the electrophysiology of tubular transport in mouse proximal tubules under control situations. Alterations of the transport in the face of hypoxia, ischemia and cooling *in vitro* will be discussed later.

### 5.1 The Control Proximal Tubule

#### 5.1.1 Diffusional potentials

Cell membrane potential originates from ionic gradients across the membrane. These gradients are maintained primarily by the  $\text{Na}^+, \text{K}^+$ -ATPase. The membrane potential

( $E_m$ ) can be approximated by the combined diffusional potentials of three major ions,  $\text{Na}^+$ ,  $\text{K}^+$  and  $\text{Cl}^-$ :

$$E_m = \frac{RT}{F} \ln \frac{P_K a_o^K + P_{\text{Na}} a_o^{\text{Na}} + P_{\text{Cl}} a_i^{\text{Cl}}}{P_K a_i^K + P_{\text{Na}} a_i^{\text{Na}} + P_{\text{Cl}} a_o^{\text{Cl}}} \quad (5.1)$$

where the  $P$ 's are permeability coefficients and subscripts  $o$  and  $i$  represent ionic activities outside and inside the cell, respectively. This is the well known *constant field equation*, also known as the *Goldman-Hodgkin-Katz equation* [76, 92].

The constant field equation also applies to the calculation of the transepithelial diffusional potential ( $E_{te}$ ). However, since symmetrical solutions were used in the perfused tubule preparation in this study, the  $E_{te}$  across the tight junction (the paracellular barrier) was assumed to be zero<sup>1</sup>.

### 5.1.2 Transepithelial and transmembrane potentials

The proximal tubule has been modeled as an electrical circuit, with a battery (the diffusional potential) and a resistor (the ionic conductance) across each barrier (apical and basolateral membranes, as well as the tight junction) [31] (Figure 5.1). According to this equivalent electrical circuit, diffusional potentials for apical ( $E_{ap}$ ) and basolateral ( $E_{bl}$ ) membranes derived from the constant field equation (Equation 5.1) are tightly coupled in proximal tubules. In other words, the electrical potentials recorded across the basolateral ( $V_{bl}$ ) membrane, the apical ( $V_{ap}$ ) membrane and the

---

<sup>1</sup>When proximal tubules are perfused with symmetrical solutions, local ionic gradient across the tight junction may develop, which makes  $E_{te}$  deviate from zero. This is because the NaCl concentration in the narrow lateral intercellular space (LIS) may be higher than that of bulk bath solution as a result of active  $\text{Na}^+$  pumping into the LIS and the slow diffusion of NaCl from this compartment to the bath. However, in *Necturus* proximal tubules, the estimated NaCl-diffusion potential across the tight junction was an order of magnitude smaller than the recorded  $V_{te}$ , suggesting that paracellular diffusional potentials contribute little to the  $V_{te}$  [31, 32]. I therefore assumed  $E_{te}$  to be zero for this discussion.

tight junction ( $V_{te}$ ) are functions of  $E_{bl}$ ,  $E_{ap}$ , the apical ( $R_{ap}$ ) and the basolateral ( $R_{bl}$ ) membrane resistances, and the transepithelial resistance ( $R_{te}$ ) [31]:

$$V_{bl} = \frac{E_{bl}(R_{ap} + R_{te}) - E_{ap}R_{bl}}{R_{bl} + R_{ap} + R_{te}} \quad (5.2)$$

$$V_{ap} = \frac{E_{ap}(R_{bl} + R_{te}) - E_{bl}R_{ap}}{R_{bl} + R_{ap} + R_{te}} \quad (5.3)$$

$$V_{te} = \frac{(E_{bl} + E_{ap})R_{te}}{R_{bl} + R_{ap} + R_{te}} \quad (5.4)$$

Conversely, the  $E_{ap}$  and  $E_{bl}$  can be expressed by  $V_{ap}$ ,  $V_{bl}$ ,  $R_{ap}$ ,  $R_{bl}$ , and  $R_{te}$ :

$$E_{ap} = \frac{V_{bl}R_{ap} + V_{ap}(R_{ap} + R_{te})}{R_{te}} \quad (5.5)$$

$$E_{bl} = \frac{V_{bl}(R_{bl} + R_{te}) + V_{ap}R_{bl}}{R_{te}} \quad (5.6)$$

The objective of the electrophysiological analysis is to understand the ionic permeabilities of each diffusional barrier (apical and basolateral cell membranes, and paracellular pathway). Such knowledge is crucial for the description of the transport characteristics of the tubular epithelium (see, for example, Figure 1.1). Determination of potentials and resistances across individual barriers would enable one to derive the diffusional potentials across these barriers ( $E_{ap}$  and  $E_{bl}$ ). Such diffusional potentials are much more informative than recorded membrane potentials ( $V_{ap}$  and  $V_{bl}$ ) in revealing ionic gradients and permeabilities across the cell membranes.

The electrophysiological analysis based on the equivalent electrical circuit just described was first developed by Boulpaep and colleagues in amphibian proximal tubules [31]. In the following section, we will apply this analysis to the mouse proximal straight tubule using electrophysiological parameters obtained from this study.

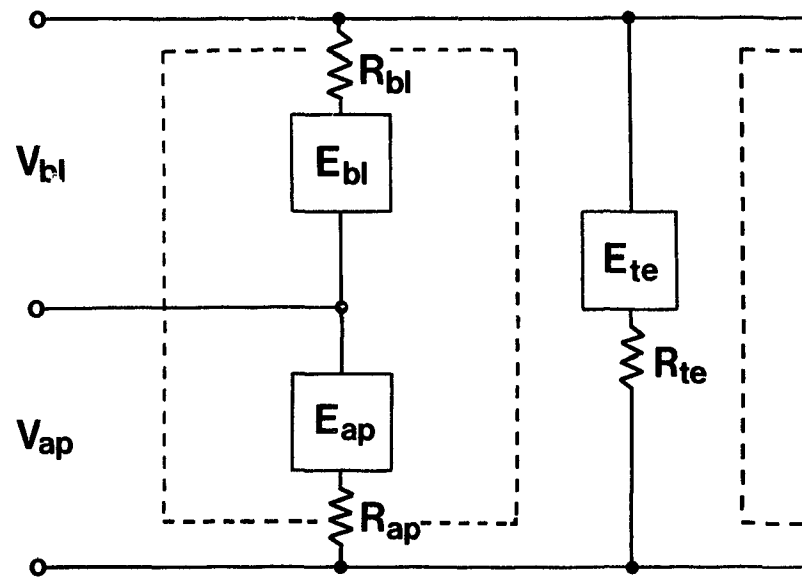


Figure 5.1: Equivalent electric circuit for the proximal tubules. The dash lines indicate cell borders. Notice that  $V_{ap} + V_{bl} \equiv V_{te}$ . See text for abbreviations. (Illustration modified from reference [31]).

### 5.1.3 Basolateral cell membrane

Using experimentally determined membrane<sup>2</sup> and transepithelial potentials ( $V_{bl} = -70.0$  mV,  $V_{te} = -1.7$  mV,  $V_{ap} = +68.3$  mV) and resistances ( $R_{bl} = 92 \Omega \cdot \text{cm}^2$ ,  $R_{te} = 13 \Omega \cdot \text{cm}^2$ ,  $R_{ap} = 369 \Omega \cdot \text{cm}^2$ , see Table 3.1),  $E_{bl}$  was calculated according to Equation 5.6:

$$\begin{aligned} E_{bl} &= \frac{-70 \times (92 + 13) + 68.3 \times 92}{13} \\ &= -82.0 \text{ mV} \end{aligned} \quad (5.7)$$

If intracellular  $\text{K}^+$  activity ( $a_i^{\text{K}}$ ) of 100 mM was assumed<sup>3</sup>, with extracellular  $\text{K}^+$  activity ( $a_o^{\text{K}}$ ) at 4.65 mM ( $a_o^{\text{K}} = [\text{K}^+]_o \times 0.93 = 5 \text{ mM} \times 0.93 = 4.65 \text{ mM}$ , 0.93 being the activity coefficient), the Nernst potential for potassium was calculated to be:

$$\begin{aligned} E_{\text{K}} &= \frac{RT}{F} \ln \frac{a_o^{\text{K}}}{a_i^{\text{K}}} \\ &= 61.5 \ln(4.65/100) \\ &= -82.0 \text{ mV} \end{aligned} \quad (5.8)$$

Therefore, the diffusional potential derived from the experimental data (Equation 5.6) can be almost perfectly approximated with the Nernst potential of the transmembrane  $\text{K}^+$  gradient (Equation 5.8). This result indicates that the  $\text{K}^+$  conductance is the predominant ionic conductance across the basolateral membrane.

<sup>2</sup> $V_{ap}$  is calculated as the difference between  $V_{te}$  and  $V_{bl}$ , see the equation in the legend to Figure 5.1.

<sup>3</sup>Although  $a_i^{\text{K}}$  of 100 mM is higher than those measured by liquid ion-exchanger microelectrodes (40 to 80 mM) [25, 61, 117], this value is very close to the values determined by electron microprobe analysis [132] and flame photometry [193] (assuming the activity coefficient of 0.7). The reason for choosing  $a_i^{\text{K}}$  as 100 mM is that the microelectrode methods may lead to an underestimation of  $a_i^{\text{K}}$ , as discussed by Laprade and colleagues [117].

The relative importance of  $K^+$ -diffusion potential to the overall basolateral diffusional potential can also be estimated by measuring basolateral potassium transference number ( $t_{K(b)}$ , see Section 2.3.3 for details). However, as pointed out by Völkl and colleagues [200], the measured  $t_{K(b)}$  is always an underestimate of the actual contribution of potassium potential (or conductance) to the overall diffusional potential (or conductance). This is because the recorded change in basolateral membrane potential ( $\Delta V_{bl}$ ) in response to bath 20-K<sup>+</sup> pulses is smaller than the actual change in the diffusional potential ( $\Delta E_{bl}$ ), with portions of  $\Delta E_{bl}$  being distributed across the apical membrane and the tight junction (see Figure 5.1). Using Equation 5.6 and assuming that resistances of all barriers were not affected by elevation of basolateral  $[K^+]$  (see discussion below), the value of  $E_{bl}$  after bath perfusion of 20-K<sup>+</sup> Ringer was calculated to be:

$$\begin{aligned} E_{bl(20K)} &= \frac{-44.0 \times (92 + 13) + 43.0 \times 92}{13} \\ &= -51.1 \text{ mV} \end{aligned} \quad (5.9)$$

where the  $V_{bl}$  and  $V_{ap}$  values were derived from the recorded magnitudes of depolarization of  $V_{bl}$  and  $V_{te}$  in the presence of 20-K<sup>+</sup> Ringer. It follows that

$$\begin{aligned} \Delta E_{bl} &= E_{bl(20K)} - E_{bl} \\ &= -51.1 - (-82.0) = +30.9 \text{ mV} \end{aligned} \quad (5.10)$$

By substituting  $\Delta V_{bl}$  with  $\Delta E_{bl}$  into Equation 2.3, the corrected  $t_{K(b)}$  ( $t'_{K(b)}$ ) can be derived as follows:

$$t'_{K(b)} = \Delta E_{bl} F Z_K / (RT \ln 4) = 0.83 \quad (5.11)$$

It appears that the experimentally determined apparent  $t_{K(\text{bl})}$  (0.70, see Section 3.1.2) is in good agreement with the corrected  $t'_{K(\text{bl})}$  (0.83).

The inherent assumption made in the measurement and analysis of  $t_{K(\text{bl})}$  is that intracellular  $K^+$  activity does not change with a brief application of 20-K<sup>+</sup> Ringer. In addition, two more assumptions were implied in this analysis. First, the potassium conductance of the basolateral membrane was assumed to be constant during the membrane depolarization with 20-K<sup>+</sup> Ringer in the bath. Unfortunately, the validity of this assumption can not be evaluated with confidence because of the limited knowledge of the properties of  $K^+$  conductances in the basolateral membrane of proximal tubular cells. The two types of  $K^+$  conductance identified so far appear to be voltage-dependent [152, 165]. The inward-rectifying potassium channel recorded in the basolateral membrane of rabbit proximal straight [70] and convoluted [152] tubules was described as “moderately voltage-dependent” and activated by depolarization [152]. In contrast, the  $K^+$  channel found in the basolateral membrane of *Necturus* proximal tubule is activated by hyperpolarization [165]. All these possible changes in basolateral  $K^+$  permeability in response to membrane depolarization were ignored in the process of obtaining both  $t_{K(\text{bl})}$  and  $t'_{K(\text{bl})}$ .

Second, we have assumed that the diffusional potential across the tight junction ( $E_{te}$ ) remained zero even though a transepithelial  $K^+$  gradient was set up during basolateral 20-K<sup>+</sup> perfusion. Because of the tight coupling of the diffusional potential across each barrier, the generation of  $E_{te}$  during basolateral 20-K<sup>+</sup> perfusion would require that  $E_{te}$  be incorporated in the calculation of  $E_{\text{bl}(20K)}$  (Equation 5.9, [31]). However, the  $E_{te}$  generated by this transepithelial  $K^+$  gradient (lumen 5 mM, bath 20

mM) appears to be small, because in the present study, the  $V_{te}$  was only depolarized by  $0.68 \pm 0.08$  mV ( $n = 6$ ) under this condition<sup>4</sup>. Considering that the calculated Nernst potential of potassium across the tight junction is 37.1 mV, it is apparent that the tight junction is almost impermeable to  $K^+$ . This finding is contradictory to the result obtained from the autoperfused dog kidney [34], in which the  $K^+$  permeability was found to be the highest among several cations (e.g.  $Na^+$ ) and anions (e.g.  $Cl^-$ ). However, it agrees with the low cation permeability observed in amphibian proximal tubules [4, 162]. Species variation may account for some of the discrepancy.

The contribution of the  $K^+$  potential to overall basolateral diffusional potential estimated from potassium transference number is lower than what one would predict if the values of  $E_K$  (Equation 5.8) and  $E_{bl}$  (Equation 5.7) were compared. That  $E_{bl}$  equals  $E_K$  would imply that the basolateral membrane potential is solely due to the  $K^+$ -diffusion potential. The  $t_{K(bl)}$ -analysis is probably more accurate than the simple comparison between  $E_K$  and  $E_{bl}$ , because the electrogenic  $Na^+, K^+$ -ATPase that is not included in this model system contributes a significant portion of the inside-negative basolateral membrane potential [164]. This means that  $E_{bl}$  is probably a combination of  $E_K$ , depolarizing Nernst potentials (e.g.  $E_{Cl}$ ) and a hyperpolarizing pump potential. The  $Na^+$  conductance can not contribute significantly to the remaining 17% of the basolateral membrane conductance (Equation 5.11)<sup>5</sup> because it would depolarized  $E_{bl}$  away from the value derived from Equation 5.8.

<sup>4</sup>Because of the low shunt resistance ( $R_s$ ) compared with resistance across the cell membranes ( $R_{ap}$  and  $R_{bl}$ , see Table 3.1), it can be predicted that  $V_{te}$  is a good approximation of  $E_{te}$ . See reference [31] for details.

<sup>5</sup>Since the sum of the individual ionic transference number must equal 1,  $t'_{X(bl)} = 1 - t'_{K(bl)} = 0.17$ ,  $t'_{X(bl)}$  being the sum the ionic transference numbers other than that of  $K^+$ .

### 5.1.4 Apical cell membrane

The origin of the apical membrane potential ( $E_{\text{ap}}$ ) is more complex. There is a significant contribution of a  $\text{Na}^+$ -diffusion potential to  $E_{\text{ap}}$  [31, 65]. According to Frömter [65],  $\text{Na}^+$ -glucose transport alone may contribute up to 20% of the apical membrane conductance in rat proximal tubules. In amphibian proximal tubules, luminal ion-substitution experiments indicate that the  $\text{K}^+$  and  $\text{Cl}^-$  conductances are lower than that of  $\text{Na}^+$  [30]. Information is quite limited on the relative importance of each ionic diffusional potential to  $E_{\text{ap}}$  in mammalian proximal tubules.

The  $E_{\text{ap}}$  can be derived from membrane potential and resistance data recorded in this study, which were given at the beginning of Section 5.1.3. According to Equation 5.5,  $E_{\text{ap}}$  was calculated to be:

$$\begin{aligned} E_{\text{ap}} &= \frac{-70.0 \times 369 + 68.3(369 + 13)}{13} \\ &= +20.0 \text{ mV} \end{aligned} \quad (5.12)$$

The positive sign implies that the cell interior is negative relative to the lumen<sup>6</sup>. Since the value of  $E_{\text{ap}}$  is far away from the Nernst potential for potassium calculated in Equation 5.8 (+82.0 mV, cell negative), it is apparent that one or several depolarizing diffusional potentials contribute significantly to  $E_{\text{ap}}$ .  $\text{Na}^+$  conductance must be involved because for all major ions, only the Nernst potential for  $\text{Na}^+$  is lower than the  $E_{\text{ap}}$  [ $E_{\text{Na}} = -52.7$  mV, lumen positive ( $a_i^{\text{Na}} = 14.6$  mM,  $a_o^{\text{Na}} = 140$  mM  $\times$  0.75 = 105 mM, 0.75 being the activity coefficient)].

---

<sup>6</sup>The convention in electrophysiological analysis of tubular transport formulates that  $V_{\text{ap}} + V_{\text{bl}} \equiv V_{\text{e}}$  (see Figure 5.1). When the bath potential is considered zero, both  $V_{\text{bl}}$  and  $V_{\text{e}}$  are negative. To satisfy the above equation, the cell interior-negative  $V_{\text{ap}}$  (as well as  $E_{\text{ap}}$ ) must be expressed as a positive value.

To estimate the contribution of  $K^+$ -diffusion potential to the  $E_{ap}$ , luminal ionic-substitution experiment was performed. The apparent  $t_{K(ap)}$  measured by luminal perfusion of 20-K<sup>+</sup> Ringer was  $0.11 \pm 0.01$  ( $n = 5$ ). Very low  $K^+$  and  $Cl^-$  conductances were also reported in amphibian proximal tubules using similar experimental manoeuvre [30]. This would suggest a substantial contribution of  $Na^+$ -potential to the  $E_{ap}$ .

However, as pointed out in Section 5.1.3, the recorded voltage change ( $\Delta V_{ap}$ ) following lumen application of 20-K<sup>+</sup> Ringer may not reflect the actual change in the diffusional potential ( $\Delta E_{ap}$ ). Equation 5.5 was used to calculate the  $E_{ap}$  during luminal perfusion of 20-K<sup>+</sup> Ringer, based on the same assumptions made when the  $E_{bl}$  was derived (see Section 5.1.3):

$$\begin{aligned} E_{ap(20K)} &= \frac{-66.6 \times 369 + 64.2 \times (369 + 13)}{13} \\ &= -3.9 \text{ mV} \end{aligned} \quad (5.13)$$

where the  $V_{bl}$  was directly measured and  $V_{ap}$  was calculated according to:  $V_{ap} = V_{lc} - V_{bl}$ .

The corrected  $t'_{K(ap)}$  was calculated according to Equation 2.4 as follows:

$$\begin{aligned} t'_{K(ap)} &= \Delta E_{ap} F Z_K / (RT \ln 4) \\ &= [20.0 - (-3.9)] / 37.1 \\ &= 0.65 \end{aligned} \quad (5.14)$$

In contrast to the  $t_{K(bl)}$ , which underestimates the  $t'_{K(bl)}$  by less than 20% (see Section 5.1.3), the  $t_{K(ap)}$  underestimates the  $t'_{K(ap)}$  by as much as 80% (0.11 vs.

0.65). This dramatic difference between  $t_{K(\text{ap})}$  and  $t'_{K(\text{ap})}$  highlights the problem of interpreting the data from luminal ionic substitution experiments.

If 65% of the apical ionic conductance is a  $K^+$  conductance, then the remaining 35% must be predominantly  $Na^+$  conductance to account for the  $E_{\text{ap}}$  of +20.0 mV (Equation 5.12). In fact, if I assume that the remaining conductance (35%) is a  $Na^+$  conductance, according to the constant field equation (Equation 5.1), the  $E_{\text{ap}}$  calculation would be:

$$\begin{aligned} E_{\text{ap}} &= -\frac{RT}{F} \ln \frac{P_K/P_{Na} a_o^K + a_o^{Na}}{P_K/P_{Na} a_i^K + a_i^{Na}} \\ &= -61.5 \lg \frac{1.86 \times 4.65 + 105}{1.86 \times 100 + 14.6} \\ &= +15.2 \text{ mV} \end{aligned} \tag{5.15}$$

where the ratio  $P_K/P_{Na}$  equals 1.86  $(0.65/0.35)^7$ . The  $E_{\text{ap}}$  so calculated is reasonably close to the value of +20.0 mV calculated according the Equation 5.12.

This calculation would indicate that in the presence of luminal substrate, about one third of the apical membrane conductance is a  $Na^+$  conductance. According to Frömter's analysis in rat proximal tubules, the  $Na^+$ -substrate cotransport pathway accounts for 47% of total apical conductance in the presence of glucose and phenylalanine (5 mM each) [65]. It may be that the  $Na^+$  conductance estimated in this study mainly originates from the  $Na^+$ -cotransport pathways<sup>8</sup>. In other words,

<sup>7</sup>The terms "conductance" and "permeability" are used interchangeably in this analysis. Strictly speaking, "conductance" and "permeability" are two directly related yet distinct electrophysiological parameters [174].

<sup>8</sup>The analysis presented here models the  $Na^+$ -substrate cotransporter as a  $Na^+$ -battery in series with a  $Na^+$ -conductance, as previously described by Frömter [65]. This model appears to be superior to a current source model (see for example reference [31]), because even though the cotransport system showed saturation with the increase in the transmembrane chemical gradient of  $Na^+$ , the transport activity was sensitive to changes in electrical gradient of  $Na^+$  around the resting mem-

the Na<sup>+</sup>-cotransport pathways may be the predominant component of apical Na<sup>+</sup> conductance. This remains to be further substantiated.

It should be pointed out that the calculation of apical potassium transference number is less reliable than the similar calculation of basolateral potassium transference number. According to Equation 5.5, the  $E_{ap}$  values are subject to large variation with relatively small errors of  $V_{bl}$  and  $V_{ap}$ <sup>9</sup>, because the apical resistance is fourfold higher than the basolateral resistance (see Table 3.1). Therefore, the above calculation can only be regarded as a first-order estimate.

### 5.1.5 Loop current

The electric circuit model presented in Figure 5.1 predicts that whenever  $E_{ap} + E_{bl} \neq 0$ , there is a closed loop current  $I_{loop}$  given by [31]:

$$I_l = -\frac{E_{ap} + E_{bl}}{R_{ap} + R_{bl} + R_{te}} \quad (5.16)$$

With the available  $E_{ap}$ ,  $E_{bl}$  and resistance data,  $I_{loop}$  was calculated to be:

$$\begin{aligned} I_l &= -\frac{20.0 - 82.0}{369 + 92 + 13} \\ &= 131 \mu\text{A}/\text{cm}^2 \end{aligned} \quad (5.17)$$

Since it was assumed that  $E_{te} = 0$  in the present symmetrical perfusion system (see footnote on page 98),  $I_{loop}$  can also be expressed by the following equation

brane potential value ( $-60$  to  $-70$  mV) [143]. In addition, inhibition of the cotransport system increased apical membrane resistance by over twofold [143]. Therefore, this transport system looks more like a battery in series with a resistor than a constant current source with infinite internal resistance.

<sup>9</sup>The error of  $V_{ap}$  originates from the experimental errors of both  $V_{bl}$  and  $V_{te}$ , because  $V_{ap}$  is calculated from  $V_{bl}$  and  $V_{te}$  (see footnote on page 101).

according to the equivalent circuit model (Figure 5.1):

$$I_1 = -V_{te}/R_s \quad (5.18)$$

In a leaky epithelium like proximal tubules, the shunt resistance is a good approximation of transepithelial resistance, and Equation 5.18 can be rewritten as

$$I_1 = -V_{te}/R_{te} \quad (5.19)$$

Therefore,  $I_{loop}$  can be directly obtained from the experimental data ( $V_{te}$  and  $R_{te}$ ). This loop current is the same expression as the *equivalent short-circuit current* ( $I_{sc}$ ) introduced by Greger [78], although the two currents are conceptually different. As pointed out by Greger, the  $I_{sc}$  is linked stoichiometrically to the rate of electrogenic  $\text{Na}^+$  reabsorption. The value obtained from this study ( $131 \mu\text{A}/\text{cm}^2$ ) is smaller than that obtained from thick ascending limbs (200 to  $600 \mu\text{A}/\text{cm}^2$ ), probably because electrogenic  $\text{Na}^+$  reabsorption accounts for a much larger proportion of total  $\text{Na}^+$  reabsorption in thick ascending limbs than in proximal tubules [78].

Results from this study and many others (for example, see [15] and [143]) illustrate that removal of organic substrate from tubular lumen abolishes the  $V_{te}$  (and  $I_{loop}$  according to Equation 5.19), suggesting that electrogenic  $\text{Na}^+$  reabsorption in this segment reflects solely the  $\text{Na}^+$ -substrate cotransport. Significant increase in apical membrane resistance was also observed following luminal substrate removal in salamander [143] and rat [65] proximal tubules. It appears that removal of luminal substrates reduces the luminal  $\text{Na}^+$  conductance to a negligible level, with the portion of  $\text{K}^+$  conductance becoming predominant (see Section 5.1.4). It follows that both luminal and basolateral membrane potentials are determined by the Nernst

potential of transmembrane  $K^+$  gradient. These two membrane potentials therefore would cancel out, causing both loop current and  $V_{te}$  to vanish.

In summary, the data analysis presented in this section confirms that the basolateral membrane of mouse proximal straight tubules is predominantly permeable to  $K^+$ . The basolateral membrane potential can be approximated by the  $K^+$ -diffusion potential. The contribution of the  $Na^+$ -diffusion potential to the basolateral membrane potential is negligible. The analysis of apical ionic permeability by means of ion-substitution experiments is complicated by the tight electrical coupling between the apical membrane, the basolateral membrane, and the tight junction. A semiquantitative calculation suggests that potassium conductance may account for a large portion of the apical membrane conductance. But unlike the basolateral membrane, there is also a significant  $Na^+$  permeability in the apical membrane, which may largely be accounted for by  $Na^+$ -coupled cotransport systems. The paracellular pathway has a very low  $K^+$  permeability. Thus, the transepithelial  $K^+$  gradient can not generate a transepithelial potential. However, we can not exclude the contribution of a local  $NaCl$  gradient to the transepithelial potential. When the diffusional potential of this local salt gradient is *assumed* to be zero, the transepithelial potential can be accounted for by an electrogenic  $Na^+$ -transport current flowing across the tight junction.

## 5.2 Effects of Hypoxia and Ischemia

Renal ischemia leads to reduction in tubular reabsorption of  $Na^+$  and water upon reperfusion (see Section 1.1.2). However, information on tubular transport during

and immediately after hypoxia or ischemia is limited. Effects of hypoxia and ischemia on the electrophysiological characteristics of mouse proximal straight tubules are discussed below.

### **5.2.1 Basolateral membrane potential and $K^+$ transference number**

In proximal straight tubules, the basolateral cell membrane is highly permeable to  $K^+$  (see Section 5.1.3). Therefore, a large portion of basolateral cell membrane potential difference ( $V_{bl}$ ) can be attributed to the  $K^+$  equilibrium potential. In this study, neither  $V_{bl}$  nor  $t_{K(bl)}$  was affected following 20-min warm hypoxia (Figures 3.2 and 3.3a) or ischemia (Figures 3.6 and 3.5a), suggesting that the hypoxic and/or ischemic insult resulted in no permanent alteration of the transmembrane  $K^+$  permeability and concentration gradient.

The  $V_{bl}$  was also continuously monitored during the 20-min hypoxic and ischemic perfusion periods. In about 75% of the tubules studied, there was no significant change in  $V_{bl}$  during the 20-min hypoxic perfusion. In the other 25% of tubules (4 out of 15),  $V_{bl}$  began to depolarize towards the end of hypoxic perfusion (Figure 3.1a, *insert*). This depolarization, which was reversible following control reperfusion, was very similar to the response produced by ouabain, suggesting that the  $Na^+,K^+$ -ATPase activity may be compromised during the hypoxic perfusion. It may be that ATP depletion in this group of tubules was more severe. This variation in  $V_{bl}$  response suggests differences in vulnerability to hypoxia among individual isolated tubular segments, or even among individual cells in a single tubule. From the assay of tubule ATP content, a 53% (ranging from 42% to 64%) reduction of cell ATP

was observed. The hypoxia-induced depolarization of  $V_{bl}$  may occur only in those tubules where a high percentage of ATP depletion was achieved. In this context, it is worthwhile to point out that in another ongoing study in our laboratory, in which proximal tubules are subjected to organic substrate deprivation, a 66% decrease in cellular ATP is observed before any significant depolarization of  $V_{bl}$  is recorded (Morgunov, personal communications).

Bilateral perfusion with the ischemic Ringer immediately induced massive depolarization of  $V_{bl}$  in all 20 tubules studied (Figure 3.5). Such a depolarization is not unexpected because the ischemic Ringer has a high concentration of  $K^+$  (20 mM, Table 2.1). In addition, a decrease in pH (7.0 in ischemic Ringer) may also initiate a depolarization of  $V_{bl}$  (possibly through the activation of  $Na^+-(HCO_3^-)_3$  cotransporter [1]). This depolarization of  $V_{bl}$  may have masked any effect of low  $P_{O_2}$  on  $V_{bl}$ , as observed in 25% of tubules subjected to hypoxia (Figure 3.1). Nevertheless, judging from the complete recovery of both  $V_{bl}$  and  $t_{K(bl)}$  immediately following the 20-min ischemic perfusion, it appears that, compared with the hypoxic experiment, exposure to an simulated ischemic environment does not initiate irreversible damage to tubule cells.

### 5.2.2 Intracellular $Na^+$ activity

$a_i^{Na}$  is good indicator of alterations in tubular transport. Because of the rapid transcellular  $Na^+$  traffic, even a slight imbalance in apical entry and basolateral exit may result in either accumulation or depletion of  $a_i^{Na}$  [175, 176]. For example, removal of organic substrates from luminal perfusate decreased  $a_i^{Na}$  (Figure 3.5, also see [143]),

whereas inhibition of basolateral  $\text{Na}^+$ -extrusion with ouabain increased  $a_i^{\text{Na}}$  (Figure 3.10)<sup>10</sup>. The well maintained  $a_i^{\text{Na}}$  following 20-min hypoxic or ischemic perfusions (Figures 3.3 and 3.5) would suggest that either 1) apical  $\text{Na}^+$ -entry and basolateral  $\text{Na}^+$ -exit mechanisms were intact, or 2) both were compromised to a same extent. Further experimental evidence would indicate that the first possibility is more likely (see Section 5.2.3). In contrast to this study, a significant increase in  $a_i^{\text{Na}}$  was observed in a whole-kidney ischemic preparation of rat within 20 min [132], suggesting that the *in vitro* perfused proximal tubules are more resistant to hypoxic or ischemic insult than proximal tubules *in situ*.

Continuous monitoring of  $a_i^{\text{Na}}$  during the 20-min hypoxic perfusion revealed no change in  $a_i^{\text{Na}}$  in all six tubules studied. Simultaneous monitoring of membrane potential in these tubules indicated that the  $V_{bl}$  was also stable throughout the experimental course. It appears that all the tubules used in the  $a_i^{\text{Na}}$  experiment belonged to the majority (75%) group described in Section 5.2.1. In contrast to hypoxic perfusion, a decrease in  $a_i^{\text{Na}}$  during ischemic perfusion was observed (Figure 3.5). Such a decrease in  $a_i^{\text{Na}}$  may result from the effect of high  $\text{K}^+$  content in the ischemic solution. High extracellular concentration of  $\text{K}^+$  depolarizes cell membrane, reducing the driving force for  $\text{Na}^+$  entry and reducing  $a_i^{\text{Na}}$ . Indeed, reduction in  $a_i^{\text{Na}}$  was also observed with bath application of 20-K<sup>+</sup> Ringer in this study (Figure 3.5) and in salamander proximal tubules [143]. Considering the accumulation of  $\text{Na}^+$  inside the

---

<sup>10</sup>It is noteworthy that the transcellular  $\text{Na}^+$  flux described here may set up an  $\text{Na}^+$  concentration gradient across the cytosol. In regions close to the basolateral membrane, where the tips of  $\text{Na}^+$  electrodes are most likely located, the  $\text{Na}^+$  concentration may be the lowest. Therefore,  $a_i^{\text{Na}}$  measured by means of  $\text{Na}^+$ -selective microelectrodes may be an underestimate of average cytosolic  $\text{Na}^+$  activity.

cell as one of the mechanisms of ischemic injury, high extracellular  $[K^+]$  may have a beneficial role by decreasing  $a_i^{Na}$ . Indeed, many preservation solutions clinically used for kidney preservation contain high concentrations of  $K^+$  [131]. However, as discussed in Section 6.2.3, high  $K^+$  content in preservation solutions has its own pitfalls, especially at warm temperatures.

### 5.2.3 Transepithelial potential and tubular resistances

A 40% reduction in both  $V_{te}$  and  $R_{te}$  was observed immediately following the 20-min hypoxic and ischemic perfusions. In agreement with these observations, in a chemical ischemic model (ATP depletion by Antimycin A [42]) in cultured LLC-PK<sub>1</sub> monolayer, the transmonolayer electrical resistance was also reduced to 60% of control after 2-h exposure to 0.1  $\mu$ M Antimycin A. A closer look at the experimental data from the present study revealed a significant correlation between the  $V_{te}$  change and the  $R_{te}$  change for each tubule studied (Figure 3.9). Such a relationship implies that even with the reduction in both electrical potential and resistance across the tubular epithelium following the hypoxic and ischemic perfusions, the loop current across the paracellular pathway ( $I_{loop} = -V_{te}/R_{te}$ ) remains unchanged. As discussed in Section 5.1.5, the loop current is closely associated with electrogenic  $Na^+$  reabsorption in proximal tubules. It follows that the  $V_{te}$  and  $R_{te}$  data predict an unaltered transcellular electrogenic  $Na^+$  transport following 20-min *in vitro* hypoxic and ischemic perfusions. This prediction is in agreement with the  $V_{bl}$ ,  $t_{K(bl)}$ , and  $a_i^{Na}$  findings, and suggests a lack of cell damage following the hypoxic or ischemic insult.

To further prove that the functional integrity of tubular cells is not affected

by the 20-min hypoxic or ischemic perfusion, the cell membrane resistances were directly measured using electrical cable analysis. Because such an analysis requires a large amount of experiment data, which are very difficult technically to obtain, cell membrane resistances were only compared between control and postischemic tubules. The membrane resistance data for control tubules obtained in this study (Table 3.1) are comparable to those obtained using other methods [65], confirming the validity of this analysis. Twenty minutes of ischemic perfusion did not significantly alter  $R_{ap}$  and  $R_{bl}$  in this model system. Such a finding, combined with the findings that the potential differences and the ionic gradients across cell membranes were restored, would indicate that electrogenic ionic flux across the membranes was not compromised. This conclusion is in agreement with the previous conclusion that  $I_{loop}$  across the paracellular pathway was unchanged (see above). In other words, the experimental data demonstrate separately that the ionic current flowing through two parts of a closed circuit, one across cell membranes and one across shunt, is not altered following the ischemic insult.

However, the unaltered electrogenic transport after 20 min of hypoxia and ischemia does not imply that the overall transepithelial transport was not affected. Proximal tubular reabsorption consists of both electrogenic and electroneutral transport [97]. Since electrogenic reabsorption is generally believed to contribute a small portion of total reabsorption<sup>11</sup>, we have to consider potential changes in electroneu-

<sup>11</sup>Net sodium flux ( $J_{Na}$ ) across the rat proximal tubule was estimated according to the volume flux ( $J_v$ ) data ( $J_v = 2 \text{ nL/mm/min}$ ) [2, 44]. Assuming the fluid reabsorption is iso-osmotic in this segment,  $J_{Na}$  was calculated as

$$J_{Na} = 140\text{mEq/L} \times 2\text{nL/mm/min} = 280\text{pEq/mm/min} \quad (5.20)$$

Taking the electrogenic  $\text{Na}^+$ -transport current ( $I_g$ ) as 28 pEq/mm/min [65], this current only

tral transport. In fact, hypoxia and ischemia made the leaky proximal tubule even more leaky, as indicated by the reduction in  $R_{te}$ . This would inevitably increase electroneutral backleaks, and therefore decrease the efficiency of total reabsorption. In other words, changes in net reabsorption do not necessarily parallel changes in electrical current or potential difference across the epithelium. Consistent with this concept, Hanley [87] has reported that the decrease in fluid reabsorption ( $J_v$ ) was greater than the decrease in transepithelial potential difference in proximal tubules of the rabbit kidney following 60 min of total ischemia.

As mentioned in Section 5.1.5, in a leaky epithelium like the proximal tubule, transepithelial resistance ( $R_{te}$ ) is a good approximation of shunt resistance ( $R_s$ ), which consists of two components: tight junction ( $R_{tj}$ ) and lateral interspace resistances ( $R_{lis}$ ) [33]

$$R_{te} \cong R_s = R_{tj} + R_{lis} \quad (5.21)$$

In mammalian proximal straight tubules  $R_{lis}$  is only 20% of  $R_s$  (refer to Appendix A). Therefore, decreases in  $R_s$ , especially when over 20%, are mainly attributable to decreases in  $R_{tj}$ . This prediction is in agreement with the morphological findings reported by Molitoris' group suggesting damage to the tight junction using *in vivo* [138] or *in vitro* [42] ischemic models.

In summary, the electrophysiological observations suggest that the proximal tubule cells are capable of maintaining their functional integrity after a 20-min exposure to oxygen tension averaging 4 mmHg. In contrast, the tight junction appears to be more susceptible to low  $P_{O_2}$  than transcellular membrane transport components. 

---

accounts for 10% of total  $Na^+$  transport ( $I_g/J_{Na} = 0.1$ ).

Damage to the tight junction may increase the leakiness of the tubular epithelium and reduce the total transepithelial transport.

### 5.3 Effects of Cooling

Previous studies in both mammalian [24, 38, 171, 172, 173, 200] and amphibian [144, 162] proximal tubules have documented a reduction of fluid transport and depolarization of transepithelial potential during cooling. However, the effects of cooling on individual barriers of the proximal tubules have only been analyzed in amphibian preparations [144, 162]. In this section, the temperature sensitivities of apical and basolateral membranes of mouse proximal straight tubules are discussed.

#### 5.3.1 Cooling to 22°C

Cooling to 22°C resulted in a depolarization of both  $V_{bl}$  and  $V_{te}$  (Figure 4.2), reduction in  $t_{K(bl)}$  (Figure 4.2), and an increase in cell membrane and transepithelial resistances (Table 4.1). Using the experimentally obtained potential and resistance data at 22°C, the diffusional potentials across the apical and the basolateral membranes were calculated according to Equations 5.5 and 5.6, respectively:

$$E_{ap} = +23.2 \text{ mV} \quad (5.22)$$

$$E_{bl} = -74.6 \text{ mV} \quad (5.23)$$

The  $E_{bl}$  calculated above is less negative than the  $E_{bl}$  derived from 37°C data (Equation 5.7). This difference may be accounted for by 1) a reduction of transmembrane  $K^+$  gradient, or 2) a decrease in the relative membrane conductance to  $K^+$  ( $t_{K(bl)}$ ). Experimentally, a decrease in  $t_{K(bl)}$  was observed during the cooling to

22°C (Figure 4.2). If the correcting procedures illustrated in Equations 5.9 to 5.11 are used, the corrected  $t_{K(b)}$  ( $t'_{K(b)}$ ) can be derived as:

$$t'_{K(b)} = 0.72 \quad (5.24)$$

Therefore, cooling from 37°C to 22°C led to a decrease in  $t'_{K(b)}$  from 0.83 (Equation 5.11) to 0.72. Assuming that the transmembrane  $K^+$  gradient is unchanged after cooling to 22°C, the reduction in  $t'_{K(b)}$  itself would account for a depolarization of  $E_{bl}$  by 11.8 mV ( $-78 \times 0.72 + 82 \times 0.83 = 11.8$  mV, where  $E_K$  of  $-82$  mV was obtained from Equation 5.8). This is comparable to the 7.4-mV depolarization of  $E_{bl}$  calculated according to Equations 5.23 and 5.7. Such a comparison implies that membrane depolarization at 22°C is mainly due to a reduction of the relative membrane permeability to  $K^+$ . The reduction in  $t_{K(b)}$  was also observed when the  $Na^+,K^+$ -ATPase was inhibited with ouabain [200], suggesting a correlation between the inactivation of the  $Na^+,K^+$ -ATPase (either by ouabain or by cooling) and the decrease in  $K^+$  permeability.

One the other hand, the apical diffusional potential was not dramatically affected by cooling to 22°C (23.2 mV at 22°C, Equation 5.22 versus 20.0 mV at 37°C, Equation 5.12). However, cooling to 22°C increased the apical membrane resistance by nearly fourfold (see Table 4.1). It appears that the various conductive pathways to ions such as  $Na^+$  and  $K^+$  in the apical membrane decrease proportionally during cooling, so that the  $E_{ap}$  remains stable.

According to Equation 5.19, the loop current at 22°C can be calculated:

$$I_l = 27 \mu A/cm^2 \quad (5.25)$$

This value is only 21% of the 37°C-control  $I_{\text{loop}}$  (Equation 5.17), suggesting that electrogenic  $\text{Na}^+$  transport is considerably reduced, but is not completely shut down. Because of the temperature sensitivity of the  $\text{Na}^+, \text{K}^+$ -ATPase [45, 62], cooling will inevitably reduce the activity of basolateral  $\text{Na}^+$  extrusion. It appears that proximal tubular cells possess ways to coordinate the transport activity in apical and basolateral membranes, so that a reduction of basolateral  $\text{Na}^+$  exit is accompanied by a reduction of apical  $\text{Na}^+$  entry, or *vice versa*. As a result, with the decrease in transcellular  $\text{Na}^+$  flux, the apical entry of  $\text{Na}^+$  still matches exactly the basolateral exit of  $\text{Na}^+$ . This conclusion is based on the experimental observation that the intracellular  $\text{Na}^+$  activity remained stable during the cooling period (Figure 4.3).

A previous study in perfused rabbit proximal straight tubules demonstrated complete elimination of both  $V_{\text{te}}$  and volume reabsorption during cooling to 21°C [173]. The analysis in the present study not only demonstrates a severely compromised tubular transport at 22°C, but also suggests that such a reduction in transport may represent a protective measure whereby cells preserve their functional integrity.

### 5.3.2 Cooling to 4°C

Compared with those recorded at 22°C, electrophysiological data recorded at 4°C deviate further from the 37°C-control (see Section 4.1). According to Equations 5.5 and 5.6, the diffusional potentials across the apical ( $E_{\text{ap}}$ ) and the basolateral ( $E_{\text{bl}}$ ) membranes can be derived from the experimentally measured membrane potentials and resistances as follows:

$$E_{\text{ap}} = +16.9 \text{ mV} \quad (5.26)$$

$$E_{bl} = -16.9 \text{ mV} \quad (5.27)$$

Note that because the  $V_{te}$  is zero, the  $V_{bl}$  and  $V_{ap}$  are perfect representations of  $E_{bl}$  and  $E_{ap}$ , respectively.

In the basolateral membrane, the dramatic increase in membrane resistance is probably due to the inactivation of  $K^+$  channels, because the  $t'_{K(bl)}$  decreased from 0.83 at 37°C to 0.32 at 4°C<sup>12</sup>. This reduction of  $t'_{K(bl)}$  may partially account for the depolarization of  $E_{bl}$ . In addition, an accumulation of intracellular  $Na^+$  (Figure 4.3) suggests that the depolarization of  $E_{bl}$  may also be due to a loss of intracellular  $K^+$ . Such a disturbance in ionic balance indicates that the activity of the  $Na^+, K^+$ -ATPase is severely compromised at 4°C that even with the dramatically reduced membrane ion permeabilities, the  $Na^+, K^+$ -ATPase is still unable to prevent the loss of intracellular  $K^+$  or the gain of intracellular  $Na^+$ . A similar increase in  $a_i^{Na}$  at temperatures below 8°C was also observed in rat medullary collecting duct, but not in medullary thick ascending limb [157, 183]. In amphibian proximal tubules, cooling to 5.5°C dramatically reduced tubular  $Na^+$  transport, but did not affect intracellular  $Na^+$  content [144]. These differences in the  $a_i^{Na}$  response to cooling may relate to the difference in temperature sensitivities of either the  $Na^+, K^+$ -ATPase or ionic permeabilities among various mammalian and amphibian preparations [144].

The apical membrane  $E_{ap}$  was only slightly lower than the 37°C control and the 22°C value. When the  $R_{ap}$  value at 22°C and at 4°C are compared, no significant difference is observed (Table 4.1), suggesting that no further decrease in total ionic permeability occurs as the preparation is cooled from 22°C to 4°C. However, the in-

---

<sup>12</sup> $t'_{K(bl)}$  equals  $t'_{K(bl)}$  at 4°C.

formation provided in this study is not sufficient to indicate if there is a change in the relative permeability for each individual ion. The fact that the diffusional potential across the apical membrane remained unchanged even after the loss of intracellular ionic balance would suggest that there is a certain change in the contributions of various ionic permeabilities to the total membrane conductance.

Cooling to 4°C abolished transepithelial potential. The loop current, as calculated according to Equation 5.19, was zero at 4°C, suggesting that the electrogenic Na<sup>+</sup> transport was completely blocked.

In summary, cooling to 22°C led to a slight depolarization of basolateral diffusional potential, which can be attributed to a reduction in the relative contribution of K<sup>+</sup> permeability to the total basolateral membrane conductance. Cooling to 22°C also dramatically increased both apical and basolateral membrane resistances and decreased transepithelial electrogenic Na<sup>+</sup> transport. The decrease in electrogenic Na<sup>+</sup> transport at 22°C, however, was not accompanied by disturbances of intracellular ionic balance. It appears that tubule cells are able to sacrifice their transport activity for their functional integrity at 22°C. On the other hand, cooling from 22°C to 4°C led to a further increase in the basolateral membrane resistance, whereas no further increase in apical membrane resistance was observed. This observation suggests that the apical ionic conductance is more sensitive than the basolateral conductance to cooling. Such a difference in temperature sensitivity would be beneficial for tubule cells to maintain their low intracellular Na<sup>+</sup> level, because with cooling, apical Na<sup>+</sup> entry is reduced before the basolateral pump-leak system [175, 176] is impaired. However, such a protective measure was no longer effective at 4°C, because

even with the decrease in ionic conductance and the absence of transcellular  $\text{Na}^+$  transport, the intracellular  $\text{Na}^+$  level still increased gradually at  $4^\circ\text{C}$ . This would suggest that the activity of the  $\text{Na}^+, \text{K}^+$ -ATPase was suppressed to such a level that it failed either to sustain any transport or to preserve cellular ionic balance.

# Chapter 6

## DISCUSSION II: Tubular Metabolism and Morphology

Kidney tubules may encounter many challenges at all stages of renal transplantation. In early clinical and experimental studies, much effort was directed towards reducing the adverse effects of cold ischemia and extend the cold-storage time [19, 50]. Recently, it became increasingly evident that two transient phases, cooling and re-warming, contributed significantly to tubular injury [28, 131]. This study examines two aspects of the tubular injury. First, the potential threat of short-term warm hypoxia and ischemia on proximal tubules in the cooling and rewarming phases, and second, reperfusion injury during implantation due to the presence of preservation solutions at warm temperatures.

### 6.1 Effects of Hypoxia and Ischemia

It has been documented by *in vivo* experiments that both morphological and functional alterations can occur in proximal tubules within 15 min from interruption of renal blood flow [72, 115, 141]. A 20-min period of hypoxia and ischemia was chosen in the present study, to detect sublethal changes in tubular morphology and

metabolism.

### 6.1.1 Morphological changes

The ultrastructural integrity of the proximal tubule is well preserved under the *in vitro* hypoxic and ischemic conditions in the present study. The only prominent change observed in tubules perfused with hypoxic or ischemic Ringer solutions appears to be the change in the appearance of vacuoles suspected of being lysosomes. Several distinct cytoplasmic vacuoles containing organelles, suggestive of autophagy, were observed (see Figure 3.12). In addition, numerous myeloid bodies were also observed in tubular cells following the hypoxic or ischemic insult.

Morphological changes in proximal tubules occurring early (15 to 30 min) in mild renal ischemia *in vivo* include clumping of the nuclear chromatin, distortion of microvilli, and changes in the shape and the redox state of mitochondria, as described by Trump and colleagues (see [118] for a review). These changes were not evident in the perfused tubule system used in this study, in which tubules were fixed after a 5-min reperfusion period following a 20-min hypoxic or ischemic period. Increase in lysosome-like structure seen in the present study, however, has been observed previously in proximal tubules recovering from 30 to 60 min of ischemia (stage B<sub>2</sub> and B<sub>3</sub> in proximal straight tubules [72] and stage A<sub>1</sub> in proximal convoluted tubules [73]). Formation of myeloid bodies following ischemia and reperfusion *in vivo* has also been observed, and has been associated with the internalization and digestion of the microvilli [73]. In the present study, however, more numerous and larger myeloid bodies were observed in the absence of major damage to the microvilli, suggesting

that these structures may be different in origin. The myeloid bodies observed in this study showed more similarity to those induced by aminoglycoside antibiotics, which have been reported to interfere with the function of lysosomal enzymes (see [105] for a review). It is not clear at this point if hypoxia and ischemia share the pathogenesis of aminoglycoside nephrotoxicity with respect to lysosomal malfunction.

In summary, it appears that proximal tubules in the present tubule-perfusion model show a slightly different spectrum of ischemic and reperfusion injury compared to that observed in *in vivo* ischemic models, suggesting differences between the two model systems in the initial metabolic and functional states of tubular cells, and in the ischemic environments with which the cells interact.

### 6.1.2 Metabolic changes

Proximal straight tubules ( $S_3$  segments) are marginally oxygenated even in intact kidneys, rendering them vulnerable to ischemic insult [36]. Studies using *in vivo* ischemic models and transplantation models indicate that the  $S_3$  segment is one of the most susceptible proximal tubular segment to ischemic injury [6, 73, 58, 201]. Single isolated perfused proximal straight tubules in the present model system are less susceptible to hypoxic and ischemic insults than tubules in whole kidney preparations. This suggests that the hypoxic/ischemic Ringer solution may not completely mimic the tubular environment in an ischemic whole kidney for the following two reasons. 1) Because of the more efficient  $O_2$  delivery in the present *in vitro* model,  $P_{O_2}$  in the hypoxic/ischemic solution may still be above the critical level. In isolated whole kidney experiments, cortical  $P_{O_2}$  levels dropped rapidly to virtually zero

within 30 sec following the termination of perfusion [121]. The bath  $P_{O_2}$  level of 4 mmHg in the present study is clearly less severe and may be above the lethal  $P_{O_2}$  that produces cell injury. In this context, it is worthwhile to mention that a study using suspensions of isolated rat kidney cells demonstrated that half-maximal oxidation of cytochromes relative to aerobic cells occurred at a  $P_{O_2}$  level of 4  $\mu$ M (or 3 mmHg) [9]. 2) This simulated ischemic condition, although taking into account factors such as the  $K^+$  and lactate accumulation, low pH, and substrate deprivation, is only a partial simulation of renal ischemia *in vivo*. Other constituents that may catalyze the process of cell injury (e.g. enzymes or hormones) need to be accounted for. Extended exposure (beyond 20 min) must also be addressed to evaluate the time course of potential tubular cell injury.

The data from tubule ATP assays support the notion that tubules perfused with hypoxic Ringer solution are marginally oxygenated. A 50% reduction of tubular ATP content was observed following a 20-min perfusion with hypoxic Ringer (see Figure 3.13a). This ATP depletion was less severe than that observed in whole-kidney ischemic model systems [16, 90, 190], suggesting that a residual ATP production was present during the hypoxic perfusion. Acidosis is unlikely to develop under this condition, because lactate produced by glycolysis (if any) is washed away by a well-buffered perfusion solution. In addition,  $H^+$  extrusion by  $H^+$ -ATPase remains fully active with 50% reduction of  $[ATP]_i$ , because  $K_m$  of the  $H^+$ -pump is approximately 80  $\mu$ M [161]. On the other hand, when acidosis and hyperkalemia were imposed by perfusion with ischemic Ringer, tubular ATP content was better preserved (Figure 3.13b). This lack of significant decrement of  $[ATP]_i$  further emphasizes that

the present *in vitro* ischemic model may not mimic the true pathological condition.  $[ATP]_i$  was better preserved due to the high- $K^+$  content of the ischemic Ringer. As shown in Figure 3.5, depolarization of the cell membrane and the transepithelial potentials and a decrease in the intracellular  $Na^+$  activity were observed during the ischemic perfusion. Because the  $Na^+,K^+$ -ATPase activity is directly regulated by  $Na^+$  in the range of physiological intracellular concentration ( $K_m = 10$  to  $20$  mM [204]), ischemic perfusion may lead to a reduction in the activity of  $Na^+,K^+$ -ATPase and subsequent curtailment of ATP expenditure (see Section 1.1.1). A low pH in the ischemic Ringer could also be protective. In an *in vitro* model of hypoxia in isolated rabbit proximal tubule suspensions [205], it has been shown that the depletion of cellular ATP by hypoxia was significantly less in tubule suspensions protected by an acidic pH.

In suspensions of isolated rabbit proximal tubules, the activity of  $Na^+,K^+$ -ATPase depends on  $[ATP]_i$  in a linear fashion, showing no saturation up to  $4$  mM [182]. This is in sharp contrast to the results obtained using lysed membranes of proximal tubular cells or digitonized tubules —  $K_m$  for  $[ATP]_i$  of  $0.3$  to  $0.4$  mM was obtained under these experimental conditions [182, 3]. Such a discrepancy would suggest that in intact cells, there is a steep  $[ATP]_i$  gradient between the mitochondria, where ATP is produced, and the sub-basolateral-membrane compartment, where ATP is hydrolyzed by the  $Na^+,K^+$ -ATPase. If  $[ATP]_i$ -dependence of  $Na^+,K^+$ -ATPase observed in suspensions of rabbit proximal tubules holds true for the present model system, one would expect a proportional reduction in  $Na^+,K^+$ -ATPase activity *during* the hypoxic perfusion. Since membrane depolarization during hypoxia was only

observed in a subpopulation of tubules where there may have been a high percentage of ATP depletion (see Section 5.2.1), it appears that there may exist a certain threshold-activity of the  $\text{Na}^+$  pump above which cells are able to maintain their ionic balance, presumably by reducing membrane ionic permeabilities. It is noteworthy that the ATP-dependent  $\text{K}^+$  conductance is not likely to be activated by a mild reduction in  $[\text{ATP}]_i$ , because in whole cell preparations, this channel opens only if  $[\text{ATP}]_i$  drops to values below 2 mM [104].

It was concluded from the discussion in Section 5.2 that 20 min of hypoxic and ischemic perfusion at 37°C damaged the tight junction. The fact that reduction in tubular ATP content was only observed during the hypoxic perfusion, but not during the ischemic perfusion, implies that ATP depletion may not be directly linked to the damage to the tight junction. This is contradictory to the study using confluent LLC-PK<sub>1</sub> cells [42], in which 2 hours of ATP depletion led to the opening of the tight junction. It is possible that both ATP depletion and low  $P_{\text{O}_2}$  act in concert to exert the damaging effects on tight junctions. Possible mediators, other than ATP depletion, of low- $P_{\text{O}_2}$ -induced damage of tight junction are alterations of a variety of intracellular second-messenger systems [12, 20]. In addition, the  $\text{Ca}^{2+}$  concentration (2 mM) in the Ringer solution used in this study is higher than serum  $\text{Ca}^{2+}$  level of 1.2 mM. Although this hypercalcemic situation alone has no effect on the integrity of the transepithelial resistance (see Figure 3.1.3), it may have a negative influence on the tight junction when cell metabolism and transport are altered by the ischemic perfusion. In this context, it is of interest to point out that the  $\text{Ca}^{2+}$ -ATPase on the basolateral membrane, which participates in the maintenance of a low intracellular

$\text{Ca}^{2+}$  concentration, is more sensitive to ATP depletion than the  $\text{Na}^+, \text{K}^+$ -ATPase is ( $K_m = 3 \text{ mM}$  for  $\text{Ca}^{2+}$ -ATPase [59] compared to  $0.4 \text{ mM}$  for  $\text{Na}^+, \text{K}^+$ -ATPase [181], both assayed in lysed-cell preparations). Therefore, with hypercalcemia, it is possible that even a slight reduction of  $[\text{ATP}]_i$  may result in cytosolic  $\text{Ca}^{2+}$  overload. The relationship between intracellular  $\text{Ca}^{2+}$  concentration and renal tubule injury certainly represents an interesting issue for further investigation.

In summary, this part of the study demonstrates the successful survival of epithelial cells of single isolated perfused proximal tubules exposed to oxygen tension averaging  $4 \text{ mmHg}$ . The tight junction appears to be more susceptible to low  $P_{\text{O}_2}$  than transcellular membrane-transport components. A decrease in transepithelial resistance precedes noticeable cell injury. Recent studies using renal cell cultures reported that significant cell injury was only observed after 20 min or longer of intracellular ATP depletion [10, 42, 128]. However, decrease in transepithelial resistance was detectable between 2 to 20 min [42, 128].

## **6.2 Effects of Temperature and Preservation Solutions**

### **6.2.1 Maintenance of cell volume at $37^\circ\text{C}$**

According to the Donnan equilibrium theory [55], the presence of negatively charged, cell-membrane impermeable macromolecules in the intracellular compartment results in the accumulation of  $\text{K}^+$  ion inside the cell.  $\text{K}^+$  is also accumulated because of the activity of the  $\text{Na}^+, \text{K}^+$ -ATPase. The Donnan system, however, is not a true equilibrium state, because the cell interior has a higher osmolarity. The "Double

Donnan” theory states that the transmembrane osmotic gradient is counterbalanced by  $\text{Na}^+$  ions, which are abundant in the interstitial fluid. The  $\text{Na}^+$  ion is an effective osmotic agent because it is constantly extruded from the cell by the  $\text{Na}^+, \text{K}^+$ -ATPase, making this ion functionally impermeable across the cell membrane. Chloride is driven out of the cell by an inside negative-membrane potential to maintain the electrical neutrality [116, 127].

### **6.2.2 Effects of temperature on cell volume**

Despite the net gain in  $a_i^{\text{Na}}$  at  $4^\circ\text{C}$ , the present study showed no significant increase in cell volume. It is generally believed that entry of  $\text{Na}^+$  and  $\text{Cl}^-$  during the cooling phase causes cell swelling [19]. In our system, we observed cell shrinkage rather than swelling (Figure 4.5). This could be explained as follows: when  $\text{Na}^+, \text{K}^+$ -ATPase is inhibited, the net loss of  $\text{K}^+$  is faster than the net gain of  $\text{Na}^+$ , resulting in a net loss of intracellular osmolarity and subsequently causing cell shrinkage [77]. An initial decrease in cell volume has been documented following ouabain treatment at  $37^\circ\text{C}$  [123]. Cell volume decrease at  $4^\circ\text{C}$  can also be visualized with electron microscopy. This was accompanied by the appearance of flattened endocytic vacuoles in the cytoplasm (see Figure 4.6). However, the overall cellular ultrastructure appears to be normal. These observations are in agreement with the study by Trump and colleagues [193], in which significant ultrastructural effects of cold temperature ( $4^\circ\text{C}$ ) were only observed beyond 1 hour of cooling.

### 6.2.3 Effects of high-K<sup>+</sup> content in preservation solutions

Preservation solutions that mimic the intracellular ionic composition appear to be beneficial in prolonging cold storage of kidney *in vitro* [28]. Both EC and UW solutions are high in K<sup>+</sup> content and low in Na<sup>+</sup> content [28, 131]. The rationale for the beneficial effect of high-K<sup>+</sup> content in preservation solutions has not been documented experimentally. Theoretically, by preserving intracellular ionic composition, less energy would be expended to restore cellular ionic balance during the initial stage of rewarming. High-K<sup>+</sup> solutions may also prevent intracellular alkalization by the Na<sup>+</sup>/H<sup>+</sup> exchanger [28].

However, high extracellular K<sup>+</sup> content has dramatic effects on electrical activity of tubular cells. It dissipates the transmembrane K<sup>+</sup> gradient and hence cell-membrane potential. Because the cell membrane is much more permeable to K<sup>+</sup> than Na<sup>+</sup>, substitution of K<sup>+</sup> for Na<sup>+</sup> in the extracellular fluid also constitutes an osmotic threat to the cell volume. The entry of K<sup>+</sup> along with Cl<sup>-</sup>, the latter being accelerated because of the dissipation of inside-negative membrane potential, may result in cell swelling [207].

The effect of a high-K<sup>+</sup> solution on cell volume depends on cell membrane permeability to K<sup>+</sup>. The K<sup>+</sup> conductance of individual cell membranes ( $g_K$ ) can be estimated according to the experimentally measured K<sup>+</sup> transference number [ $t_{K(bl)}$  and  $t_{K(ap)}$ ] and membrane resistance data ( $R_{ap}$  and  $R_{bl}$ )

$$g_{K(ap)} = t_{K(ap)} / R_{ap} \quad (6.1)$$

Table 6.1: Estimated cell membrane  $K^+$  conductances<sup>a</sup>

Temperatures	37°C		22°C		4°C	
Barriers <sup>b</sup>	AP	BL	BL	BL	BL	BL
$g_K^c$	0.3	7.3	1.2	0.2		
$g_K'^{c,d}$	1.8	9.0	1.6	0.2		

<sup>a</sup>Calculated from membrane resistances ( $R_{ap}$  and  $R_{bl}$ ) and  $K^+$  transfer numbers [ $t_{K(ap)}$  and  $t_{K(bl)}$ ] according to Equations 6.1 and 6.2.

<sup>b</sup>AP, apical cell membrane; BL, basolateral cell membrane.

<sup>c</sup> $\times 10^{-3}$  mho/cm<sup>2</sup>.

<sup>d</sup>derived according to calibrated  $t'_{K(ap)}$  and  $t'_{K(bl)}$  data (see Sections 5.1.3 and 5.1.4).

$$g_{K(bl)} = t_{K(bl)} / R_{bl} \quad (6.2)$$

At 37°C, the basolateral cell membrane is highly permeable to  $K^+$  (Table 6.1). Therefore, bath perfusion with high- $K^+$  solutions is highly dangerous, for it can cause drastic cell swelling.

On the other hand, the apical cell membrane is much less permeable to  $K^+$  (Table 6.1). Accordingly, luminal perfusion of high- $K^+$  solutions should have a less effect on cell volume. Indeed, bath application of the high- $K^+$  EC solution led to dramatic cell swelling, whereas luminal application of the EC solution led to cell shrinkage instead (Figure 4.13).

Temperature modifies cell membrane permeability to  $K^+$ . As shown in Table 6.1, cooling to 22°C decreased the  $g_K$  of basolateral membrane ( $g_{K(bl)}$ ) to one-sixth of the  $g_{K(bl)}$  at 37°C. However, this value is still six times higher than the  $g_K$  of the apical membrane ( $g_{K(ap)}$ ) at 37°C. Cooling to 4°C further decreased the  $g_{K(bl)}$  to the

level of  $g_{K(ap)}$  at 37°C. These K<sup>+</sup> conductance data may partially explain the effects of EC solution on cell volume at the three different temperatures. EC perfusion at 37°C resulted in rapid cell swelling (Figures 4.11 and 4.13). Exposure to EC solution at 22°C also led to cell swelling, but after a 10-min delay (Figures 4.7 and 4.9). No cell swelling was observed in EC solution at 4°C for up to 1 hour (data not shown). However, one should be aware that the control of cell volume under such conditions depends not only on the membrane permeability to K<sup>+</sup>, but also on the effectiveness of membrane impermeants in the preservation solutions, as discussed in the following section. The relative contribution of each factor in preventing cell swelling is not clear.

#### **6.2.4 Effects of membrane impermeants in preservation solutions**

Because of the potential osmotic threat from the high-K<sup>+</sup> content in preservation solutions, membrane impermeants are added to the solutions to provide additional extracellular osmolarity, stabilizing the cell volume. Glucose is used as a membrane impermeant in the EC solution. Raffinose and lactobionate are added to the UW solution as membrane impermeants (Table 2.2).

Both EC and UW perfusion had no effect on cell volume in tubules perfused at 4°C for up to 1 hour. This is in part due to the beneficial effects of cold temperature in reducing membrane permeability to K<sup>+</sup> (Table 6.1). In addition, the presence of effective membrane impermeant in both solutions further ensured the stability of cell volume.

However, at 22°C, although cells were faced with similar osmotic threats from

the high- $K^+$  content in both EC and UW solutions, cell volume increased in tubules exposed to the EC solution (Figures 4.7 and 4.9) but not in tubules exposed to the UW solution (Figures 4.8 and 4.9). These data suggest that the membrane impermeants in UW solution are more effective than the glucose, the membrane impermeant in EC solution, in stabilizing the cell volume at 22°C. An explanation of this may be that glucose is membrane permeable at 22°C.

Tubular cells exposed to high- $K^+$  solutions at 37°C are at the highest risk of swelling because the basolateral membrane permeability to  $K^+$  is the highest at this temperature. However, no cell swelling was observed in UW solution (Figures 4.12 and 4.13), indicating that the membrane impermeants in this solution remain effective at 37°C. On the other hand, perfusion with EC solution (bath side or both sides) produced dramatic cell swelling (Figures 4.11 and 4.13). It appears that at 37°C, glucose is highly membrane permeable. The striking difference in cell volume changes between tubules perfused with EC and UW solutions was further supported by the ultrastructural study, as illustrated in Figure 4.14. Our data strongly support Andrews' and Coffey's observation that at 37°C, renal ischemia in the presence of EC solution was more detrimental to tubular morphology than simple ischemia in a rat *in vivo* model [7].

The opposite effect of lumen versus bath EC perfusion on cell volume (Figure 4.13) is in agreement with the observed difference in  $K^+$  conductance between apical and basolateral membranes (Table 6.1). In addition, the presence of glucose in the luminal perfusate may also be protective, because the glucose permeability across the apical membrane is substantially lower in the absence of a transmembrane  $Na^+$

gradient (10 mM of  $\text{Na}^+$  in the EC solution). The observed cell shrinkage with EC solution present in lumen only (Figure 4.13) could be accounted for by the hyperosmolarity of this solution. The difference of osmolarities between luminal EC solution (320 mOsm/L, Table 2.2) and bath Ringer solution (300 mOsm/L, Table 2.1) may lead to water flux from the bath to the lumen, increasing the hydrostatic pressure of the tubular lumen. This increase in luminal hydrostatic pressure decreases the thickness of the cell layer (i.e. cell volume) because the cells are compressed against the rigid basement membrane.

Both experimental [166] and clinical [79] renal transplantation studies suggest a better prognosis using EC-mannitol compared to normal EC as a preservation solution. In this study, substitution of glucose with mannitol greatly reduced cell swelling at 37°C (Figure 4.13), suggesting that mannitol is much less membrane permeable than glucose. Since mannitol and glucose have a similar molecular weight and polarity, the rates of simple diffusion across the cell membrane for these two molecules should be similar [56]. It appears that the high glucose permeability of the basolateral cell membrane is attributable to mechanisms other than simple diffusion, possibly carrier mediated transport systems [46, 110]. The superiority of EC-mannitol over normal EC solution for long-term (12 to 48 h) preservation of tubular morphology at 0 to 2°C has been demonstrated in an isolated kidney model [6]. In fact, replacing mannitol (182 MW) with a larger saccharide, sucrose (342 MW), is even more beneficial [6]. Several studies have also suggested that EC-mannitol is more effective than normal EC solution in preventing ischemic damage at 37°C [166, 189]. Similar results were obtained when sucrose was used as the

membrane impermeant [7]. These studies emphasize the importance of membrane impermeants in renal preservation solutions, and highlight Belzer and colleagues' choice of a large-molecular-weight anion (lactobionate, 358 MW) and saccharide (raffinose, 594 MW) as membrane impermeants in the UW solution [19].

Since the renal medulla utilizes glucose as its main metabolic fuel [210], does replacing glucose with mannitol affect glucose metabolizing segments of the nephron? As pointed out by Belzer and Southard [19], glucose in EC solution may have a negative influence on liver preservation by stimulating acidosis, because the liver has a high capability to metabolize glucose. It appears that providing metabolic substrates during cold ischemia does not improve the outcome of renal preservation. Raffinose in the UW solution is nonmetabolizable, so is mannitol in the EC-mannitol solution. Therefore, it may be justifiable from the metabolic point of view to replace glucose in the EC solution with mannitol.

### **6.2.5 Correlation between cell swelling and deterioration of transepithelial potential**

The reduction of  $V_{te}$  following EC perfusion at 22°C (Figure 4.10) and 37°C (Figure 4.15) suggests that tubular transport may be compromised due to the initial cell swelling associated with the exposure of the tubule to the EC solution. This could be accounted for by 1) the destruction of cell integrity, or 2) the damage to cell-to-cell junctions. Evaluation of vital dye uptake at the end of the experiments would be a simple and useful way to assess cell integrity. In fact, significant dye uptake was observed during reperfusion with dye-containing control Ringer solution in the lumen after a 20-min EC perfusion at 37°C. Minimal dye uptake was observed after

a 20-min EC perfusion at 22°C. These observations, however, are merely qualitative.

With electron microscopy, severe tubular cell damage was seen after 9 min of EC-perfusion followed by a 5-min control reperfusion. The cell damage, however, did not occur uniformly in a proximal tubule, but was limited to only one or two cells in any given cross section (Figure 4.16). Increasing EC-perfusion time to 20 min produced a more profound and uniform cell damage. On the other hand, cell integrity was better preserved after 10 min of UW-perfusion followed by a 15-min control reperfusion. Although UW perfusion for up to 20 min had little effect on the structural integrity of the tubular cells (Figure 4.14), numerous large vacuoles were detected under the light microscope immediately following control reperfusion. Normal morphology of cells appeared to be regained during the 15-min reperfusion period, although some large vacuoles persisted (Figure 4.16b). However, these vacuoles appear to have little effect on the electrical integrity of the tubular epithelium, because a nearly complete recovery of  $V_{te}$  was observed after 15 min of reperfusion. In addition, in agreement with the intact electrical integrity of proximal tubules recovering from 10 min of EC-mannitol perfusion, the overall ultrastructure of tubular epithelium appeared normal under such conditions (Figure 4.16). It may be worthwhile to note that the EC-mannitol solution is much less viscous than the UW solution. As a result, 5 min of reperfusion with control Ringer was enough to restore the  $V_{te}$  and morphology. It is not clear from the information presented here what causes the appearance of the large vacuoles during the slow wash out of the UW solution in this model system. It is noteworthy that HES (approximately 250,000 MW), which is responsible for the high viscosity of the UW solution, can not be filtered by the glomeruli, nor can it

cross the peritubular capillary endothelium. It appears that under *in vivo* conditions, renal tubules are exposed to a UW solution which is less viscous. This implies that transient vacuolization during reperfusion observed in this study may not occur in clinical transplantation.

In summary, EC perfusion at 22°C and 37°C led to profound cell swelling, accompanied by the damage to electrogenic tubular transport upon reperfusion with control Ringer. UW perfusion at these temperatures had no effect on cell volume. Tubular transport was also better preserved. UW solution appears to be superior to EC solution at warmer temperatures because of the presence of membrane impermeants which are effective over a wide temperature range compared to glucose in the EC solution, which is membrane permeable at warm temperatures. The damaging effects reported in this study may partially explain the higher percentage of delayed graft function and decreased graft survival as a result of using Euro-Collins' (EC) solution, compared with using University of Wisconsin (UW) solution in renal preservation [156].

## Chapter 7

# CONCLUDING REMARKS

The *in vitro* perfusion system used in this study appears to be an effective way to characterize detailed structural and functional alterations of individual tubular segments under conditions that would be experienced during renal transplantation.

Renal hypoxia was simulated in this model system by low- $P_{O_2}$  perfusion, accomplished by adding Oxyrase<sup>TM</sup> to the perfusion solutions. The data suggest that functional integrity of tubular cells is well preserved at an average oxygen tension ( $P_{O_2}$ ) of 4 mmHg for up to 20 min, whereas the overall tubular transport may be compromised because of the damage to tight junctions. It would appear that damage to the cell-to-cell junction is one of the earliest events in tubular hypoxic injury, preceding the injury to the cell body. Low  $P_{O_2}$  in combination with glucose depletion, lactate and  $K^+$  accumulation, and acidic pH was used to simulate the *in vivo* ischemic environment. Similar electrophysiological alterations were observed when tubules were perfused with the ischemic solution. More profound tubular injury may be expected if the hypoxic/ischemic perfusion time is prolonged, or if total anoxia is achieved. Alternatively, tubular injury may be induced by respiratory inhibitors that deplete cellular ATP. Further investigation of the electrophysiological

and morphological profiles of perfused tubules under these condition would help us to better understand the structure-function relationship of the renal tubules subjected to hypoxic/ischemic injury.

Tubular perfusion with warm preservation solutions reveals the damaging effect of the EC solution on tubular transport at 22°C and 37°C due to its ineffectiveness in maintaining cell volume. The UW solution and the EC-mannitol solution are far superior to the EC solution in preserving cell volume and tubular transport at these temperatures. If we interpret the observed structural and functional changes at warm temperatures as an accelerated injury process occurring at temperatures close to 0°C, the data in this study would indicate a better outcome of renal preservation using UW or EC-mannitol solution than that of using EC solution. Possibilities exist that the EC-mannitol may be used as a less expensive alternative of the UW solution in clinical practice.

From the data presented in this study, it is evident that rinsing the organ prior to implantation would be beneficial in preserving tubular structure. Several recent studies have demonstrated the beneficial effect of terminal rinse in organ preservation [51, 69, 153]. However, the effectiveness of terminal rinse solutions on transplantation outcome cannot be solely explained by the tubular effect(s) observed in this study [51]. The situation appears to be more complicated. As research goes on in search of more efficient preservation solutions for organ transplantation, the present model provides a useful system to evaluate the cellular effects of these new solutions. Moreover, understanding the mechanisms of protection may directly lead to the development of new preservation solutions.

# Appendix A

## Cable Analysis in Mammalian Proximal Tubules

Electric cable analysis has been used extensively to determine resistances of different barriers in amphibian proximal tubules [5, 81]. The proximal tubule was modeled as a concentric electrical cable in these studies. Cable equations were simplified, considering the dimensions and geometry of amphibian proximal tubules. One of the most important simplifications was to separate the concentric cable into two independent cables, namely, luminal cable for determination of  $R_{te}$  and  $\alpha$ , and cellular cable for determination of  $R_z$  (also refer to Section 2.3.4).

Previous data on cable analysis in mammalian tubule preparations are limited. Although the transepithelial resistance was determined in a few studies [34, 200],  $R_{ap}$  and  $R_{bl}$  of mammalian proximal tubules have never been, to the best of our knowledge, measured using cable analysis. Mammalian proximal tubules differ remarkably from their amphibian counterparts in geometry and dimension. Therefore, any simplification of cable theory made for amphibian proximal tubules should be reevaluated. The application of cable theory to mouse proximal straight tubules is described as follows. Basics of cable theory can be found in studies by Anagnos-

topoulos and colleagues [5] and by Guggino and colleagues [81].

## A.1 General Theory

The mouse proximal straight tubule was modeled as a double-cylindrical concentric cable of infinite length. The equivalent electric circuit is shown in Figure A.1. The voltage distributions along the double cable, following a current injection, are described by the following equations:

$$\Delta V_{te} = A e^{-x/\vartheta} + B e^{-x/\eta} \quad (\text{A.1})$$

$$\Delta V_{bl} = C e^{-x/\vartheta} + D e^{-x/\eta} \quad (\text{A.2})$$

where  $\vartheta$  and  $\eta$  are combined double-cable length constants ( $\vartheta < \eta$ ), and  $x$  is the distance from the current source.  $A, B, C$  and  $D$  are constants to be determined by boundary conditions (see below).

Equations A.1 and A.2 reflect the concept of “cross talk” between luminal and cellular cables. That is, the voltage changes of each cable are determined not only by its own exponential term (usually the main term), but also by an exponential term of the other cable. Both  $\vartheta$  and  $\eta$  are expressions of intrinsic length constants of luminal ( $\lambda_l$ ) and cellular ( $\lambda_c$ ) cables.

Simplifications and complications in applying the cable equations for resistance measurements are discussed as follows under the conditions of luminal and cellular current injections, respectively.

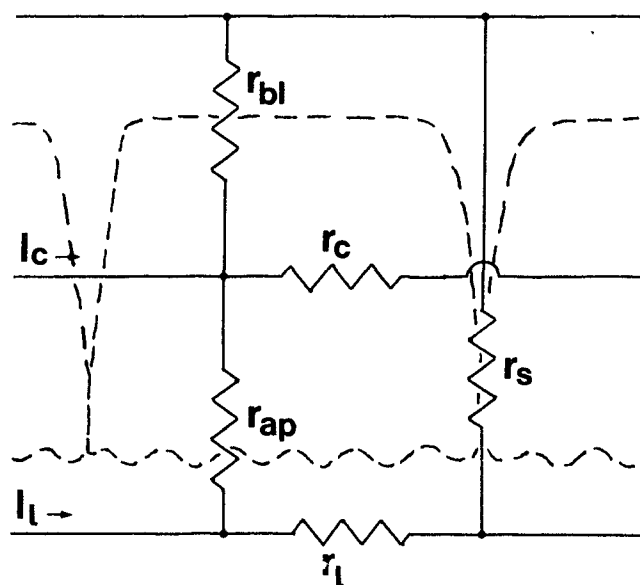


Figure A.1: Equivalent electrical circuit of mouse proximal tubule for cable analysis. Only one elementary unit of the circuit is shown. Dashed lines indicate cell borders.  $I_c$  and  $I_l$  designate current flow along cellular and luminal cables, respectively;  $r_{ap}$ ,  $r_{bl}$  and  $r_s$  are transverse resistances of apical, basolateral and shunt per unit length, respectively;  $r_c$  and  $r_l$  are core resistances of cellular and luminal cables, respectively. Modified from Figure 1 in [5]

## A.2 Intraluminal Current Injection and Luminal Cable

The values of A and B in equation A.1 and A.2 which satisfy the boundary conditions of luminal current ( $I_0$ ) stimulation are [5]:

$$A = \frac{r_1 I_0 \vartheta^3 (\lambda_1^2 - \eta^2)}{2 \lambda_1^2 (\vartheta^2 - \eta^2)} \quad (\text{A.3})$$

$$B = \frac{r_1 I_0 \eta^3 (\lambda_1^2 - \vartheta^2)}{2 \lambda_1^2 (\vartheta^2 - \eta^2)} \quad (\text{A.4})$$

where  $r_1$  is the core resistance per unit length:  $r_1 = \rho/2\pi a$ ,  $\rho$  and  $a$  being core resistivity and the radius of the tubule, respectively.

The cellular cable term (A-term) is negligible compared with the luminal cable term (B-term) under the following two assumptions:

$$\vartheta e^{-x/\vartheta} \ll \eta e^{-x/\eta} \quad (\text{A.5})$$

$$\vartheta^2 \ll \eta^2 \quad (\text{A.6})$$

When experimentally measured length constants were incorporated in Equations A.5 and A.6, it was found that these assumptions were met when  $x > 50 \mu\text{m}$ . Since tubules less than  $50 \mu\text{m}$  were never used in the study, Equation A.1 was simplified as:

$$\begin{aligned} \Delta V_{te} &= \frac{r_1 I_0}{2} \lambda_1 e^{-x/\lambda_1} \\ &= V_0 e^{-x/\lambda_1} \end{aligned} \quad (\text{A.7})$$

where  $V_0$  denotes the  $\Delta V_{te}$  at the current-injection site.

For a finite cable with length  $X$ , Equation A.7 becomes:

$$\Delta V_c = \frac{\Delta V_p}{\cosh(X/\lambda_l)} \quad (\text{A.8})$$

where  $\Delta V_c$  and  $\Delta V_p$  denote  $\Delta V_{te}$  at the perfusion and collection ends, respectively. According to Equation A.8,  $\lambda_l$  was determined from experimentally measured  $\Delta V_c$  and  $\Delta V_p$  (see equation 2.5).  $R_{te}$  was subsequently determined according to Equation 2.6.

### A.3 Intraluminal Current Injection and Voltage Divider Ratio

The voltage divider ratio ( $\alpha$ , see Section 2.3.4) was used as an approximation of  $R_{ap}/R_{bl}$  in amphibian proximal tubules. The assumption was that transepithelial current flow occurred first across the apical cell membrane, then across the basolateral cell membrane. However, this assumption may not be true for the following two reasons: 1) If the resistance of the lateral intercellular spaces ( $R_{lis}$ ) is not negligible compared with  $R_s$ , a significant portion of current entering the cell from the tubule lumen can exit via  $R_{lis}$  rather than  $R_{bl}$  [53]; 2) The current flowing across the apical membrane may not equal the current flowing across the basolateral membrane because of the intercellular current exchange through cell-to-cell junctions [53].

#### A.3.1 $\alpha$ and $R_{lis}$

The first error mentioned above always results in an underestimate of  $R_{ap}/R_{bl}$  by overestimating  $R_{bl}$ . This systematic error has to be considered in epithelia with narrow lateral intercellular spaces, such as mammalian proximal tubules. The degree

of deviation of  $\alpha$  from  $R_{ap}/R_{bl}$  depends both on fractional interspace resistance ( $R_{lis}/R_s$ ) and on the ratios of cell membrane to shunt resistance ( $R_{ap}/R_s$  and  $R_{bl}/R_s$ ).

To correct for this error, the  $R_{lis}$  was calculated according to [33]

$$R_{lis} = (d \times \rho)/(l \times w_i) \quad (\text{A.9})$$

where  $d$  (cm) is the interspace depth,  $\rho$  ( $\Omega \cdot \text{cm}$ ) is the resistivity of the Ringer solution (Figure 2.2),  $w_i$  (cm) is the interspace width, and  $l$  (cm/cm<sup>2</sup>-epithelium) is the total linear extent. Dimensional data ( $d$ ,  $w_i$  and  $l$ ) were obtained from electron micrographic studies in rabbit proximal tubules [188, 208]. The estimated  $R_{lis}$  was  $2.7 \Omega \cdot \text{cm}^2$ .  $\alpha$  was then modified using equations 31 to 37 in reference [33].

### A.3.2 $\alpha$ and intercellular current exchange

The second error leads to a fall in  $\alpha$  with distance ( $x$ ), from overestimate near the current-injection site to underestimate further away from the current source. Two parameters used to evaluate the degree of deviation are

$$p = \sqrt{\frac{r_l}{r_c}} \left(1 + \frac{r_{ap}}{r_s}\right) \quad (\text{A.10})$$

$$q = \sqrt{\frac{r_c}{r_l}} \left(1 + \frac{r_{ap}}{r_{bl}}\right) \quad (\text{A.11})$$

where  $r_l$  and  $r_c$  are core resistances per unit length of luminal and cellular cable, respectively. Resistances  $r_{ap}$ ,  $r_{bl}$  and  $r_s$  are expressed as ohm per unit length of luminal membrane, basolateral membrane, and shunt pathway, respectively. The greater the ratio  $q/p$ , the smaller the length dependence of  $\alpha$ , and the smaller the error. The  $q/p$  ratio calculated using experimental data was greater than 150. In addition, experimentally measured  $\alpha$  showed no dependency on distance ( $x$ ). These

observations suggest that  $\alpha$  is not affected by intercellular current exchange in tubule preparations used in the present study.

## A.4 Intracellular Current Injection and Cellular Cable

### A.4.1 Cross talk

When the current is injected intracellularly, the voltage deflection along the cellular cable is [5]:

$$\Delta V_{bl} = \frac{r_c I_0}{2} \lambda_c e^{-x/\vartheta} \left[ 1 + \frac{m\eta}{4\vartheta} e^{x(\frac{1}{\vartheta} - \frac{1}{\eta})} \right] \quad (\text{A.12})$$

where  $r_c$  is the core resistance of cell cable per unit length, and

$$m = \frac{4r_c r_l}{r_{ap}^2} \left( \frac{1}{\lambda_c^2} - \frac{1}{\lambda_l^2} \right)^{-2} \quad (\text{A.13})$$

$r_{ap}$  being the resistance of luminal membrane per unit length.

The magnitude of the second term in equation A.12 determines if  $\Delta V_{bl}$  can be simplified to a single exponential. This requires that 1) the term  $m\eta/4\vartheta$  be much smaller than 1 (0.02 for *Necturus*, for example), and 2)  $x < 5\vartheta$ . Using experimental data recorded in mouse proximal tubules, it was found that both requirements were met, and that the second term in equation A.12 contributed less than 5% of  $\Delta V_{bl}$  if  $x < 55\mu\text{m}$ . The effect of ‘‘cross talk’’ was therefore not taken into account in the present analysis because  $\Delta V_{bl}$  was never measured at  $x > 55\mu\text{m}$  (see Figure 3.9).

### A.4.2 Point-current distortion

One of the assumptions inherent in the foregoing analysis is that the injected currents are uniformly distributed across the cross section of tubules. In the case of luminal

current injection, a disc current source with diameter similar to that of tubular lumen is assumed. In the case of cellular current injection, a ring current source covering the cross section of cell layer is assumed. Although the tip of the perfusion pipette mimics the disc current source in luminal analysis, the tip of an intracellular electrode is by no means close to the ring shape, but rather a perfect point source.

The attenuation of  $\Delta V_{bl}$  along the tubule in response to a point-current injection is given by [81]

$$\Delta V_{bl} (x,y=0) = \frac{V_0}{2} \sum_{n=-\infty}^{+\infty} \frac{\exp -[(x/a)\sqrt{(a/\lambda_c)^2 + n^2}]}{\sqrt{(a/\lambda_c)^2 + n^2}} \quad (\text{A.14})$$

where  $V_0$  is the  $\Delta V_{bl}$  at current-injection site,  $a$  is the radius of the tubule,  $\lambda_c$  is the length constant of cellular cable, and subscript  $x, y = 0$  indicates that both current-injection and  $\Delta V_{bl}$ -sensing electrodes are on a same axis parallel to the longitudinal axis of the tubule. Experimentally, the condition  $x, y = 0$  was met by laying tubule tightly against the flat bottom of the chamber and impaling both electrodes into cells located in a same focusing plane of an inverted microscope (200 $\times$ ). In the working range of  $17\mu\text{m} < x < 55\mu\text{m}$  ( $0.5 < x/a < 1.5$ ), up to 7 terms in Equation A.14 have to be included ( $-3 \leq n \leq +3$ ).  $V_0$  and  $\lambda_c$  in Equation A.14 were determined from the experimentally measured  $\Delta V_{bl} \sim x$  relationship by recursive calculation with the aid of a personal computer (see Section A.5).  $R_z$  (see Section 2.3.4) was then calculated as

$$R_z = 4\pi a \lambda_c V_0 / I_0 \quad (\text{A.15})$$

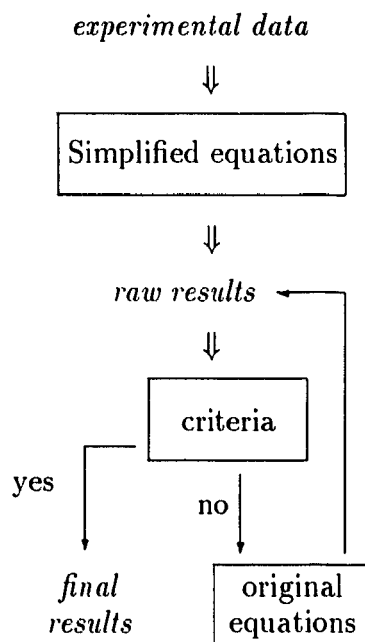
$I_0$  being the input current (3 to 20 nA<sup>1</sup>).

---

<sup>1</sup>For each pair of impalement, at least two current amplitudes were used. Data were considered reliable only if the recorded  $\Delta V_{bl}$  changed proportionally with changes in current amplitude.

## A.5 Data Analysis

The following flow chart shows the general format employed to analyze the data obtained from measurements of cell membrane and transepithelial resistances. To start with the calculation, all simplifications mentioned above were assumed valid. Raw results were obtained from experimental data based on these simplified equations. The raw results were regarded as final results only if all the foregoing criteria were met. Otherwise, the experimental data were fit to the original equations by means of recursive analysis, which generated a new set of results. These results then replaced the last version of raw results. This cycle continued until final results were obtained. It is worthwhile to note that this type of analysis allows one to refine an experimental model recursively using a single experimental-data pool — with each cycle of data processing, an increasing amount of information is extracted from the experimental data.



The standard errors of experimental data were transferred to the results using error propagation equations

$$\delta f(x_1, x_2, \dots, x_n) = \sqrt{\sum_{i=1}^n \left( \frac{\partial f(x_1, x_2, \dots, x_n)}{\partial x_i} \delta x_i \right)^2} \quad (\text{A.16})$$

where  $x_i$  and  $\delta x_i$  denote an experimental datum and its standard error, respectively, and  $f(x_1, x_2, \dots, x_n)$  and  $\delta f(x_1, x_2, \dots, x_n)$  are calculated result and its standard error, respectively.

The basic concept of this flow chart was written into the following BASIC program, which was run on a personal computer (IBM PC/XT).

```

1 REM
2 REM *** A BASIC PROGRAM FOR CABLE ANALYSIS ***
3 REM
10 DIM X(11), VXVO(10,11)
99 REM
100 REM *** Print Out the Title of the Programme ***
101 REM
110 CLS
120 FOR I=1 TO 4:PRINT:NEXT I
130 PRINT TAB(10)"#####"TAB(24)"####"TAB(33)"#####"TAB(46)"###"
    TAB(58)"#####"
140 PRINT TAB(9)"###"TAB(23)"#"TAB(26)"###"TAB(33)"###"TAB(39)"###"
    TAB(46)"###"TAB(58)"###"
150 PRINT TAB(9)"###"TAB(22)"#####"TAB(33)"#####"TAB(46)"###"
    TAB(58)"#####"
160 PRINT TAB(9)"###"TAB(21)"#"TAB(26)"###"TAB(33)"###"TAB(39)"###"
    TAB(46)"###"TAB(58)"###"
170 PRINT TAB(10)"#####"TAB(20)"#"TAB(26)"###"TAB(33)"#####"
    TAB(46)"#####"TAB(58)"#####"
180 PRINT:PRINT:PRINT TAB(23)"THE SYSTEM FOR CABLE ANALYSIS"
190 PRINT TAB(22)"_____ "
200 PRINT:PRINT TAB(22)"(C) COPYRIGHT 1991, YONGDONG YOU"
210 FOR I=1 TO 5:PRINT:NEXT I
220 PRINT "Press 'F5' key to continue..."
230 STOP

```

```

299 REM
300 REM *** Main Programme -- Menu ***
301 REM
310 CLS
320 PRINT:PRINT:PRINT:PRINT:PRINT TAB(32)"### MENU ###":PRINT
330 IF L1=0 THEN GOTO 350
340 FOR I=L1 TO 1 STEP -1:PRINT TAB(20-I);CHR$(251);:NEXT I
350 PRINT TAB(20)"1. Data Input"
360 IF L2=0 THEN GOTO 380
370 FOR I=L2 TO 1 STEP -1:PRINT TAB(20-I);CHR$(251);:NEXT I
380 PRINT TAB(20)"2. Calculations of Membrane Resistances"
390 IF L3=0 THEN GOTO 410
400 FOR I=L3 TO 1 STEP -1:PRINT TAB(20-I);CHR$(251);:NEXT I
410 PRINT TAB(20)"3. Luminal Cable"
420 IF L4=0 THEN GOTO 440
430 FOR I=L4 TO 1 STEP -1:PRINT TAB(20-I);CHR$(251);:NEXT I
440 PRINT TAB(20)"4. Cellular Cable, Cross Talk"
450 IF L5=0 THEN GOTO 470
460 FOR I=L5 TO 1 STEP -1:PRINT TAB(20-I);CHR$(251);:NEXT I
470 PRINT TAB(20)"5. Cellular Cable, Point Distortion"
480 IF L6=0 THEN GOTO 500
490 FOR I=L6 TO 1 STEP -1:PRINT TAB(20-I);CHR$(251);:NEXT I
500 PRINT TAB(20)"6. VDR, Cross Talk"
510 IF L7=0 THEN GOTO 530
520 FOR I=L7 TO 1 STEP -1:PRINT TAB(20-I);CHR$(251);:NEXT I
530 PRINT TAB(20)"7. VDR, Effect of Rlis"
540 IF L8=0 THEN GOTO 560
550 FOR I=L8 TO 1 STEP -1:PRINT TAB(20-I);CHR$(251);:NEXT I
560 PRINT TAB(20)"8. Print Out the Final Results"
570 PRINT TAB(20)"9. Quit"
580 FOR I=1 TO 5:PRINT:NEXT I
590 INPUT "Your choice";CHOICE
600 ON CHOICE GOSUB 1000,2000,3000,4000,5000,6000,7000,8000,9000
990 END
999 REM
1000 REM *** Subroutine 1, Data Input ***
1001 REM
1010 CLS
1012 IF L1=0 THEN GOTO 1020
1014 PRINT:PRINT:PRINT"Data input has already been completed!"
1016 GOTO 1900
1020 PRINT:PRINT:PRINT TAB(30)"### DATA INPUT ###"
1030 PRINT:PRINT CHR$(224);"(";CHR$(230);"m) =";:INPUT ALPHA
1040 PRINT "S.E.M. of ";CHR$(224);"(% of mean)";:INPUT EALPHA
1050 PRINT CHR$(225);"(";CHR$(230);"m) =";:INPUT BETA

```

```

1060 PRINT "S.E.M. of ";CHR$(225);"% of mean";:INPUT EBETA
1070 INPUT "VO(mV) =";VO
1080 INPUT "S.E.M. of VO(% of mean)";EVO
1090 PRINT "Rte(";CHR$(234);"cm";CHR$(253);") =";:INPUT RTE
1100 INPUT"S.E.M. of Rte(% of mean)";ERTE
1110 PRINT"ao(";CHR$(230);"m) =";:INPUT AO
1120 INPUT "S.E.M. of ao(% of mean)";EAO
1130 INPUT"VDR =",VDR
1140 INPUT "S.E.M. of VDR(% of mean)";EVDR
1150 PRINT"Ri(";CHR$(234);"cm) =";:INPUT RI
1160 PRINT"d(";CHR$(230);"m) =";:INPUT D
1170 INPUT"S.E.M. of d(% of mean)";ED
1900 PRINT:PRINT"Press 'F5' key to go back to menu..."
1910 STOP
1920 L1=1
1930 GOTO 300
1990 RETURN
1999 REM
2000 REM *** Subroutine 2, Calculations of Membrane Resistances ***
2001 REM
2010 CLS
2015 IF L1=0 THEN GOTO 2800
2020 PRINT:PRINT:PRINT TAB(17)"### CALCULATIONS OF MEMBRANE
RESISTANCES ###"
2030 RZ=.00628*AO*VO*ALPHA
2040 SRZ=.00628*SQR((VO*ALPHA*EAO/100*AO)^2+(AO*ALPHA*EVO/100*VO)^2
+(AO*VO*EAPLHA/100*ALPHA)^2)
2050 RBL=(VDR+1)/VDR*RZ
2060 SRBL=SQR((RZ/VDR*EVDR/100)^2+((VDR+1)/VDR*SRZ)^2)
2070 RAP=VDR*RBL
2080 SRAP=SQR((RBL*EVDR/100*VDR)^2+(VDR*SRBL)^2)
2090 RS=RTE*(RAP+RBL)/(RAP+RBL-RTE)
2100 SRS=RS^2*SQR((ERTE/100/RTE)^2+(SRAP^2+SRBL^2)/(RAP+RBL)^4)
2500 RINPUT=VO/.00002
2510 RAP1=1592*RAP/AO
2520 SRAP1=1592*SQR((SRAP/AO)^2+(RAP/AO*EAO/100)^2)
2530 RBL1=1592*RBL/(AO+D)
2540 SRBL1=1592*SQR((SRBL/(AO+D))^2+(RBL/(AO+D)^2*EAO/100*AO)^2
+(RBL/(AO+D)^2*ED/100*D)^2)
2550 RS1=1592*RS/(AO+D/2)
2560 SRS1=1592*SQR((SRS/(AO+D/2))^2+(RS/(AO+D/2)^2*EAO/100*AO)^2
+(RS/(AO+D/2)^2*ED/200*D)^2)
2600 PRINT:PRINT
2610 PRINT "Rap =";CINT(RAP);CHR$(241);CINT(SRAP);CHR$(234);
"cm";CHR$(253)

```

```

2620 PRINT " =";RAP1;CHR$(241);SRAP1;CHR$(234);"cm"
2630 PRINT "Rbl =";CINT(RBL);CHR$(241);CINT(SRBL);CHR$(234);
      "cm";CHR$(253)
2640 PRINT " =";RBL1;CHR$(241);SRBL1;CHR$(234);"cm"
2650 PRINT "Rs =";CINT(10*RS)/10;CHR$(241);CINT(10*SRS)/10;
      CHR$(234);"cm";CHR$(253)
2660 PRINT " =";RS1;CHR$(241);SRS1;CHR$(234);"cm"
2670 PRINT:PRINT "Rz =";CINT(RZ);CHR$(241);CINT(SRZ);CHR$(234);"cm";
      CHR$(253)
2770 PRINT "Rinput =";RINPUT;CHR$(234)
2780 PRINT CHR$(224);" =";ALPHA;CHR$(241);EALPHA*ALPHA/100;
      CHR$(230);"m"
2790 PRINT CHR$(225);" =";BETA;CHR$(241);EBETA*BETA/100;
      CHR$(230);"m"
2795 L2=L2+1
2798 GOTO 2900
2800 PRINT:PRINT:PRINT"Warning: This system is not functional
      without input data."
2810 PRINT:PRINT"Go back to 'Data Input' first."
2900 PRINT:PRINT:PRINT"Press 'F5' key to return to menu..."
2910 STOP
2930 GOTO 300
2990 RETURN
2999 REM
3000 REM *** Subroutine 3, Luminal Cable ***
3001 REM
3010 CLS
3020 IF L3<>0 THEN GOTO 3200
3050 PRINT:PRINT:PRINT TAB(20)"### LUMINAL CABLE (ZL) ###"
3060 PRINT:PRINT"What is the ";CHR$(225);" and Rte after ZL
      correction?"
3070 PRINT CHR$(225);"(";CHR$(230);"m) =";:INPUT BETA
3080 PRINT "Rte(";CHR$(234);"cm";CHR$(253);") =";:INPUT RTE
3090 FOR I=1 TO 6:PRINT:NEXT I
3100 PRINT"Press 'F5' key to continue..."
3150 STOP
3200 CLS
3220 PRINT:PRINT:PRINT TAB(20)"### LUMINAL CABLE (CROSS TALK) ###"
3230 PRINT:PRINT"x(";CHR$(230);"m)"TAB(20);CHR$(224);"*exp(-x/";
      CHR$(224);")"TAB(40);CHR$(225);"*exp(-x/";CHR$(225);")"
      TAB(60);CHR$(224);"*exp/";CHR$(225);"*exp"
3240 FOR I=1 TO 6
3250 X=50*I
3260 XA=ALPHA*EXP(-X/ALPHA)
3270 FOR J=1 TO 50

```

```

3280 XA=XA*10
3290 IF XA>1000 THEN GOTO 3310
3300 NEXT J
3310 XA=CINT(XA)/1000
3320 XB=BETA*EXP(-X/BETA)
3330 FOR K=1 TO 50
3340 XB=XB*10
3350 IF XB>1000 THEN GOTO 3370
3360 NEXT K
3370 XB=CINT(XB)/1000
3400 PRINT X;TAB(20);XA;"E";-J+3;TAB(40);XB;"E";-K+3;
      TAB(60);XA/XB;"E";K-J
3410 NEXT I
3450 PRINT:PRINT CHR$(225);CHR$(253);"/";CHR$(224);CHR$(253);" =";
      CINT(BETA^2/ALPHA^2)
3500 FOR I=1 TO 5:PRINT:NEXT I
3510 INPUT "Is modification needed (Y/N)";A$
3520 IF A$<>"Y" THEN GOTO 3900
3530 CLS
3540 PRINT:PRINT"Sorry, this part of the programme is not available
      right now."
3900 PRINT:PRINT"Press 'F5' key to go back to menu..."
3910 STOP
3920 L3=L3+1
3930 GOTO 300
3990 RETURN
3999 REM
4000 REM *** Subroutine 4, Cellular Cable -- Cross Talk ***
4001 REM
4010 CLS
4020 PRINT:PRINT:PRINT TAB(20)"### CELLULAR CABLE, CROSS TALK ###"
4030 RHOC=2*AO*VO/ALPHA/(2*AO+D)*1E+09
4040 RHOL=3.183*RI/AO^2*1E+07
4050 M=4*RHOL*RHOC/RAP1^2/((1/ALPHA^2-1/BETA^2)^2*1E-16
4060 PRINT:PRINT"m-term: ";M*BETA/ALPHA/4;"*";"exp(";
      1/ALPHA-1/BETA;"x)"
4070 PRINT:PRINT "x(";CHR$(230);"m)"TAB(20)"m-term"
4080 FOR I=1 TO 10
4090 X=10*I
4100 MTERM=M*BETA/ALPHA/4*EXP((1/ALPHA-1/BETA)*X)
4110 PRINT X;TAB(20);CINT(1000*MTERM)/1000
4120 NEXT I
4200 PRINT:INPUT"Is modification needed (Y/N)";B$
4210 IF B$<>"Y" THEN GOTO 4900
4300 CLS

```

```

4310 PRINT:PRINT"Sorry, this part of the programme is not available
      right now."
4900 PRINT:PRINT"Press 'F5' key to continue..."
4910 STOP
4920 L4=L4+1
4930 GOTO 300
4990 RETURN
4999 REM
5000 REM *** Subroutine 5, Cell Cable -- Point Distortion ***
5001 REM
5010 CLS
5020 IF L5=1 THEN GOTO 5700
5030 PRINT:PRINT:PRINT TAB(10)"### CELL CABLE, POINT DISTORTION ###"
      :PRINT
5040 FOR I=1 TO 3
5050 C(I)=1/SQR(1+I*I*(ALPHA/AO)^2)
5060 E(I)=1/ALPHA*(1-1/C(I))
5070 PRINT I;"-term =";2*C(I);"*exp(";E(I);"x)"
5080 NEXT I
5090 PRINT:PRINT"x(";CHR$(230);"m)"TAB(20)"1st-term"
      TAB(40)"2nd-term"TAB(60)"3rd-term"
5100 FOR I=1 TO 10
5110 X=10*I
5120 PRINT X;
5130 FOR J=1 TO 3
5140 PRINT TAB(20*J);CINT(1000*2*C(J)*EXP(E(J)*X))/1000;
5150 NEXT J
5160 PRINT
5170 NEXT I
5200 PRINT:INPUT"Is modification needed (Y/N)";C$
5210 IF C$<>"Y" THEN GOTO 5750
5250 CLS
5260 PRINT:INPUT"How many terms do you want to include in
      modification (1-3)";N
5270 PRINT:PRINT"OK! I'm modifying now, please wait..."
5300 S(0)=.5
5310 FOR I=1 TO 10
5315 PRINT"*";
5320 A(I)=ALPHA*(1.07+I/100)
5330 FOR J=1 TO N
5340 D(I,J)=1/SQR(1+J^2*(A(I)/AO)^2)
5350 F(I,J)=1/A(I)-1/AO*SQR((AO/A(I))^2+J^2)
5360 NEXT J
5370 FOR K=0 TO 10
5380 X(K)=20+K*4

```

```

5390 VXVO=0
5400 FOR L=1 TO N
5410 VXVO=VXVO+2*D(I,L)*EXP(F(I,L)*X(K))
5420 NEXT L
5430 VXVO(I,K)=EXP(-X(K)/A(I))*(1+VXVO)
5440 NEXT K
5450 NEXT I
5460 GOSUB 5800
5500 PRINT:PRINT CHR$(224);"(i)";TAB(20)"1/S(i)"TAB(40)"intercept"
5510 FOR I=1 TO 10
5520 PRINT CINT(100*A(I))/100;TAB(20);CINT(-100/S(I))/100;TAB(40);
      CINT(100*EXP(I(I)))/100
5530 NEXT I
5540 FOR I=1 TO 10
5550 IF ABS(-1/S(I)-ALPHA)=(-1/S(I)-ALPHA) THEN GOTO 5570
5560 NEXT I
5570 ALPHA=(A(I)+A(I-1))/2
5580 PRINT:PRINT"The new ";CHR$(224);" =";ALPHA
5590 COEF=EXP((I(I)+I(I-1))/2)
5600 PRINT"The coefficient =";COEF
5610 VO=VO/COEF
5620 PRINT "The new VO =";VO
5630 GOTO 5750
5700 CLS
5710 PRINT:PRINT"This programme can not be repeated!"
5750 PRINT:PRINT"Press 'F5' key to return to menu..."
5760 STOP
5770 L5=1
5780 GOTO 300
5790 RETURN
5799 REM
5800 REM *** Sub-subroutine 5(1), Linear Regression ***
5801 REM
5810 FOR I=1 TO 10
5815 PRINT"#";
5820 O=0:P=0:Q=0:R=0
5830 FOR J=0 TO 10
5840 O=O+X(J)
5850 P=P+LOG(VXVO(I,J))
5860 Q=Q+X(J)*LOG(VXVO(I,J))
5870 R=R+X(J)*X(J)
5880 NEXT J
5890 S(I)=(Q-O*P/11)/(R-O*O/11)
5900 I(I)=P/11-S(I)*O/11
5910 NEXT I

```



```
7210 PRINT:PRINT"Modified VDR =";VDR1
7220 VDR=VDR1
7230 GOTO 7900
7240 CLS
7250 PRINT:PRINT"This part of the programme cannot be repeated!"
7900 FOR I=1 TO 7:PRINT:NEXT I
7910 PRINT"Press 'F5' key to return to menu..."
7920 STOP
7930 L7=1
7940 GOTO 300
7990 RETURN
7999 REM
8000 REM *** Subroutine 8, Print out the Final Results ***
8001 REM
8010 CLS
8020 PRINT:PRINT:PRINT TAB(24)"### PRINT OUT THE FINAL RESULTS ###"
8030 PRINT:PRINT:PRINT:PRINT TAB(35)"Please wait..."
8040 FOR I=1 TO 7:PRINT:NEXT I
8050 LPRINT:LPRINT:LPRINT"Cell Membrane Resistances"
8060 IF RI<60 THEN CHOICE1=1
8070 IF RI>60 AND RI<80 THEN CHOICE1=2
8080 IF RI>80 THEN CHOICE1=3
8090 ON CHOICE1 GOSUB 8800,8830,8860
8100 LPRINT "Rap =" ;CINT(RAP) ;CHR$(241) ;CINT(SRAP) ;CHR$(234) ;"cm" ;
      CHR$(253)
8110 LPRINT " =" ;RAP1 ;CHR$(241) ;SRAP1 ;CHR$(234) ;"cm"
8120 LPRINT "Rb1 =" ;CINT(RBL) ;CHR$(241) ;CINT(SRBL) ;CHR$(234) ;"cm" ;
      CHR$(253)
8130 LPRINT " =" ;RBL1 ;CHR$(241) ;SRBL1 ;CHR$(234) ;"cm"
8140 LPRINT "Rs =" ;CINT(10*RS)/10 ;CHR$(241) ;CINT(10*SRS)/10 ;
      CHR$(234) ;"cm" ;CHR$(253)
8150 LPRINT " =" ;RS1 ;CHR$(241) ;SRS1 ;CHR$(234) ;"cm"
8160 LPRINT:LPRINT "Rz =" ;CINT(RZ) ;CHR$(241) ;CINT(SRZ) ;CHR$(234) ;
      "cm" ;CHR$(253)
8170 LPRINT "Rinput =" ;RINPUT ;CHR$(234)
8180 LPRINT CHR$(224) ;" =" ;ALPHA ;CHR$(241) ;EALPHA*ALPHA/100 ;
      CHR$(230) ;"m"
8190 LPRINT CHR$(225) ;" =" ;BETA ;CHR$(241) ;EBETA*BETA/100 ;
      CHR$(230) ;"m"
8500 PRINT"Press 'F5' key to return to menu..."
8510 STOP
8520 L8=L8+1
8530 GOTO 300
8590 RETURN
8799 REM
```

```
8800 REM *** Sub-subroutine 8(1), Temp.:37 C ***
8801 REM
8810 LPRINT"Mammalian Proximal Tubules, Temp.:37";CHR$(248);"C"
      :LPRINT
8820 RETURN
8829 REM
8830 REM *** Sub-subroutine 8(2), Temp.:22 C ***
8831 REM
8840 LPRINT"Mammalian Proximal Tubules, Temp.:22";CHR$(248);"C"
      :LPRINT
8850 RETURN
8859 REM
8860 REM *** Sub-subroutine 8(3), Temp.:4 C ***
8861 REM
8870 LPRINT"Mammalian Proximal Tubules, Temp.:4";CHR$(248);"C"
      :LPRINT
8880 RETURN
8999 REM
9000 REM *** Subroutine 9, End of the Programme ***
9001 REM
9010 CLS
9020 FOR I=1 TO 5:PRINT:NEXT I
9030 PRINT TAB(18)"#####"TAB(32)"###"TAB(40)"###"
      TAB(47)"#####"
9040 PRINT TAB(18)"###"TAB(32)"### #"TAB(40)"###"TAB(47)"###"
      TAB(54)"###"
9050 PRINT TAB(18)"#####"TAB(32)"### #"TAB(40)"###"TAB(47)"###"
      TAB(54)"###"
9060 PRINT TAB(18)"###"TAB(32)"### #"TAB(40)"###"TAB(47)"###"
      TAB(54)"###"
9070 PRINT TAB(18)"#####"TAB(32)"###"TAB(40)"###"
      TAB(47)"#####"
9080 PRINT:PRINT:PRINT TAB(17)"--- THIS IS THE END OF THE
      PROGRAMME ---"
9090 FOR I=1 TO 7:PRINT:NEXT I
9990 RETURN
```

# Bibliography

- [1] R.J. Alpern. Cell mechanisms of proximal tubule acidification. *Physiol Rev*, 70:79–114, 1990.
- [2] R.J. Alpern, K.J. Howlin, and P.A. Preisig. Active and passive components of chloride transport in the rat proximal convoluted tubule. *J Clin Invest*, 76:1360–1366, 1985.
- [3] H. Ammann, J. Noël, Y. Boulanger, and P. Vinay. Relationship between intracellular ATP and the sodium pump activity in dog renal tubules. *Can J Physiol Pharmacol*, 68:57–67, 1990.
- [4] T. Anagnostopoulos. Biionic potentials in the proximal tubule of *Necturus* kindey. *J Physiol*, 233:375–394, 1973.
- [5] T. Anagnostopoulos, J. Teulon, and A. Edelman. Conductive properties of the proximal tubule in *Necturus* kidney. *J Gen Physiol*, 75:553–587, 1980.
- [6] P.M. Andrews and A.K. Coffey. Factors that improve the preservation of nephron morphology during cold storage. *Lab Invest*, 46:100–120, 1982.
- [7] P.M. Andrews and A.K. Coffey. Protection of kidneys from acute renal failure resulting from normothermic ischemia. *Lab Invest*, 49:87–98, 1983.
- [8] H.-J. Apell. Electrogenic properties of the Na,K pump. *J Membr Biol*, 110:103–114, 1989.
- [9] T.Y. Aw, E. Wilson, T.M. Hagen, and D.P. Jones. Determinants of mitochondrial O<sub>2</sub> dependence in kidney. *Am J Physiol*, 253:F440–447, 1987.
- [10] R. Bacallao and L. Mandel. Internalization of E-cadherin and Na<sup>+</sup>,K<sup>+</sup>-ATPase in cultured renal cells occurs rapidly with energy depletion (abstract). *J Am Soc Nephrol*, 2:643, 1991.
- [11] R.S. Balaban and L.J. Mandel. Metabolic substrate utilization by rabbit proximal tubule. An NADH fluorescence study. *Am J Physiol*, 254:F407–F416, 1988.
- [12] M.S. Balda. Intracellular signals in the assembly and sealing of tight junctions. In M. Cereijido, editor, *Tight Junctions*, chapter 9, pages 121–137. CRC Press, Boca Raton, 1992.

- [13] M. Barac-Nieto and J.J. Cohen. Nonesterified fatty acid uptake by dog kidney: effects of probenecid and chlorothiazide. *Am J Physiol*, 215:98–107, 1968.
- [14] M. Barac-Nieto, H. Murer, and R. Kinne. Asymmetry in the transport of lactate by basolateral and brush border membranes of rat kidney cortex. *Pflügers Arch*, 392:366–371, 1982.
- [15] L.J. Barratt, F.C. Rector, Jr., J.P. Kokko, and D.W. Seldin. Factors governing the transepithelial potential difference across the proximal tubule of the rat kidney. *J Clin Invest*, 53:454–464, 1974.
- [16] J. Bastin, N. Cambon, M. Thompson, O.H. Lowry, and H.B. Burch. Change in energy reserves in different segments of the nephron during brief ischemia. *Kidney Int*, 31:1239–1247, 1987.
- [17] G. Baverel, M. Bonnard, E.D'A. de Castanet, and M. Pellet. Lactate and pyruvate metabolism in isolated renal tubules of normal dogs. *Kidney Int*, 14:567–575, 1978.
- [18] J.S. Beck, S. Breton, H. Mairbäurl, R. Laprade, and G. Giebisch. Relationship between sodium transport and intracellular ATP in isolated perfused rabbit proximal convoluted tubule. *Am J Physiol*, 261:F634–F639, 1991.
- [19] F.O. Belzer and J.H. Southard. Principles of solid-organ preservation by cold storage. *Transplantation*, 45:673–676, 1988.
- [20] C.J. Bentzel, C.E. Palant, and M. Fromm. Physiological and pathological factors affecting the tight junction. In M. Cereijido, editor, *Tight Junctions*, chapter 11, pages 151–173. CRC Press, Boca Raton, 1992.
- [21] C.A. Berry and F.C. Rector, Jr. Mechanism of proximal NaCl reabsorption in the proximal tubule of the mammalian kidney. *Semin Nephrol*, 11:86–97, 1991.
- [22] C.A. Berry and F.C. Rector, Jr. Renal transport of glucose, amino acids, sodium, chloride, and water. In B.M. Brenner and F.C. Rector, Jr., editors, *The Kidney*, chapter 7, pages 245–282. W.B. Saunders Company, Philadelphia, 4th edition, 1991.
- [23] C.A. Berry, D.G. Warnock, and F.C. Rector, Jr. Ion selectivity and proximal salt reabsorption. *Am J Physiol*, 235:F234–F245, 1978.
- [24] B. Biagi and G. Giebisch. Temperature dependence of transepithelial potential in isolated perfused rabbit proximal tubules. *Am J Physiol*, 236:F302–F310, 1979.
- [25] B. Biagi, M. Sohtell, and G. Giebisch. Intracellular potassium activity in the rabbit proximal straight tubule. *Am J Physiol*, 241:F677–F686, 1981.

- [26] D. Biemesderfer, R.F. Reilly, M. Exner, P. Igarashi, and P.S. Aronson. Immunocytochemical characterization of  $\text{Na}^+$ - $\text{H}^+$  exchanger isoform NHE-1 in rabbit kidney. *Am J Physiol*, 263:F833–F840, 1992.
- [27] J.V. Bonventre. Mediators of ischemic renal injury. *Ann Rev Med*, 39:531–544, 1988.
- [28] J.V. Bonventre and J.M. Weinberg. Kidney preservation ex vivo for transplantation. *Annu Rev Med*, 43:523–553, 1992.
- [29] P.J. Bore, I. Papatheofanis, and R.A. Sells. Adenosine triphosphate regeneration and function in the rat kidney following warm ischemia. *Transplantation*, 27:235–237, 1979.
- [30] E.L. Boulpaep. Ion permeability of the peritubular and luminal membrane of the renal tubular cell. In F. Krück, editor, *Transport und Funktion Intracellulärer Elektrolyte*, pages 98–107. Urban and Schwarzenberg, Munich, 1967.
- [31] E.L. Boulpaep. Electrical phenomena in the nephron. *Kidney Int*, 9:88–102, 1976.
- [32] E.L. Boulpaep. Recent advances in electrophysiology of the nephron. *Annu Rev Physiol*, 38:20–36, 1976.
- [33] E.L. Boulpaep and H. Sackin. Electrical analysis of intraepithelial barriers. In E.L. Boulpaep, editor, *Current Topics in Membranes and Transport*, volume 13, chapter 12, pages 169–197. Academic Press, New York, 1980.
- [34] E.L. Boulpaep and J.F. Seely. Electrophysiology of proximal and distal tubules in the autoperfused dog kidney. *Am J Physiol*, 221:1084–1096, 1971.
- [35] M. Brezis. Forefronts in nephrology: summary of the newer aspects of renal cell injury. *Kidney Int*, 42:523–539, 1992.
- [36] M. Brezis, S. Rosen, P. Silva, and F.H. Epstein. Renal ischemia: A new perspective. *Kidney Int*, 26:375–383, 1984.
- [37] M.B. Burg. Renal handling of sodium, chloride, water, amino acids, and glucose. In B.M. Brenner and F.C. Rector, Jr., editors, *The Kidney*, volume 1, chapter 5, pages 145–175. W. B. Saunders Company, Philadelphia, 3rd edition, 1986.
- [38] M.B. Burg and J. Orloff. Control of fluid absorption in the renal proximal tubule. *J Clin Invest*, 47:2016–2024, 1968.
- [39] M.B. Burg and J. Orloff. Electrical potential difference across proximal convoluted tubules. *Am J Physiol*, 219:1714–1716, 1970.

- [40] K. Burridge, T. Kelly, and P. Mangeat. Nonerythrocyte spectrins: actin-membrane attachment proteins occurring in many cell types. *J Cell Biol*, 95:478–486, 1982.
- [41] D.M. Canafax, A. Torres, D.S. Fryd, J.E. Heil, M.H. Strand, N.L. Ascher, W.D. Payne, D.E.R. Sutherland, R.L. Simmons, and J.S. Najarian. The effects of delayed function on recipients of cadaver renal allografts. A study of 158 patients randomized to cyclosporine or ALG-azathioprine. *Transplantation*, 41:177–181, 1986.
- [42] P.E. Canfield, A.M. Geerdes, and B.A. Molitoris. Effect of reversible ATP depletion on tight-junction integrity in LLC-PK<sub>1</sub> cells. *Am J Physiol*, 261:F1038–F1045, 1991.
- [43] J. Cardinal, M.D. Lutz, M.B. Burg, and J. Orloff. Lack of relationship of potential difference to fluid absorption in the proximal renal tubule. *Kidney Int*, 7:94–102, 1975.
- [44] B.M. Chanterlle, M.G. Cogan, and F.C. Rector, Jr. Active and passive components of NaCl absorption in the proximal convoluted tubule of the rat kidney. *Miner Electrolyte Metab*, 11:209–214, 1985.
- [45] J.S. Charnock, D.M. Doty, and J.C. Russell. The effect of temperature on the activity of (Na<sup>+</sup> + K<sup>+</sup>)-ATPase. *Arch Biochem Biophys*, 142:633–637, 1971.
- [46] P.T. Cheung and M.R. Hammerman. Na<sup>+</sup>-independent D-glucose transport in rabbit renal basolateral membranes. *Am J Physiol*, 254:F711–F718, 1988.
- [47] J.J. Cohen and Kamm D.E. Renal metabolism: Relation to renal function. In B.M. Brenner and F.C. Rector, Jr, editors, *The Kidney*, chapter 4, pages 76–109. W.B. Saunders Company, Philadelphia, 2nd edition, 1981.
- [48] J.J. Cohen and J.R. Little. Lactate metabolism in the isolated perfused rat kidney: Relations to renal function and gluconeogenesis. *J Physiol*, 255:399–414, 1976.
- [49] J.J. Cohen, L.S. Merkens, and O.W. Peterson. Relation of Na<sup>+</sup> reabsorption to utilization of O<sub>2</sub> and lactate in the perfused rat kidney. *Am J Physiol*, 238:F415–F427, 1980.
- [50] G.M. Collins, M. Bravo-Shugarman, and P.I. Terasaki. Kidney preservation for transportation. *Lancet*, 2:1219–1222, 1969.
- [51] G.M. Collins and W.N. Wicomb. New organ preservation solutions. *Kidney Int*, 42 (Suppl 38):S197–S202, 1992.
- [52] R.G. Contreras, A. Ponce, and J.J. Boliva. Calcium and tight junctions. In M. Cerejido, editor, *Tight Junctions*, pages 139–173. CRC Press, Inc., Boca Raton, 1992.

- [53] D.I. Cook and E. Frömter. Is the voltage divider ratio a reliable estimate of the resistance ratio of the cell membranes in tubular epithelia? *Pflügers Arch*, 403:388–395, 1985.
- [54] E. Coudrier, D. Kerjaschki, and D. Louvard. Cytoskeleton organization and submembranous interactions in intestinal and renal brush borders. *Kidney Int*, 34:309–320, 1988.
- [55] H. Davson. *A Textbook of General Physiology*. Williams & Williams, Baltimore, 4th edition, 1970.
- [56] J.M. Diamond and Y. Katz. Interpretation of nonelectrolyte partition coefficients between dimyristoyl lecithin and water. *J Membr Biol*, 17:121–154, 1974.
- [57] K.G. Dickman and L.J. Mandel. Differential effects of respiratory inhibitors on glycolysis in proximal tubules. *Am J Physiol*, 258:F1608–F1615, 1990.
- [58] J.F. Donohoe, M.A. Venkatachalam, D.B. Bernard, and N.G. Levinsky. Tubular leakage and obstruction after renal ischemia: Structural-functional correlations. *Kidney Int*, 13:208–222, 1978.
- [59] A. Doucet and A.I. Katz. High-affinity Ca-Mg-ATPase along the rabbit nephron. *Am J Physiol*, 242:F346–F352, 1982.
- [60] T.D. DuBose, Jr. Reclamation of filtered bicarbonate. *Kidney Int*, 38:584–589, 1990.
- [61] A. Edelman, S. Curci, I. Samaržija, and E. Frömter. Determination of intracellular  $K^+$  activity in rat kidney proximal tubular cells. *Pflügers Arch*, 378:37–45, 1978.
- [62] M. Esmann and J.C. Skou. Temperature-dependencies of various catalytic activities of membrane-bound  $Na^+/K^+$ -ATPase from ox brain, ox kidney and shark rectal gland and of  $C_{12}E_8$ -solubilized shark  $Na^+/K^+$ -ATPase. *Biochim Biophys Acta*, 944:344–350, 1988.
- [63] J.F. Figueiredo, D. Falkenstein, S.A. Draibe, D. Sigulem, and O.L. Ramos. The effect of Collins' solution on the function and structure of isolated proximal convoluted tubules from rabbit kidneys. *Transplantation*, 42:80–83, 1986.
- [64] W.F. Finn. Nephrology forum: Prevention of ischemic injury in renal transplantation. *Kidney Int*, 37:171–182, 1990.
- [65] E. Frömter. Electrophysiological analysis of rat renal sugar and amino acid transport. I. Basic phenomena. *Pflügers Arch*, 393:179–189, 1982.
- [66] E. Frömter and K. Geßner. Active transport potentials, membrane diffusion potentials and streaming potentials across rat kidney proximal tubule. *Pflügers Arch*, 351:85–98, 1974.

- [67] E. Frömter and K. Geßner. Free-flow potential profile along rat kidney proximal tubule. *Pflügers Arch*, 351:69–83, 1974.
- [68] D.C. Gadsby. The Na/K pump of cardiac cells. *Ann Rev Biophys Bioeng*, 13:373–398, 1984.
- [69] W. Gao, Y. Takei, I. Marzi, K.A. Lindert, J.C. Caldwell-Kenkel, R.T. Currin, Y. Tanaka, J.J. Lemasters, and R.G. Thurman. Carolina rinse solution – a new strategy to increase survival time after orthotopic liver transplantation in the rat. *Transplantation*, 52:417–424, 1991.
- [70] H. Gögelein and R. Greger. Properties of single K<sup>+</sup> channels in the basolateral membrane of rabbit proximal straight tubules. *Pflügers Arch*, 410:288–295, 1987.
- [71] B. Glaumann, H. Glaumann, I.K. Berezesky, and B.F. Trump. Studies on the pathogenesis of ischemic cell injury. II. Morphological changes of the pars convoluta (P<sub>1</sub> and P<sub>2</sub>) of the proximal tubule of the rat kidney made ischemic *in vivo*. *Virch Arch [B] (Cell Pathol)*, 19:281–302, 1975.
- [72] B. Glaumann, H. Glaumann, I.K. Berezesky, and B.F. Trump. Studies of cellular recovery from injury. II. Ultrastructural studies on the recovery of the pars convoluta of the proximal tubule of the rat kidney from temporary ischemia. *Virch Arch [B] (Cell Pathol)*, 24:1–18, 1977.
- [73] B. Glaumann, H. Glaumann, and B.F. Trump. Studies of cellular recovery from injury. III. Ultrastructural studies on the recovery of the pars recta of the proximal tubule (P<sub>3</sub> segment) of the rat kidney from temporary ischemia. *Virch Arch [B] (Cell Pathol)*, 25:281–308, 1977.
- [74] B. Glaumann and B.F. Trump. Studies on the pathogenesis of ischemic cell injury. III. Morphological changes of the proximal pars recta tubules (P<sub>3</sub>) of the rat kidney made ischemic *in vivo*. *Virch Arch [B] (Cell Pathol)*, 19:303–323, 1975.
- [75] H.G. Glitsch. Electrogenic Na pumping in the heart. *Annu Rev Physiol*, 44:389–400, 1982.
- [76] D.E. Goldman. Potential, impedance, and rectification in membranes. *J Gen Physiol*, 27:37–60, 1944.
- [77] J.J. Grantham, C.M. Lowe, M. Dellasega, and B.R. Cole. Effects of hypotonic medium on K and Na content of proximal renal tubule. *Am J Physiol*, 232:F42–F49, 1977.
- [78] R. Greger. Ion transport mechanisms in thick ascending limb of Henle's loop of mammalian nephron. *Physiol Rev*, 65:760–797, 1985.

- [79] J.M. Griño, R. Miravittles, A.M. Castelao, R. Sabater, S. Gil-Vernet, E. Franco, E. Andres, P. Maestre, and J. Alsina. Flush solution with mannitol in the prevention of post-transplant renal failure. *Transplant Proc*, 19:4140-4142, 1987.
- [80] W.G. Guder and G. Wirthensohn. Metabolism of isolated kidney tubules. Interactions between lactate, glutamine and oleate metabolism. *Eur J Biochem*, 99:577-584, 1979.
- [81] W.B. Guggino, E.E. Windhager, E.L. Boulpaep, and G. Giebisch. Cellular and paracellular resistances of the *Necturus* proximal tubule. *J Membr Biol*, 67:143-154, 1982.
- [82] S.R. Gullans, P.C. Brazy, V.W. Dennis, and L.J. Mandel. Interactions between gluconeogenesis and sodium transport in rabbit proximal tubule. *Am J Physiol*, 246:F859-F869, 1984.
- [83] S.R. Gullans, P.C. Brazy, S.P. Soltoff, V.W. Dennis, and L.J. Mandel. Metabolic inhibitors: effects on metabolism and transport in the proximal tubule. *Am J Physiol*, 243:F133-F140, 1982.
- [84] S.R. Gullans, S.I. Harris, and L.J. Mandel. Glucose-dependent respiration in suspensions of rabbit cortical tubules. *J Membr Biol*, 78:257-262, 1984.
- [85] S.R. Gullans and S.C. Hebert. Metabolic basis of ion transport. In B.M. Brenner and F.C. Rector, Jr, editors, *The Kidney*, chapter 2, pages 76-109. W.B. Saunders Company, Philadelphia, 4th edition, 1991.
- [86] M.L. Halperin, M.B. Goldstein, B.J. Stinebaugh, and R.L. Jungas. Biochemistry and physiology of ammonium excretion. In D.W. Seldin and G. Giebisch, editors, *The Kidney: Physiology and Pathophysiology*. Raven Press, New York, 1985.
- [87] M.J. Hanley. Isolated nephron segments in a rabbit model of ischemic acute renal failure. *Am J Physiol*, 239:F17-F23, 1980.
- [88] Y. Hatefi. The mitochondrial electron transport and oxidative phosphorylation system. *Ann Rev Biochem*, 54:1015-1069, 1985.
- [89] J. Heil, D.E.R. Sutherland, D.S. Fryd, N.L. Ascher, R.L. Simmons, and J.S. Najarian. Acute tubular necrosis of cadaver renal allografts does not correlate with organ sharing or preservation time but portends a poorer prognosis for long-term graft survival. *Transplant Proc*, 16:270-272, 1984.
- [90] D.A. Hems and J.T. Brosnan. Effects of ischemia on content of metabolites in rat liver and kidney *in vivo*. *Biochem J*, 120:105-111, 1970.
- [91] D. Herminghuysen, C.J. Welbourne, and T.C. Welbourne. Renal sodium reabsorption, oxygen consumption, and  $\gamma$ -glutamyltransferase excretion in the postischemic rat kidney. *Am J Physiol*, 248:F804-F809, 1985.

- [92] A.L. Hodgkin and B. Katz. The effect of sodium ions on the electrical activity of the giant axon of the squid. *J Physiol*, 108:37–77, 1949.
- [93] M. Hoelscher, M. Klaess, G. Kallerhoff, and H.J. Bretschneider. Is Euro-Collins' solution losing its protective ability above 15°C? *Transplant Proc*, 16:166–169, 1984.
- [94] J.F. Hoffman. Active transport of Na<sup>+</sup> and K<sup>+</sup> by red blood cells. In T.E. Andreoli, J.F. Hoffman, D.D. Fanestil, and S.G. Schultz, editors, *Membrane Physiology*, chapter 13, pages 221–234. Plenum Publishing Corporation, New York, 1987.
- [95] C. Holmberg, J.P. Kokko, and H.R. Jacobson. Determination of chloride and bicarbonate permeabilities in proximal convoluted tubules. *Am J Physiol*, 241:F386–F394, 1981.
- [96] T. Hoshi. Electrophysiology of *Triturus* nephron: Cable properties and electrogenic transport systems. *Kidney Int*, 37:157–170, 1990.
- [97] K.J. Howlin, R.J. Alpern, C.A. Berry, and F.C. Rector, Jr. Evidence for electroneutral sodium chloride transport in rat proximal convoluted tubules. *Am J Physiol*, 250:F644–F648, 1986.
- [98] P. Jablonski, C. Harrison, B. Howden, D. Rae, G. Tavanlis, V.C. Marshall, and J.D. Tange. Cyclosporine and the ischemic rat kidney. *Transplantation*, 41:147–151, 1986.
- [99] H.R. Jacobson and J.P. Kokko. Intrinsic differences in various segments of the proximal convoluted tubule. *J Clin Invest*, 57:818–825, 1976.
- [100] W.E. Jacobus, R.W. Moreadith, and K.M. Vandegaer. Mitochondrial respiratory control. Evidence against the regulation of respiration by extramitochondrial phosphorylation potential or by [ATP]/[ADP] ratios. *J Biol Chem*, 257:2397–2404, 1982.
- [101] P.A. Johnston, H. Rennke, and N.G. Levinsky. Recovery of proximal tubular function from ischemic injury. *Am J Physiol*, 246:F159–F166, 1984.
- [102] D.P. Jones. Renal metabolism during normoxia, hypoxia and ischemic injury. *Ann Rev Physiol*, 48:33–50, 1986.
- [103] J.K. Joseph, D. Bunnachak, T.J. Burke, and R.W. Schrier. A novel method of inducing and assuring total anoxia during *in vitro* studies of O<sub>2</sub> deprivation injury. *J Am Soc Nephrol*, 1:837–840, 1990.
- [104] M. Kakei, A. Noma, and T. Shibasaki. Properties of adenosine-triphosphate-regulated potassium channels in guinea-pig ventricular cells. *J Physiol*, 363:441–462, 1985.

- [105] G.J. Kaloyanides and E. Pastoriza-Munoz. Aminoglycoside nephrotoxicity. *Kidney Int*, 18:571–582, 1980.
- [106] S. Kawamura, M. Imai, D.W. Seldin, and J.P. Kokko. Characteristics of salt and water transport in superficial and juxtamedullary straight segments of proximal tubules. *J Clin Invest*, 55:1269–1277, 1975.
- [107] P.S. Kellerman and R.T. Bogusky. Microfilament disruption occurs very early in ischemic proximal tubule cell injury. *Kidney Int*, 42:896–902, 1992.
- [108] P.S. Kellerman, R.A.F. Clark, C.A. Hoilien, S.L. Linas, and B.A. Molitoris. Role of microfilaments in maintenance of proximal tubule structural and functional integrity. *Am J Physiol*, 259:F279–F285, 1990.
- [109] R.H. Kessler. Effects of ischemia on the concentration of adenine nucleotides in the kidney of anaesthetized dogs. *Pro Soc Exp Biol Med*, 134:1091–1095, 1970.
- [110] R. Kinne, H. Murer, E. Kinne-Saffran, M. Thees, and G. Sachs. Sugar transport by renal plasma membrane vesicles: Characterization of the systems in the brush-border microvilli and basal-lateral plasma membranes. *J Membr Biol*, 21:375–395, 1975.
- [111] A.G. Kléber. Resting membrane potential, extracellular potassium activity, and intracellular sodium activity during acute global ischemia in isolated perfused guinea pig hearts. *Cir Res*, 52:442–450, 1983.
- [112] K.L. Klein, M.-S. Wang, S. Torikai, W.D. Davidson, and K. Kurokawa. Substrate oxidation by isolated single nephron segments of the rat. *Kidney Int*, 20:29–35, 1981.
- [113] J.P. Kokko. Proximal tubule potential difference. Dependence on glucose,  $\text{HCO}_3$  and amino acids. *J Clin Invest*, 52:1362–1367, 1973.
- [114] J.P. Kokko and F.C. Rector. Flow dependence of transtubular potential difference in isolated perfused segments of rabbit proximal convoluted tubule. *J Clin Invest*, 50:2745–2750, 1971.
- [115] A. Kotowski, A. Ruhrberg, and P. Kaufmann. The influence of hypoxic cell-free perfusion and ischemia on cell morphology in the proximal tubular S2-segment of the rat kidney. *Virchows Arch [B] (Cell Pathol)*, 59:329–337, 1990.
- [116] F. Lang, H. Völkl, and D. Häussinger. General principles in cell volume regulation. In K.W. Beyenbach, editor, *Cell Volume Regulation. Comp Physiol*, volume 4, pages 1–25. Karger, Basel, 1990.
- [117] R. Laprade, J.-Y. Lapointe, S. Breton, M. Duplain, and J. Cardinal. Intracellular potassium activity in mammalian proximal tubule: Effect of perturbations in transepithelial sodium transport. *J Membr Biol*, 121:249–259, 1991.

- [118] A. Leaf, A.D.C. Macknight, J.Y. Cheung, and J.V. Bonventre. The cellular basis of ischemic acute renal failure. In T.E. Andreoli, J.F. Hoffman, D.D. Fanestil, and S.G. Schultz, editors, *Physiology of Membrane Disorders.*, chapter 42. Plenum Publishing Corporation, New York and London, 2nd edition, 1986.
- [119] J.B. Lee and H.M. Peter. Effect of oxygen tension on glucose metabolism in rabbit kidney cortex and medulla. *Am J Physiol*, 217:1464–1471, 1969.
- [120] J.B. Lee, V.K. Vance, and G.F. Cahill, Jr. Metabolism of C<sup>14</sup>-labelled substrates by rabbit kidney cortex and medulla. *Am J Physiol*, 203:27–36, 1962.
- [121] H.P. Leichtweiss, D.W. Lubbers, C. Weiss, H. Baumgartl, and W. Reschke. The oxygen supply of the rat kidney: Measurements of intrarenal pO<sub>2</sub>. *Pflügers Arch*, 309:328–349, 1969.
- [122] M.N. Levy. Oxygen consumption and blood flow in the hypothermic, perfused kidney. *Am J Physiol*, 197:1111–1114, 1959.
- [123] M.A. Linshaw and F.B. Stapleton. Effect of ouabain and colloid osmotic pressure on renal tubule cell volume. *Am J Physiol*, 235:F480–F491, 1978.
- [124] M.A. Linshaw, F.B. Stapleton, F.E. Cuppage, and J.J. Grantham. Effect of basement membrane and colloid osmotic pressure on renal tubule cell volume. *Am J Physiol*, 233:F325–F332, 1977.
- [125] A. Lukas and G.R. Ferrier. Electrophysiological effects of amrinone and milrinone in an isolated canine cardiac tissue model of ischemia and reperfusion. *J Pharmacol Exp Ther*, 244:348–354, 1988.
- [126] M.D. Lutz, J. Cardinal, and M.B. Burg. Electrical resistance of renal proximal tubule perfused in vitro. *Am J Physiol*, 225:729–734, 1973.
- [127] A.D.C. Macknight and A. Leaf. Regulation of cellular volume. In T.E. Andreoli, J.F. Hoffman, D.D. Fanestil, and S.G. Schultz, editors, *Membrane Physiology*, pages 311–328. Plenum Publishing Corporation, New York, 2nd edition, 1987.
- [128] L. Mandel and R. Bacallao. Alterations in the cytoskeleton and transepithelial resistance (RTE) during ATP depletion in cultured renal epithelial cells (abstract). *J Am Soc Nephrol*, 2:651, 1991.
- [129] L.J. Mandel. Metabolic substrates, cellular energy production, and the regulation of proximal tubular transport. *Ann Rev Physiol*, 47:85–101, 1985.
- [130] L.J. Mandel and R.S. Balaban. Stoichiometry and coupling of active transport to oxidative metabolism in epithelial tissues. *Am J Physiol*, 240:F357–F371, 1981.

- [131] V.C. Marshall, P. Jablonski, and D.F. Scott. Renal preservation. In P.J. Morris, editor, *Kidney Transplantation. Principles and Practice*, pages 151–182. W.B. Saunders Company, Philadelphia, 3rd edition, 1988.
- [132] J. Mason, F. Beck, A. Dörge, R. Rick, and K. Thurau. Intracellular electrolyte composition following renal ischemia. *Kidney Int*, 20:61–70, 1981.
- [133] D.L. Maude. Mechanism of salt transport and some permeability properties of rat proximal tubule. *Am J Physiol*, 218:1590–1595, 1970.
- [134] W.J. Mergner, S.M. Chang, and B.F. Trump. Studies on the pathogenesis of ischemic cell injury. V. Morphological changes of the pars convoluta ( $P_1$  and  $P_2$ ) of the proximal tubule of rat kidney made ischemic *in vitro*. *Virch Arch [B] (Cell Pathol)*, 21:211–228, 1976.
- [135] O.W. Moe, P.A. Preisig, and R.J. Alpern. Cellular model of proximal tubule NaCl and NaHCO<sub>3</sub> absorption. *Kidney Int*, 38:605–611, 1990.
- [136] B.A. Molitoris. Ischemia-induced loss of epithelial polarity: Potential role of the actin cytoskeleton. *Am J Physiol*, 260:F769–F778, 1991.
- [137] B.A. Molitoris, L.K. Chan, J.I. Shapiro, J.D. Conger, and S.A. Falk. Loss of epithelial polarity: a novel hypothesis for reduced proximal tubule Na<sup>+</sup> transport following ischemic injury. *J Membr Biol*, 107:119–127, 1989.
- [138] B.A. Molitoris, S.A. Falk, and Dahl R.H. Ischemia-induced loss of epithelial polarity. Role of the tight junction. *J Clin Invest*, 84:1334–1339, 1989.
- [139] B.A. Molitoris, A. Geerdes, and J.R. McIntosh. Dissociation and redistribution of Na<sup>+</sup>,K<sup>+</sup>-ATPase from its surface membrane actin cytoskeletal complex during cellular ATP depletion. *J Clin Invest*, 88:462–469, 1991.
- [140] B.A. Molitoris, C.A. Hoilien, R. Dahl, D.J. Ahnen, P.D. Wilson, and J. Kim. Characterization of ischemia-induced loss of epithelial polarity. *J Membr Biol*, 106:233–242, 1988.
- [141] B.A. Molitoris and R. Kinne. Ischemia induces surface membrane dysfunction. Mechanism of altered Na<sup>+</sup>-dependent glucose transport. *J Clin Invest*, 80:647–654, 1987.
- [142] B.A. Molitoris, P.D. Wilson, R.W. Schrier, and F.R. Simon. Ischemia induces partial loss of surface membrane polarity and accumulation of putative calcium ionophores. *J Clin Invest*, 76:2097–2105, 1985.
- [143] N. Morgunov and E.L. Boulpaep. Electrochemical analysis of renal Na<sup>+</sup>-glucose cotransport in salamander proximal tubules. *Am J Physiol*, 252:F154–F169, 1987.
- [144] N.S. Morgunov and D.J. Hirsch. Sodium transport in salamander proximal tubule at 5.5°C. *Am J Physiol*, 260:F323–F330, 1991.

- [145] W.J. Nelson and R.W. Hammerton. A membrane-cytoskeletal complex containing  $\text{Na}^+$ ,  $\text{K}^+$ -ATPase, ankyrin, and fodrin in Madin-Darby canine kidney (MDCK) cells: implications for the biogenesis of epithelial cell polarity. *J Cell Biol*, 108:893–902, 1989.
- [146] W.J. Nelson and P.J. Veshnock. Dynamics of membrane-skeleton (fodrin) organization during development of polarity in Madin-Darby canine kidney epithelial cells. *J Cell Biol*, 103:1751–1765, 1986.
- [147] W.J. Nelson and P.J. Veshnock. Ankyrin binding to  $(\text{Na}^+ + \text{K}^+)\text{ATPase}$  and implications for the organization of membrane domains in polarized cells. *Nature (Lond.)*, 328:533–536, 1987.
- [148] W.J. Nelson and P.J. Veshnock. Modulation of fodrin (membrane skeleton) stability by cell-cell contact in Madin-Darby canine kidney epithelial cells. *J Cell Biol*, 104:1527–1537, 1987.
- [149] J.T. Nielsen and E.I. Christensen. Ultrastructure of isolated perfused proximal tubules from rabbit kidney. A comparison with proximal tubules fixed by perfusion *in vivo*. *Lab Invest*, 49:400–411, 1983.
- [150] A.C. Novick, H. Ho-Hsieh, D. Steinmuller, S.B. Stroom, R.J. Cunningham, D. Steinhilber, M. Goormastic, and C. Buszta. Detrimental effect of cyclosporine on initial function of cadaver renal allografts following extended preservation. Results of a randomized prospective study. *Transplantation*, 42:154–158, 1986.
- [151] Oxyrase, Inc., Ashland, OH, USA. *Properties of the Oxyrase™ Enzyme System*, 1988.
- [152] L. Parent, J. Cardinal, and R. Sauvé. Single-channel analysis of a K channel at basolateral membrane of rabbit proximal convoluted tubule. *Am J Physiol*, 254:F105–F113, 1988.
- [153] N.R. Parrott, J.L.R. Forsythe, J.N.S. Matthews, T.W.J. Lennard, K.M. Rigg, G. Proud, and R.M.R. Taylor. Later perfusion. A simple remedy for renal allograft primary nonfunction. *Transplantation*, 49:913–915, 1990.
- [154] S. Pirie and D.J. Potts. A comparison of the relative effectiveness of three transplant preservation fluids upon the integrity and function of rabbit proximal convoluted tubules perfused *in vitro*. *Clin Sci*, 70:443–452, 1986.
- [155] R.J. Ploeg, D. Goossens, J.F. McAnulty, J.H. Southard, and F.O. Belzer. Successful 72-hour cold storage of dog kidneys with UW solution. *Transplantation*, 46:191–196, 1988.

- [156] R.J. Ploeg, J.H. van Bockel, P.T.H. Langendijk, M. Groenewegen, F.J. van der Woude, G.G. Persijn, J. Thorogood, and J. Hermans. (for the European Multicentre Study Group). Effect of preservation solution on results of cadaveric kidney transplantation. *Lancet*, 340:129–137, 1992.
- [157] R.M. Rajerison, M. Faure, and F. Morel. Effects of temperature, ouabain and diuretics on the cell sodium and potassium contents of isolated rat kidney tubules. *Pflügers Arch*, 406:285–290, 1986.
- [158] K.A. Reimer, C.E. Ganote, and R.B. Jennings. Alterations in renal cortex following ischemic injury. III. Ultrastructure of proximal tubules after ischemia or autolysis. *Lab Invest*, 26:347–363, 1972.
- [159] C.E. Ruegg and L.J. Mandel. Bulk isolation of renal PCT and PST. I. Glucose-dependent metabolic differences. *Am J Physiol*, 259:F164–F175, 1990.
- [160] C.E. Ruegg and L.J. Mandel. Bulk isolation of renal PCT and PST. II. Differential responses to anoxia or hypoxia. *Am J Physiol*, 259:F176–F185, 1990.
- [161] I. Sabolić and G. Burckhardt. Characteristics of the proton pump in rat renal cortical endocytotic vesicles. *Am J Physiol*, 250:F817–F826, 1986.
- [162] H. Sackin. Electrophysiology of salamander proximal tubule. I. Effects of rapid cooling. *Am J Physiol*, 251:F319–F333, 1986.
- [163] H. Sackin and E.L. Boulpaep. Isolated perfused salamander proximal tubule: methods, electrophysiology, and transport. *Am J Physiol*, 241:F39–F52, 1981.
- [164] H. Sackin and E.L. Boulpaep. Rheogenic transport in the renal proximal tubule. *J Gen Physiol*, 82:819–851, 1983.
- [165] H. Sackin and L.G. Palmer. Basolateral potassium channels in renal proximal tubule. *Am J Physiol*, 253:F476–F487, 1987.
- [166] S.A. Sacks, P.H. Petritsch, and J.J. Kaufman. Canine kidney preservation using a new perfusate. *Lancet*, 1:1024–1028, 1973.
- [167] F. Sanfilippo, W.K. Vaughn, E.K. Spees, and B.A. Lucas. The detrimental effects of delayed graft function in cadaver donor renal transplantation. *Transplantation*, 38:643–648, 1984.
- [168] F. Sanfilippo, W.K. Vaughn, E.K. Spees, and B.A. Lucas. The effects of delayed graft function on renal transplantation. *Transplant Proc*, 17:13–15, 1985.
- [169] S. Sasaki, T. Shiigai, N. Yoshiyama, and J. Takeuchi. Mechanism of bicarbonate exit across basolateral membrane of rabbit proximal straight tubule. *Am J Physiol*, 252:F11–F18, 1987.

- [170] J.A. Schafer. Transepithelial osmolality differences, hydraulic conductivities, and volume absorption in the proximal tubule. *Annu Rev Physiol*, 52:709–726, 1990.
- [171] J.A. Schafer, C.S. Patlak, and T.E. Andreoli. A component of fluid absorption linked to passive ion flows in the superficial pars recta. *J Gen Physiol*, 66:445–471, 1975.
- [172] J.A. Schafer, C.S. Patlak, and T.E. Andreoli. Fluid absorption and active and passive ion flows in the rabbit superficial pars recta. *Am J Physiol*, 233:F154–F167, 1977.
- [173] J.A. Schafer, S.L. Troutman, and T.E. Andreoli. Volume reabsorption, transepithelial potential difference, and ionic permeability properties in mammalian superficial proximal straight tubules. *J Gen Physiol*, 64:582–607, 1974.
- [174] S.G. Schultz. *Basic Principles of Membrane Transport*. Cambridge University Press, Cambridge, 1980.
- [175] S.G. Schultz. Regulatory mechanisms in sodium-absorbing epithelia. In D.W. Seldin and G. Giebisch, editors, *The Kidney: Physiology and Pathophysiology*, chapter 10, pages 189–198. Raven Press, New York, 1985.
- [176] S.G. Schultz and R.L. Hudson. How do sodium-absorbing cells do their job and survive? *News Physiol Sci*, 1:185–189, 1986.
- [177] A.E. Senior. ATP synthesis by oxidative phosphorylation. *Physiol Rev*, 68:177–231, 1988.
- [178] A.W. Siebens and W.F. Boron. Effect of electroneutral luminal and basolateral lactate transport on intracellular pH in salamander proximal tubules. *J Gen Physiol*, 90:799–831, 1987.
- [179] P. Silva. Energy and fuel substrate metabolism in the kidney. *Semin Nephrol*, 10:432–444, 1990.
- [180] M. Silverman, P. Vinay, L. Shinobu, A. Gougoux, and G. Lemieux. Luminal and antiluminal transport of glutamine in dog kidney: Effect of metabolic acidosis. *Kidney Int*, 20:359–365, 1981.
- [181] S.P. Soltoff and L.J. Mandel. Active ion transport in the renal proximal tubule. I. Transport and metabolic studies. *J Gen Physiol*, 84:601–622, 1984.
- [182] S.P. Soltoff and L.J. Mandel. Active ion transport in the renal proximal tubule. III. the ATP dependence of the Na pump. *J Gen Physiol*, 84:643–662, 1984.
- [183] J.-I. Sudo and F. Morel. Na<sup>+</sup> and K<sup>+</sup> cell concentrations in collagenase-treated rat kidney tubules incubated at various temperatures. *Am J Physiol*, 246:C407–C414, 1984.

- [184] M.G. Suranyi and B.M. Hall. Current status of renal transplantation. *West J Medicine*, 152:687–696, 1990.
- [185] R.L. Tannen. Ammonia metabolism. *Am J Physiol*, 235:F265–F277, 1978.
- [186] A. Tejedor, J. Noel, P. Vinay, Y. Boulanger, and A. Gougoux. Characterization and metabolism of canine proximal tubules, thick ascending limbs and collecting ducts in suspension. *Can J Physiol Pharmacol*, 66:997–1009, 1988.
- [187] R.C. Thomas. Electrogenic sodium pump in nerve and muscle cells. *Physiol Rev*, 52:563–594, 1972.
- [188] C.C. Tisher and J.P. Kokko. Relationship between peritubular oncotic pressure gradients and morphology in isolated proximal tubules. *Kidney Int*, 6:146–156, 1974.
- [189] J. Torras, J.R. Bordalba, D. Seron, M. Carrera, A.M. Castelao, R. Poveda, J. Alsina, and J. Griño. An experimental comparison between isotonic saline solution, Euro-Collins, and a flush solution with mannitol in the prevention of renal damage due to warm ischemia. *Transplant Proc*, 24:54–55, 1992.
- [190] A.L. Trifillis, M.W. Kahng, R.A. Cowley, and B.F. Trump. Metabolic studies of postischemic acute renal failure in the rat. *Exp Mol Pathol*, 40:155–168, 1984.
- [191] S. Tripathi, E.L. Boulpaep, and A.B. Manunsbach. Isolated perfused *ambystoma* proximal tubule: hydrodynamics modulates ultrastructure. *Am J Physiol*, 252:F1129–F1147, 1987.
- [192] S. Tripathi, N. Morgunov, and E.L. Boulpaep. Submicron tip breakage and silanization control improve ion-selective microelectrodes. *Am J Physiol*, 249:C514–C521, 1985.
- [193] B.F. Trump, J.M. Strum, and R.E. Bulger. Studies on the pathogenesis of ischemic cell injury. I. Relation between ion and water shifts and cell ultrastructure in rat kidney slices during swelling at 0–4°C. *Virch Arch [B] (Cell Pathol)*, 16:1–34, 1974.
- [194] C.-M. Tse, S.R. Brant, M.S. Walker, J. Pouyssegur, and M. Donowitz. Cloning and sequencing of a rabbit cDNA encoding an intestinal and kidney-specific Na<sup>+</sup>/H<sup>+</sup> exchanger isoform (NHE-3). *J Biol Chem*, 267:9340–9346, 1992.
- [195] C.M. Tse, A.I. Ma, V.W. Wang, A.J.M. Watson, S. Levine, M.H. Montrose, J. Potter, C. Sardet, J. Pouyssegur, and M. Donowitz. Molecular cloning and expression of a cDNA encoding the rabbit ileal villus cell basolateral membrane Na<sup>+</sup>/H<sup>+</sup> exchanger. *EMBO J*, 10:1957–1967, 1991.
- [196] S. Uchida and H. Endou. Substrate specificity to maintain cellular ATP along the mouse nephron. *Am J Physiol*, 255:F977–F983, 1988.

- [197] Y. Ueda, S. Todo, O. Inventarza, H. Furukawa, A. Oks, Y.M. Wu, S. Oguma, and T.E. Starzl. The UW solution for canine kidney preservation. Its specific effect on renal hemodynamics and microvasculature. *Transplantation*, 48:913-918, 1989.
- [198] K.J. Ullrich and F. Papavassiliou. Contraluminal transport of small aliphatic carboxylates in the proximal tubule of the rat kidney in situ. *Pflügers Arch*, 407:488-492, 1986.
- [199] A. Vandewalle, G. Wirthensohn, H.-G. Heidrich, and W.G. Guder. Distribution of hexokinase and phosphoenolpyruvate carboxykinase along the rabbit nephron. *Am J Physiol*, 240:F492-F500, 1981.
- [200] H. Völkl, J. Geibel, R. Greger, and F. Lang. Effects of ouabain and temperature on cell membrane potentials in isolated perfused straight proximal tubules of the mouse kidney. *Pflügers Arch*, 407:252-257, 1986.
- [201] M.A. Venkatachalam, D.B. Bernard, J.F. Donohoe, and N.G. Levinsky. Ischemic damage and repair in the rat proximal tubule: Differences among the S<sub>1</sub>, S<sub>2</sub> and S<sub>3</sub> segments. *Kidney Int*, 14:31-49, 1978.
- [202] M.A. Venkatachalam, Y.J. Patel, J.I. Kreisberg, and J.M. Weinberg. Energy thresholds that determine membrane integrity and injury in a renal epithelial cell line (LLC-PK<sub>1</sub>). Relationships to phospholipid degradation and unesterified fatty acid accumulation. *J Clin Invest*, 81:745-758, 1988.
- [203] D.G. Warnock and V.J. Yee. Anion permeabilities of the isolated perfused rabbit proximal tubule. *Am J Physiol*, 242:F395-F405, 1982.
- [204] P.D. Weer. Cellular sodium-potassium transport. In D.W. Seldin and G. Giebisch, editors, *The Kidney: Physiology and Pathophysiology*, chapter 3, pages 31-48. Raven Press, New York, 1985.
- [205] J.M. Weinberg. Oxygen deprivation-induced injury to isolated rabbit kidney tubules. *J Clin Invest*, 76:1193-1208, 1985.
- [206] J.M. Weinberg. The cell biology of ischemic renal injury. *Kidney Int*, 39:476-500, 1991.
- [207] J.M. Weinberg, J.A. Davis, M. Abarzua, R.K. Smith, and R. Kunkel. Ouabain-induced lethal proximal tubule cell injury is prevented by glycine. *Am J Physiol*, 258:F346-F355, 1990.
- [208] L.W. Welling and D.J. Welling. Shape of epithelial cells and intercellular channels in the rabbit proximal nephron. *Kidney Int*, 9:385-394, 1976.
- [209] A.A.M. Wilde and A.G. Kléber. The combined effects of hypoxia, high K<sup>+</sup>, and acidosis on the intracellular sodium activity and resting potential in Guinea pig papillary muscle. *Circ Res*, 58:249-256, 1986.

- [210] G. Wirthensohn and W.G. Guder. Renal substrate metabolism. *Physiol Rev*, 66:469–497, 1986.
- [211] K. Wulff and W. Döppen. ATP: Luminometric method. In H.U. Bergmeyer, J. Bergmeyer, and M. Graßl, editors, *Methods of Enzymatic Analysis*, volume 7, chapter 3.9.3. VCH, Weinheim, Germany, 3rd edition, 1985.